

**STRUCTURE-FUNCTION STUDIES OF THE INTIATION RESPONSE OF HUMAN
MISMATCH REPAIR PROTEINS TO DNA CONTAING A MISMATCH**

Kira Caitlin Bradford

A dissertation submitted to the faculty at the University of North Carolina at Chapel Hill in partial fulfillment of the requirements for the degree of Doctor of Philosophy in the Department of Chemistry.

Chapel Hill
2015

Approved by:

Dorothy Erie

Matt Redinbo

Linda Spremulli

Tom Kunkel

Dale Ramsden

© 2015
Kira Caitlin Bradford
ALL RIGHTS RESERVED

ABSTRACT

Kira Caitlin Bradford: Structure-Function Studies of the Initiation Response of Human Mismatch Repair Proteins to DNA Containing a Mismatch
(Under the direction of Dorothy A. Erie)

DNA mismatch repair (MMR) is the post-replicative process that recognizes and repairs misincorporated bases that occur during replication. Deficiencies in MMR are linked to greater than 80% of hereditary non-polyposis colorectal cancer. To better understand the initiation of MMR in humans, two proteins, MSH2-MSH6 (hMutS α) and MLH1-PMS2 (hMutL α), were studied. hMutS α first recognizes and binds to the mismatch in an ADP-dependent manner; however, it then undergoes an ATP-dependent conformational change(s) into a mobile clamp. The ATP activated form of hMutS α also recruits hMutL α to the DNA. Together, these proteins signal the downstream events of MMR that results in the repair of the misincorporated base.

Currently, the conformations of the hMutS α -DNA complexes in the presence of ATP are not well characterized. hMutS α in the presence of ADP has previously been crystallized in complex with mismatched DNA. This crystal structure shows that hMutS α induces a kink on the DNA, consistent with other studies done with MutS homologs. However, no crystal structures have yet been solved of hMutS α in the presence of ATP. Additionally, the conformational state of hMutS α that interacts with hMutL α is not well understood, and little is known on the conformations of the hMutS α -hMutL α -DNA complexes.

In this work, I used atomic force microscopy (AFM) to examine the conformational properties of hMutS α and hMutS α -hMutL α on DNA containing a single mismatch and in various adenine nucleotide conditions. The data suggests that hMutS α recognizes and binds to the mismatch in the presence of ADP, and, surprisingly, remains localized to the mismatch in the presence of ATP. The data also show that ATP induces hMutS α -hMutS α interactions, and multiple hMutS α form a complex on the mismatch. I also characterized the hMutS α -induced DNA bend angle properties and saw unique changes in bending depending on the adenine nucleotide conditions. Additionally, I observed unique properties of the complexes of hMutS α and hMutL α in the presence of ATP including: complex volumes becoming larger, DNA lengths appearing shorter, and some population of these complexes remain localized to the mismatch. Taken together, these data provide mechanistic insights and allows us to propose a molecular model for MMR initiation.

To Robert,

For all of his love, support, and encouragement,

To my family,

For always believing in me and pushing me to be the best I can be.

ACKNOWLEDGEMENTS

First, I'd like to thank my advisor, Dorothy Erie. I am forever grateful that she is a “gambling” woman that took a chance with me and accepted me as a graduate student in her lab. She gave me the freedom and independence to pursue the research I found most intriguing, and made time for me once I banged my head against the brick wall a time too many. She also supported me with my endeavors outside the lab, as I try and find my path in life. She encouraged, supported, and guided me as I navigated through my research project, and taught me how to think like a scientist. I will always be grateful that I was lucky to have the opportunity to learn from her.

I want to thank my colleagues within the Erie lab. I'd like to thank all of the Erie lab members past and present for listening to my stumbling research talks and providing constructive feedback. I especially want to thank Vanessa, Jake, Hunter, Jackie, Zimeng, and Sarah for reading the drafts of my paper and my thesis. Thank you all for the Fridays, for the lunchroom crossword puzzles, and for the meaningful scientific discussions. Each of you helped me to grow as a scientist and forced me to learn how to be a better lab citizen. You all have helped keep me sane and made me realize time and again that there is light at the end of the tunnel.

Thank you to all the people who contributed their time and expertise to make this body of work possible. For providing the protein and DNA substrate that I would not have been able to do my experiments without, I want to thank Chungwei Du and Peggy Hsieh, for continuing to provide the resources I needed to complete my experiments. I also want to acknowledge to Matt Meiners for teaching my undergraduate students and me how to do cesium chloride preps. I also

would like to thank my committee members, especially Tom Kunkel for giving me valuable expertise.

I'd like to thank my friends who have become my new family here in NC. I am lucky to have you all in my life. I am grateful for the time commiserating our failed experiments, encouraging each other out of graduate student guilt, and for the many fun game nights that we had. I am also grateful for our many runs, during the day, and especially at night.

I would also like to thank my husband, Robert. Thanks do not begin to adequately describe how your strength, encouragement, and tough love have gotten me to this point. You are my rock that keeps me centered and strong. You put up with the emotional turmoil, the ups and downs of science, and the many tears of failure and despair. When I want to do something risky or off the wall, you do not hold me back but help me find ways to achieve it. You are so wonderful and I am so happy and grateful that you are in my life.

Finally, I would like to thank my family especially Papa Jim for encouraging me to venture into science. I would also like to thank my mom, whose strength and sheer force of will are characteristics that I will always strive to achieve. My brothers, who always believe in me, even when "the thingy isn't thingy-ing." The love and support of my family are what helps keep me going, and I will always be thankful for that.

TABLE OF CONTENTS

LIST OF TABLES	xiv
LIST OF FIGURES	xv
LIST OF ABBREVIATIONS	xvii
CHAPTER 1: DNA MISMATCH REPAIR AND ATOMIC FORCE MICROSCOPY: STUDYING BLOBS AND TWISTING KNOBS	1
Introduction	1
Human MMR	2
MutSα	3
<i>Structure of MutSα</i>	<i>3</i>
<i>Properties and Functions of MutSα</i>	<i>7</i>
<i>DNA Bending by MutSα</i>	<i>11</i>
<i>ATPase activity of MutSα and the Formation of the Mobile Clamp</i>	<i>12</i>
MutLα	15
<i>Structure of MutLα</i>	<i>15</i>
<i>Properties of MutLα</i>	<i>18</i>
<i>MutLα Endonuclease Activity</i>	<i>19</i>
<i>The Strand Discrimination Signal</i>	<i>20</i>
MutSα and MutLα Complexes	20
<i>Role of MutSα–MutLα Complexes</i>	<i>20</i>

Atomic Force Microscopy	24
Thesis Statement	29
REFERENCES	31
CHAPTER 2: STRUCTURE-FUNCTION INVESTIGATION OF HUMAN MUTSA AND MUTSA–MUTLA ON DNA CONTAINING A MISMATCH	37
Introduction.....	37
Materials and Methods.....	40
<i>Protein expression and purification.....</i>	<i>40</i>
<i>DNA substrate preparation.....</i>	<i>40</i>
<i>Sample preparation and deposition</i>	<i>40</i>
<i>Imaging</i>	<i>41</i>
<i>Image Analysis</i>	<i>41</i>
Results	43
<i>In the presence of ADP, one MutSa binds to the mismatch</i>	<i>43</i>
<i>In the presence of ATP, MutSa binds with high specificity to the mismatch</i>	<i>46</i>
<i>ATP induces mismatch-dependent multimerization of MutSa</i>	<i>47</i>
<i>MutSa and MutLa form large complexes on the DNA.....</i>	<i>49</i>
<i>Large MutSa–MutLa complexes exhibit shortened DNA lengths</i>	<i>51</i>
<i>MutSa–MutLa complexes are less specific to the mismatch.....</i>	<i>54</i>
Discussion.....	57
<i>Multimers of MutSa localize to the mismatch in the presence of ATP</i>	<i>57</i>

<i>MutLα traps MutSα mobile clamps and multiple MutLα are recruited.....</i>	58
REFERENCES	62
CHAPTER 3: INVESTIGATION OF THE ROLE OF ATP HYDROLYSIS IN MUTSA MOBILE CLAMP FORMATION AND MOVEMENT: AN AFM STUDY WITH ATPγS	65
Introduction.....	65
Materials and Methods.....	67
<i>Protein expression and purification.....</i>	67
<i>DNA substrate preparation.....</i>	67
<i>Sample preparation and deposition</i>	68
<i>Imaging</i>	68
<i>Image Analysis</i>	69
Results	69
<i>In the presence of ATPγS, up to two MutSa bind the mismatch.....</i>	69
<i>In the presence of ATPγS and ADP, one MutSa binds the mismatch</i>	75
Discussion.....	77
Future Directions	78
REFERENCES	80
CHAPTER 4: EXAMINATION OF THE EFFECT OF DIFFERENT ADENINE NUCLEOTIDES ON MUTSα-INDUCED DNA BENDING: AN AFM BEND ANGLE ANALYSIS STUDY	84
Introduction.....	84
Materials and Methods.....	86

<i>Protein expression and purification.....</i>	86
<i>DNA substrate preparation.....</i>	87
<i>Sample preparation and deposition.....</i>	87
<i>Imaging.....</i>	88
<i>Image Analysis.....</i>	88
Results.....	90
<i>In the presence of ADP, MutSα at the mismatch bends the DNA at 45 °.....</i>	90
<i>Mismatch-bound MutSα in the presence of ATP exhibits two DNA bend angles.....</i>	91
<i>MutSα induced DNA bend angles are independent of ATP hydrolysis.....</i>	97
Discussion.....	100
Future Directions.....	102
REFERENCES.....	104
CHAPTER 5: AFM STUDIES TO GAIN INSIGHT INTO OTHER BIOMOLECULAR PROCESSES.....	107
Introduction.....	107
REFERENCES.....	108
CHAPTER 5.1: STRUCTURE-FUNCTION INVESTIGATION OF ANGPTL4.....	109
Introduction.....	109
Materials and Methods.....	110
<i>Protein Purification.....</i>	110
<i>Atomic Force Microscopy.....</i>	110

Results	111
Discussion.....	114
REFERENCES	116
CHAPTER 5.2: STRUCTURE-FUNCTION INVESTIGATIONS OF TRAK.....	117
Introduction.....	117
Materials and Methods.....	118
<i>TraK and DNA substrate purification.....</i>	<i>118</i>
<i>Sample preparation and deposition</i>	<i>118</i>
<i>Imaging</i>	<i>119</i>
<i>Image Analysis</i>	<i>119</i>
Results	120
<i>TraK exists as a monomer and dimer in vitro.....</i>	<i>120</i>
<i>Large complexes of TraK form on DNA</i>	<i>120</i>
Conclusions and Future Work.....	123
REFERENCES	124
CHAPTER 5.3: AFM STUDIES OF THE OLIGMERIZATION STATE OF THE VACCINIA VIRUS ENDORIBONUCLEASE H5.....	125
Introduction.....	125
Materials and Methods:.....	126
<i>Protein Purification</i>	<i>126</i>
<i>Atomic Force Microscopy.....</i>	<i>126</i>
Results	128
<i>H5 exists primarily as a monomer</i>	<i>128</i>

Conclusions and Future Work.....	128
REFERENCES	130
APPENDIX A: SUPPLEMENTAL FIGURES - CHAPTER 2	131
Supplemental Figures	131
Supplemental Methods Figures	137
APPENDIX B: AFM DATA ANALYSIS PROTOCOL	140
Part 1: Flattening raw AFM images.....	140
Part 2: Volume Analysis.....	140
Part 3: DNA Contour Trace analysis	143
REFERENCES	146

LIST OF TABLES

Table 1.1 : Comparison of prokaryotic and eukaryotic MutS and MutL homologs	6
Table 4.1 : Summary of MutS α -induced DNA bend angles	99
Table 5.1 : Predicted AFM volumes based on the linear dependency of AFM volume to protein molecular weight: $V = 1.2 * M - 14.7$, where V is AFM volume in nm ³ , and M is molecular mass in kDa	112

LIST OF FIGURES

Figure 1.1 : DNA Mismatch Repair in Humans	5
Figure 1.2 : Crystal Structure of Human MutS	10
Figure 1.3 : Structure of MutL α	17
Figure 1.4 : Models of MutS α –MutL α Interactions	23
Figure 1.5 : AFM Experimental Methods	28
Figure 2.1 : AFM images and position and volume analysis of MutS α bound to GT–DNA	45
Figure 2.2 : AFM images and volume analysis of MutS α –MutL α complexes bound to GT–DNA	53
Figure 2.3 : Position analysis of MutS α –MutL α complexes bound to GT–DNA	56
Figure 2.4 : Model of MutS α and MutL α Interaction	59
Figure 3.1 : AFM images and analysis of MutS α bound to GT–DNA in the presence of ATP γ S	71
Figure 3.2 : AFM images and analysis of MutS α bound to circular GT–DNA in the presence of ATP γ S	74
Figure 3.3 : AFM images and analysis of MutS α bound to GT–DNA in the presence of ATP γ S and ADP	76
Figure 4.1 : AFM bend angle analysis	89
Figure 4.2 : MutS α -induced GT-DNA bend angles in the presence of various adenine nucleotides	93
Figure 4.3 : MutS α -induced GC-DNA bend angles	94
Figure 4.4 : Non-specifically bound MutS α -induced GT-DNA bend angles in the presence of ATP	96
Figure 4.5 : Model of MutS α -induced DNA Bending	101

Figure 5.1 : Distribution of AFM particle volumes in cubic nanometers	113
Figure 5.2 : AFM images and volume analysis of TraK.....	121
Figure 5.3 : AFM image and position analysis of TraK on DNA.....	122
Figure 5.4 : AFM images and volume analysis of H5	127
Figure S2.1 : Number of complexes bound to DNA	131
Figure S2.2 : Position distribution of MutS α on GC–DNA in the presence of ADP vs.ATP	132
Figure S2.3 : Images of multimers of MutS α on GT–DNA in the presence of ATP.....	133
Figure S2.4 : Asymmetry of multimers of MutS α on GT–DNA in the presence of ATP.....	134
Figure S2.5 : Distribution of the conformational shapes of MutS α and MutS α –MutL α complexes on GT–DNA.	135
Figure S2.6 : AFM images of MutS α and MutS α –MutL α complexes bound to GT–DNA	136
Figure SM2.1 : AFM images of the non–crosslinked control experiment of MutS α bound to GT–DNA in the presence of ATP	137
Figure SM2.2 : Normalization of MutS α volumes	138
Figure SM2.3 : Position analysis of MutS α on DNA	139

LIST OF ABBREVIATIONS

°	Degree
'	Prime
μm	Micron
μM	Micromolar
3D	Three-dimensional
ABC	ATP binding cassette
ADP	Adenine diphosphate
AFM	Atomic force microscopy
ANGPTL4	Angiopoietin-like Protein 4
ATP	Adenine triphosphate
ATP _γ S	Adenine 5'-(gamma-thio) triphosphate
Bp	Base pair
CC	Cytosine-cytosine mismatch
ddH ₂ O	Doubly deionized water
DNA	Deoxyribonucleic acid
dsDNA	Double stranded DNA
DTT	Dithiothreitol
<i>E. coli</i>	<i>Escherichia coli</i>
EDTA	Ethylamine diamine tetraacetic acid
EXO1	Exonuclease I
FRET	Fluorescence resonance energy transfer
GT	Guanine-thymine mismatch

HEPES	4-(2-hydroxyethyl)-1-piperazineethanesulfonic acid
HNPCC	Hereditary non-polyposis colorectal cancer
IDL	Insertion deletion loop
IRC	Initial recognition complex
k_{cat}	Catalysis rate constant
KCl	Potassium chloride
K_d	Dissociation constant
LPL	Lipoprotein Lipase
m	Meter
M	Molar
mg	Milligram
Mg	Magnesium
MgCl_2	Magnesium chloride
MgOAc	Magnesium Acetate
min	Minute
mL	Milliliter
MLH1	Human MutL homolog 1
Mlh1	<i>S. cerevisiae</i> MutL homolog 1
MLH1-PMS2	Human MutL homolog 1 and postmeiotic segregation increased 2
Mlh1-Pms1	<i>S. cerevisiae</i> MutL homolog 1 and postmeiotic segregation increased 1
mM	Millimolar
mmDNA	Mismatch DNA
MMR	Mismatch repair

mol	Mole
MSH2	Human MutS homolog 2
Msh2	<i>S. cerevisiae</i> MutS homolog 2
MSH2-MSH6	Human MutS homologs 2 and 6
Msh2-Msh6	<i>S. cerevisiae</i> MutS homologs 2 and 6
MSH6	Human MutS homolog 6
Msh6	<i>S. cerevisiae</i> MutS homolog 6
MutS(α)	MutS and MutS α
MutS α	Heterodimer of eukaryotic MutS homologs 2 and 6
MW	Molecular weight
NaCl	Sodium chloride
NaOAc	Sodium acetate
NaOH	Sodium hydroxide
NIDDK	National Institute of Diabetes and Digestive and Kidney Diseases
NIH	National Institutes of Health
nm	Nanometer
nM	Nanomolar
nm ³	Cubic nanometer
PAGE	Polyacrylamide gel electrophoresis
PCNA	Proliferating cell nuclear antigen
PDB ID	Protein database identification
Phe-X-Glu	Phenylalanine-amino acid-glutamic acid motif
Pms1	<i>S. cerevisiae</i> postmeiotic segregation increased 1

PMS2	Human postmeiotic segregation increased 2
Pol α	Polymerase α
Pol δ	Polymerase δ
Pol ε	Polymerase ε
RFC	Replication factor C
RPA	Replication protein A
s	Second
<i>S. cerevisiae</i>	<i>Saccharomyces cerevisiae</i>
SDS	Sodium dodecyl sulfate
smFRET	Single-molecule fluorescence resonance energy transfer
ssDNA	Single stranded DNA
T bulge	Single thymine insert
<i>Taq</i>	<i>Thermus aquaticus</i>
TIRF	Total internal reflection fluorescence
Tris	tris(hydroxymethyl)aminomethane buffer
URC	Ultimate recognition complex
VLDL	Very low-density lipoproteins
WT	Wild type
yMutS α	yeast Msh2-Msh6

CHAPTER 1: DNA MISMATCH REPAIR AND ATOMIC FORCE MICROSCOPY: STUDYING BLOBS AND TWISTING KNOBS

Introduction

For every organism, from prokaryotes to eukaryotes, the ability to survive relies on the accurate replication of its genome. However, the fidelity of genome replication is dependent on the accuracy of DNA polymerases, and despite the high fidelity of these polymerases, mistakes do occur. During one round of DNA replication, DNA polymerases will introduce one incorrect base (e.g. a non-Watson-Crick base pair) for every $\sim 10^7$ bases synthesized (Kunkel and Erie 2005, Iyer, Pluciennik et al. 2006). The human genome is composed of approximately 6 billion bases, which means these mistakes result in approximately 600 misincorporated bases per round of DNA replication (Iyer, Pluciennik et al. 2006). These misincorporated bases or mismatches, if not corrected, will lead to mutations in genomic DNA, genomic instability, and may promote the development of cancer (Kunkel and Erie 2005, Erie and Weninger 2014). There are several pathways to repair DNA mismatches such as base excision repair and nucleotide excision repair. However, the main pathway that will be discussed in this thesis is the bidirectional and post-replicative process of mismatch repair (MMR). MMR is highly conserved between prokaryotes and eukaryotes, and this pathway increases the fidelity of DNA synthesis 100 – 1000 fold (Schofield and Hsieh 2003, Kunkel and Erie 2005, Iyer, Pluciennik et al. 2006, Modrich 2006, Spampinato, Gomez et al. 2009). Deficiencies in the MMR pathway are linked to greater than 80% of cases of hereditary non-polyposis colorectal cancer (HNPCC), which highlight the importance of a functional mismatch repair pathway (Kaur, Masoud et al. 2011).

Human MMR

Mismatch repair proteins, MutS and MutL homologs, recognize and initiate the repair of misincorporated bases following DNA replication, shown in Figure 1.1. In humans, initiation of MMR occurs when MutS recognizes an error in the DNA. A base-base mismatch or a small insertion-deletion loop is recognized by MSH2-MSH6 (MutS α) and large insertion deletion loops are recognized by MSH2-MSH3 (MutS β). MutS α (or MutS β) then binds to the mismatch site and undergoes an ATP-dependent conformational change(s) into a mobile clamp that facilitates the interactions with one or more MutL α (Kunkel and Erie 2005, Iyer, Pluciennik et al. 2006, Hsieh and Yamane 2008, Erie and Weninger 2014). PCNA activates the latent endonuclease activity of MutL α and directs the MutS α –MutL α complex to nick the daughter strand either distally (preferentially, depicted in Figure 1.1 by the larger lightning bolt) or proximally up to hundreds of base pairs away (Kadyrov, Dzantiev et al. 2006, Kadyrov, Holmes et al. 2007). Subsequently, MutS α interacts with and increases the processivity of EXO1. EXO1 excises the mismatch-containing DNA in a 5' to 3' direction, and RPA binding stabilizes single-stranded DNA (Genschel, Bazemore et al. 2002, Constantin, Dzantiev et al. 2005). A DNA polymerase, such as Pol δ for lagging strand replication, synthesizes across the gap using the parent DNA strand as a template, and DNA ligase seals the nicks in the newly synthesized strand of DNA (Longley, Pierce et al. 1997, Constantin, Dzantiev et al. 2005).

MutS α

Structure of MutS α

MutS α in humans is a heterodimer composed of two subunits: MutS homolog 2 (MSH2) and MutS homolog 6 (MSH6). The crystal structure of a truncated mutant of MutS α with 341 amino acid (aa) residues deleted from the N-terminus of MSH6 is shown in Figure 1.2A (Warren, Pohlhaus et al. 2007). MutS α has two ATPase sites, located at the C-terminus of each subunit (1.2A and 1.2B, red arrows pointed to the red ATP molecules) and a DNA-binding domain near the N-terminus (1.2A and 1.2C, orange arrows) (Warren, Pohlhaus et al. 2007). Yellow spheres seen in Figure 1.2A indicate magnesium ions that play an important role in ADP/ATP binding to the nucleotide binding sites (Kunkel and Erie 2005, Iyer, Pluciennik et al. 2006). In Figure 1.2C, the DNA is bent by MutS α , which is consistent with other MutS homolog crystal structures that also show a MutS-induced kink in the DNA (Lamers, Perrakis et al. 2000, Obmolova, Ban et al. 2000, Natrajan, Lamers et al. 2003). Once a mismatch has been located, the highly conserved mismatch-recognition motif (located in MSH6 of human MutS α), Phe-X-Glu, comes into play (Kunkel and Erie 2005, Hsieh and Yamane 2008, Erie and Weninger 2014). The mispaired base stacks with the aromatic ring of the phenylalanine, and the glutamate forms a hydrogen bond with the N3 of a mismatched thymine or the N7 of mismatched purines. Replacing either of these conserved regions within MutS α results in impaired mismatch discrimination and compromises MMR (Hsieh and Yamane 2008).

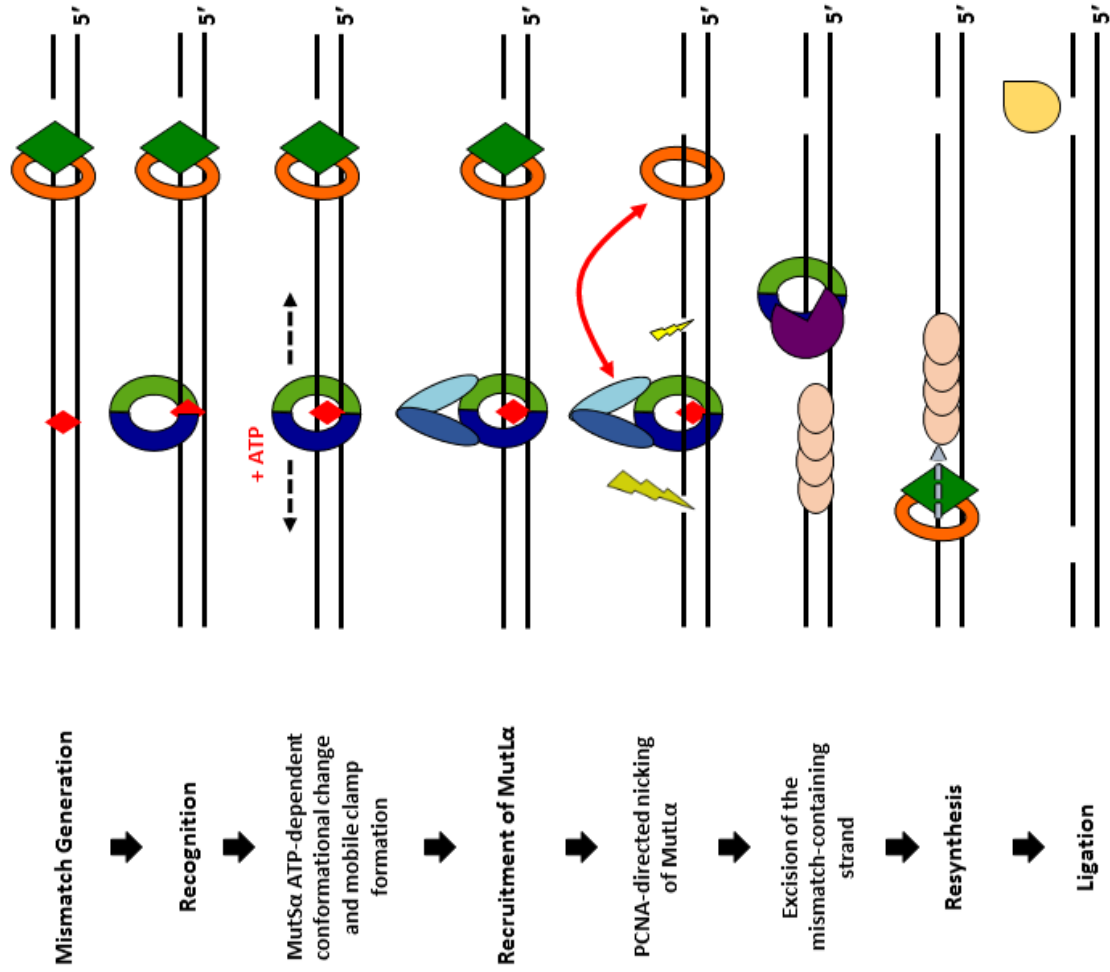
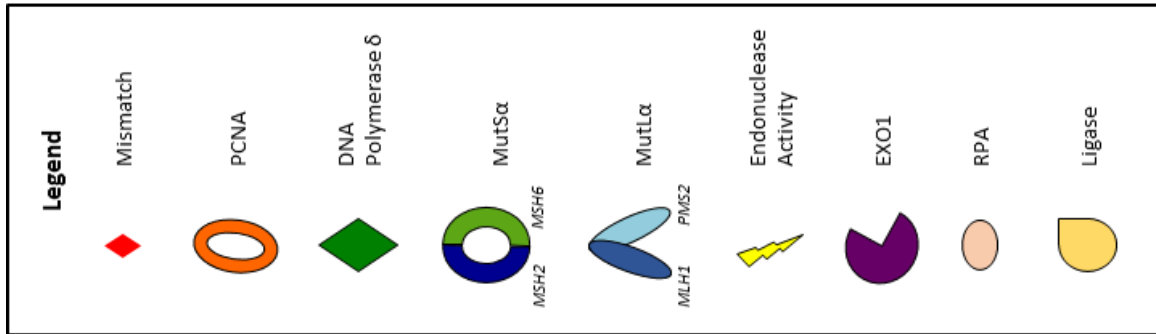


Figure 1.1 : DNA Mismatch Repair in Humans

Mismatch generation occurs when DNA polymerase, such as Pol δ , misincorporates the wrong base. The heterodimer MutS α initiates repair by recognizing and binding the mismatch. MutS α then undergoes an ATP-dependent conformational change(s) that allows MutS α to form a mobile clamp (black dashed arrows) and facilitates its recruitment of MutL α . PCNA activates (red double-headed arrow) the endonuclease activity of MutL α to nick the daughter strand. MutS α recruits EXO1 to excise the mismatch-containing strand. RPA stabilizes single-stranded DNA until a DNA polymerase resynthesizes across the gap (blue dashed arrow). DNA ligase seals the nicks.

Table 1.1 : Comparison of prokaryotic and eukaryotic MutS and MutL homologs

Prokaryotes		Eukaryotes	
	Function(s)		Function(s)
MutS	<ul style="list-style-type: none"> Recognizes base-base mismatches and IDLs 	MSH2-MSH6 (MutSα)	<ul style="list-style-type: none"> Recognizes base-base mismatches and 1-2 base IDL Initiates MMR
		MSH2-MSH3 (MutSβ)	<ul style="list-style-type: none"> Recognizes 2 or more base IDLs Initiates MMR
		MSH4-MSH5	<ul style="list-style-type: none"> Involved in meiosis
MutL	<ul style="list-style-type: none"> Interacts in an ATP-dependent manner with MutS once a mismatch has been identified Facilitates MMR by interacting with downstream proteins 	MLH1-PMS2 (MutLα) (Mlh1-Pms1 in <i>S. cerevisiae</i>)	<ul style="list-style-type: none"> Interacts in an ATP-dependent manner with MutS once a mismatch has been identified Directed by PCNA to nick the daughter strand
		MLH1-MLH3 (MutLγ)	<ul style="list-style-type: none"> Repair of some IDLs Functions in meiosis

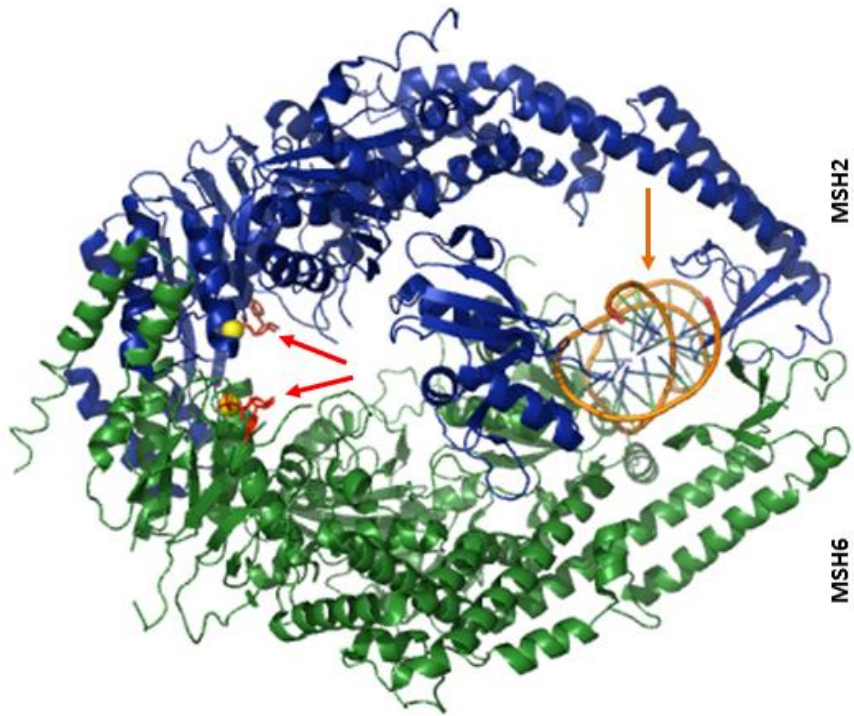
Properties and Functions of MutS α

Human MutS α and its homologs (MutS(α)) are highly conserved proteins in prokaryotes and eukaryotes. As shown in Table 1.1, one of the main roles of MutS homologs in all organisms is to serve as the mismatch-recognition signal (Kunkel and Erie 2005, Iyer, Pluciennik et al. 2006, Spampinato, Gomez et al. 2009, Erie and Weninger 2014). In humans, MutS α is primarily responsible for recognizing and repairing single base-base mismatches and one to two base insertions or deletions (Kunkel and Erie 2005, Iyer, Pluciennik et al. 2006, Erie and Weninger 2014). How MutS α is able to scan hundreds of thousands of base pairs in search of a single mismatch appears to be an enormous task. To accomplish this task, data suggests that MutS α binds non-specifically to the DNA and then bends it in search of a mismatch (Wang, Yang et al. 2003, Kunkel and Erie 2005, Erie and Weninger 2014). MutS α has a high affinity for binding to a mismatch; however, different mismatches, like GT and CC mismatches, are repaired with different efficiencies. One hypothesis for why MutS α repairs different mismatches with different efficiencies is that the efficiency of repair is governed by the stability of the MutS α -mismatch complex, which depends on both the type of mismatch and its sequence context (Kunkel and Erie 2015). Previous studies, however, indicate that binding of MutS to the mismatch alone is not sufficient to induce repair (Su, Lahue et al. 1988). Other studies with human MutS α shows that MutS α has varying affinities for different mismatches that are dependent on the presence or absence of ATP (Mazurek, Johnson et al. 2009). This and previous results suggests that the ATP-dependent conformational change of MutS α is required for mismatch repair (Gradia, Acharya et al. 1997).

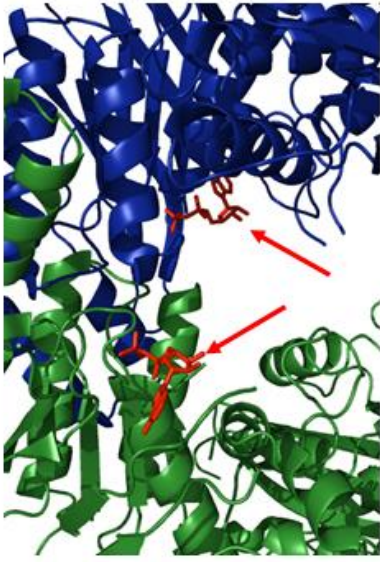
It is widely accepted that ATP and a mismatch are required for interactions of MutS α with MutL α (Iyer, Pluciennik et al. 2006, Hsieh and Yamane 2008, Kunkel and Erie 2015). An

important MutS α function is to recruit one or more MutL α to the mismatch site. It is unclear whether MutS α recruits MutL α before or after forming a mobile clamp. In *Saccharomyces cerevisiae* (*S. cerevisiae*), studies done with an ATPase mutant of MutS α that is incapable of forming a mobile clamp show that MutL α is able to interact with MutS α . This observation suggests that MutS α is able to undergo multiple ATP-induced conformational changes before forming a mobile clamp, and that one or more of these states is able to interact with MutL α (Hess, Gupta et al. 2002, Qiu, DeRocco et al. 2012). A recent study, however, with *Escherichia coli* (*E. coli*) proteins indicated that MutL appears to interact with MutS after it has formed a sliding clamp (Groothuizen, Winkler et al. 2015).

A



B



C

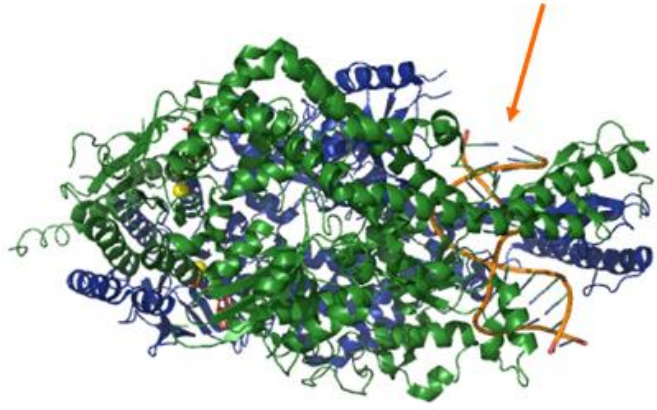


Figure 1.2 : Crystal Structure of Human MutS

(A) Front view of the human MutS α heterodimer in complex with DNA (orange arrow pointing at the orange helix) containing a single GT mismatch (PDB ID: 208B). The blue subunit is MSH2 and the green subunit is MSH6. Red stick models (indicated by red arrows) indicate ADP in the ATPase sites and yellow spheres indicate magnesium ions. (B) Zoom-in of the ATPase sites of the heterodimer of MutS α . Red arrows point to the red stick models that show ADP in the ATPase sites. (C) 90° rotation of the front-view of MutS α . An orange arrow points to DNA that is bent by MutS α .

DNA Bending by MutS α

As noted previously, the crystal structure in Figure 1.2C shows that human MutS α binds to a mismatch and bends the DNA at the GT mismatch at a $\sim 45^\circ$ angle (Warren, Pohlhaus et al. 2007). This result is similar to crystal structures of other MutS homologs, such as *Thermus aquaticus* (*Taq*) and *E. coli* MutS that were found to bend the DNA at the mismatch at a $\sim 60^\circ$ (Lamers, Perrakis et al. 2000, Obmolova, Ban et al. 2000, Natrajan, Lamers et al. 2003). AFM studies of *E. coli* and *Taq* MutS with homoduplex DNA and DNA containing a mismatch showed that MutS induces different bends in the DNA depending if MutS is located at the mismatch or at a homoduplex site (Wang, Yang et al. 2003, Erie and Weninger 2014). When MutS was bound to homoduplex DNA, the DNA was slightly bent; however, when MutS was incubated with DNA containing a single mismatch, two populations of DNA bend angles emerged. One population is associated with unbent DNA, the second is a bent population where MutS induced a bend angle of $\sim 60^\circ$. These data suggested that MutS scanned the DNA in a slightly bent state, and Wang et. al. proposed that upon recognition of the a mismatch, MutS kinks the DNA (Initial Recognition Complex, IRC) before forming a mobile clamp and unbending the DNA (Ultimate Recognition Complex, URC). Single molecule fluorescence studies of *Taq* MutS further suggested that MutS is conformationally dynamic when searching the DNA for a mismatch, but upon mismatch binding, the conformations become limited (Qiu, DeRocco et al. 2012). While prokaryotic MutS exists in different dynamic states that have different DNA bend angles associated with them, it is not known if human MutS α follows the same pattern.

ATPase activity of MutS α and the Formation of the Mobile Clamp

MutS(α) proteins are members of the ABC transporter ATPase superfamily, and the ATPase activity of the human MutS α subunits, MSH2 and MSH6, is essential for MMR in humans (Kunkel and Erie 2005, Iyer, Pluciennik et al. 2006, Hsieh and Yamane 2008). The heterodimer of MutS α has two composite nucleotide binding sites. These nucleotide binding sites are composed of six highly conserved motifs that include the Walker A and Walker B motifs from one protein subunit, and an ABC signature motif contributed by the other subunit. The loss of subunit dimerization results in the loss of ATPase activity because the ATP binding sites are “composite”, meaning that they are formed as a result of the interactions between the two subunits (Kunkel and Erie 2005, Hsieh and Yamane 2008, Spampinato, Gomez et al. 2009). Notably, the majority of the conserved residues across all homologs of MutS are within the ATPase domain (Spampinato, Gomez et al. 2009). Mutations in the conserved residues in the ATPase active sites of either MSH2 or MSH6 impair MMR activity (Schofield and Hsieh 2003).

Studies have shown that each composite ATPase site of MutS α has different affinities for nucleotide binding. Numerous biochemical studies show that MSH6 has a higher affinity for binding ATP whereas MSH2 has a higher affinity for ADP (Antony and Hingorani 2003, Bjornson and Modrich 2003, Martik, Baitinger et al. 2004, Antony, Khubchandani et al. 2006). Both subunits of MutS α can bind adenine nucleotides simultaneously, and each subunit can have different adenine nucleotides bound. Because the two subunits can bind different adenine nucleotides, this can lead to multiple liganded species of MutS α (Kunkel and Erie 2005, Iyer, Pluciennik et al. 2006). Additionally, studies have shown what appears to be an anti-cooperative effect, in that once MSH6 binds ATP, it decreases the affinity of MSH2 for ADP, allowing for MSH2 to more readily bind ATP (Mazur, Mendillo et al. 2006, Heinen, Cyr et al. 2011).

Both homoduplex and heteroduplex DNA (DNA containing a mismatch) stimulate the ADP–ATP exchange activity of MutS α , but only heteroduplex DNA appears to delay the turnover of ATP. Binding heteroduplex DNA increases the lifetime of MutS bound with ATP and suggests that in the presence of heteroduplex DNA, the rate-limiting step for turnover of ATP occurs at or prior to hydrolysis of ATP (Kunkel and Erie 2005, Iyer, Pluciennik et al. 2006). MutS α exhibits different ATPase activity in the presence of homoduplex or heteroduplex DNA, suggesting that the recognition of a mismatch leads to a longer lived ATP-bound state of MutS α (Kunkel and Erie 2005, Iyer, Pluciennik et al. 2006).

Multiple studies agree that upon binding ATP, mismatch-bound MutS α can form a mobile clamp that is able to move along the DNA (Blackwell, Martik et al. 1998, Gradia, Subramanian et al. 1999, Blackwell, Bjornson et al. 2001, Acharya, Foster et al. 2003, Jeong, Cho et al. 2011, Qiu, DeRocco et al. 2012). It is important to note, however, that not all MutS(α) proteins that recognize and bind to a mismatch go on to form a mobile clamp state (Qiu, DeRocco et al. 2012). In a fluorescence study with *Taq* MutS, results indicate that ADP-bound MutS can bind to the mismatch and then dissociate without ever transitioning into forming a mobile clamp state (Qiu, DeRocco et al. 2012). Additionally, the states of MutS(α) complexes depend on the conformations of the MutS(α)-DNA complexes as well as the ligation state of the MutS(α) ATPase sites (Tessmer, Yang et al. 2008, Qiu, DeRocco et al. 2012). There is some debate in the field about what liganded state of MutS α ATPase sites leads to the formation of a mobile clamp. Studies utilizing smFRET with *Taq* MutS revealed that MutS can bind the mismatch in a ADP:ADP or ADP:ATP liganded state. If MutS binds the mismatch in a ADP:ADP state, then MutS will dissociate from the DNA, however if MutS is bound to the mismatch in an ADP:ATP liganded state, then MutS is able to form a mobile clamp, which may

further result in a doubly liganded ATP state of MutS (Qiu, DeRocco et al. 2012). However, these results contrast with another study that suggested that the ADP:ATP liganded state may be a “dead-end” state (Heinen, Cyr et al. 2011). This study suggested that human MutS α activity was controlled by MSH2 with Mg⁺² and ADP, and found that destabilization of Mg⁺² resulted in the loss of ADP with MSH6 rapidly binding ATP. MSH6-ATP promotes binding of ATP to MSH2, and the doubly liganded ATP state of MutS α is thought to form the mobile clamp (Heinen, Cyr et al. 2011).

While it appears that ATP hydrolysis is not needed for MutS α to form a mobile clamp, there is much debate on whether ATP hydrolysis is required for the movement of these MutS α mobile clamps along the DNA (Iyer, Pluciennik et al. 2006, Erie and Weninger 2014). Studies that examined the rate of dissociation of MutS from short DNA substrates with blocked or unblocked ends upon the addition of ATP or ATP γ S found that MutS is able to form a mobile clamp in the absence of ATP hydrolysis (Acharya, Wilson et al. 1996, Gradia, Acharya et al. 1997, Schofield, Nayak et al. 2001). Because these studies used shorter DNA substrates, it is unclear if ATP hydrolysis is required for MutS mobile clamps to travel long distances on the DNA (Erie and Weninger 2014). Other studies found that MutS α failed to form long-lived mobile clamps in the presence of slowly hydrolyzing, ATP γ S or non-hydrolyzable ATP analogs, AMPPNP (Blackwell, Martik et al. 1998). These studies were further supported with other results that found that using a mutant of MutS α that was able to bind ATP, but not able to hydrolyze it also could not form a long lived mobile clamp (Iaccarino, Marra et al. 2000).

There is much debate on how the mobile clamp of MutS α is formed and if the movement of the clamp along the DNA is dependent on ATP hydrolysis, but it is also unclear what the function of the mobile clamp is. It is not clear if MutS α interacts with MutL α before or after

forming a mobile clamp as multiple studies indicate that ATP induces more than one conformational change in MutS homologs (Hess, Gupta et al. 2002, Qiu, DeRocco et al. 2012, Groothuizen, Winkler et al. 2015). It is also unknown if ATP hydrolysis is important for the formation of the MutS α –MutL α complexes (Iyer, Pluciennik et al. 2006). In spite of these questions, it is generally accepted that MutS α and MutL α interactions play a key role in MMR signaling (Kunkel and Erie 2005, Iyer, Pluciennik et al. 2006, Hsieh and Yamane 2008, Spampinato, Gomez et al. 2009).

MutL α

Structure of MutL α

MutL α is a highly conserved protein that is a heterodimer composed of MutL homolog 1 (MLH1) and post meiotic segregation increased 2 (PMS2) in humans (see Table 1.1 for MutL homologs) (Kunkel and Erie 2005, Iyer, Pluciennik et al. 2006, Hsieh and Yamane 2008, Spampinato, Gomez et al. 2009). Figure 1.3A shows a cartoon depiction of human MutL α . Both prokaryotic and eukaryotic MutL α dimerize at the C-terminal domains, and PMS2 (Pms1 in *S. cerevisiae*) contains the endonuclease site (Figure 1.3A). The N-terminal domains of both MLH1 and PMS2 contain ATPase and DNA binding activities. Long flexible linker arms link the N- and C- terminal domains together (Gueneau, Dherin et al. 2013). Figure 1.3B shows the endonuclease site in the C-terminus of Pms1 in yeast (yellow). This figure shows that a portion of Mlh1 contributes to the endonuclease site (green). AFM studies of both human and yeast MutL α in the presence of ATP shows large changes in the structure of MutL α . These studies found that MutL α could form condensed structures in which the flexible linker arms bring the N-

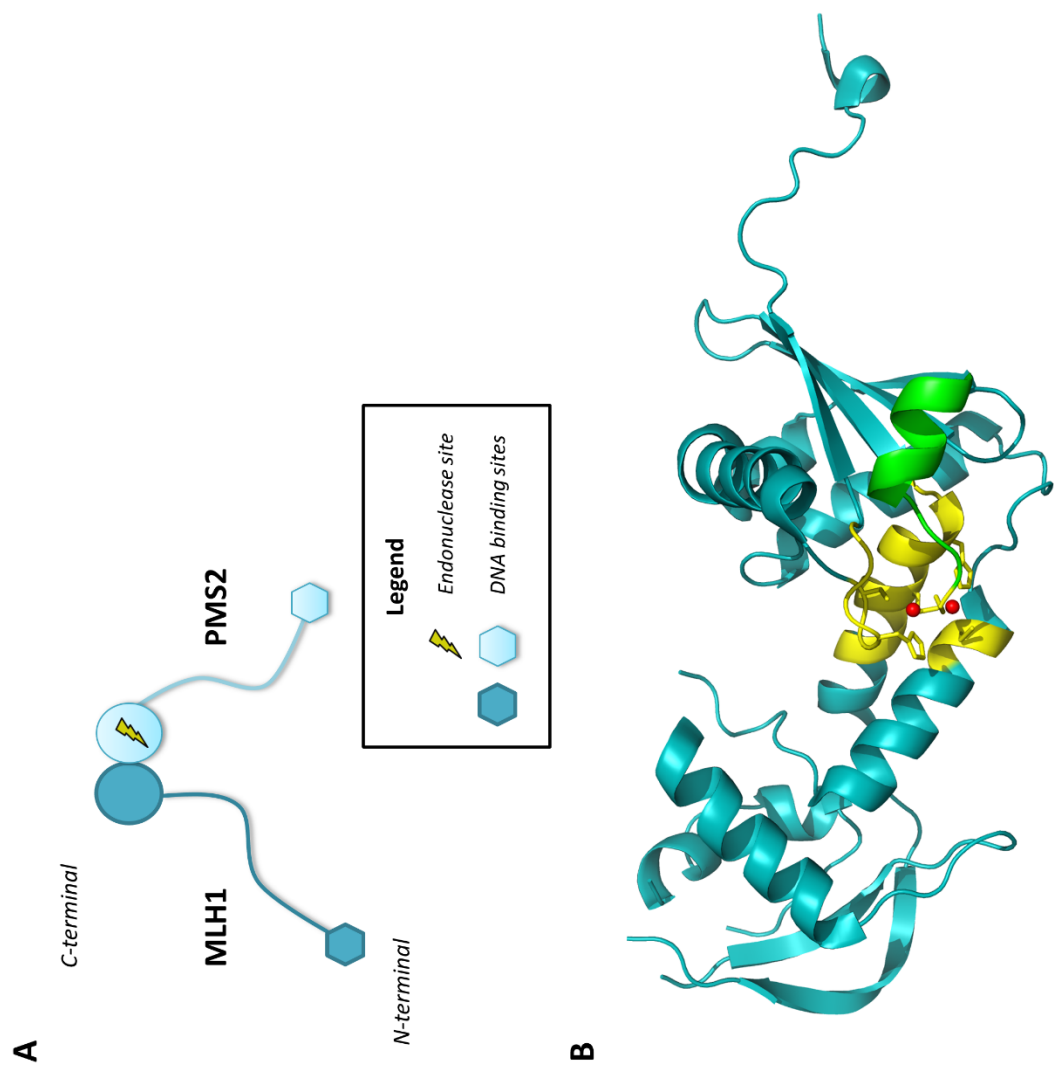


Figure 1.3 : Structure of MutL α

(A) Cartoon structure of the human MutL α heterodimer. MutL α is composed of two subunits that dimerize at the C-termini. The endonuclease activity of MutL α is located in the C-terminal domain of PMS2 (Pms1 in *S. cerevisiae*). DNA-binding domains and ATPase sites are located at the N-terminus for both subunits. Long linker arms connect the N- and C- terminal domains of each subunit, and are predicted to be unstructured. (B) C-terminal domain of *S. cerevisiae* Pms1 (PDB ID: 4E4W). The C-terminal domain of Pms1 is colored in teal, the endonuclease domain is colored in yellow, and in green is the part of Mlh1 that contributes to endonuclease activity. Red spheres indicate magnesium ions.

and C- termini together, or semi-condensed structures where either the N-terminus of PMS2 or MLH1 is brought close to the C-terminus of that subunit (Sacho, Kadyrov et al. 2008).

Properties of MutL α

MutL homologs are members of the GHL ATPase family, which includes DNA Gyrase and Hsp90 (Hsieh and Yamane 2008, Erie and Weninger 2014). ATP binding and ATP hydrolysis induces significant conformational changes in GHL proteins, which are thought to be important for the signaling function of these proteins (Geng, Sakato et al. 2012, Erie and Weninger 2014). Like MutS homologs, MutL homologs have two asymmetric nucleotide binding sites that affect the interactions and functions of MutL homologs (Hsieh and Yamane 2008). However, in contrast to MutS homologs, MutL proteins have weak ATPase activity (Hall, Shcherbakova et al. 2002). The weak ATPase activity is indicated by a low turnover of ATP, which suggests that ATP binding rather than hydrolysis facilitates MutL α interactions with other proteins by inducing conformational changes (Kunkel and Erie 2005). AFM studies of MutL α found that adenine nucleotides induce large asymmetrical conformational changes. These conformational changes are thought to mediate the interactions of MutL α with other proteins in the MMR pathway (Sacho, Kadyrov et al. 2008).

While MutL and MutL α exhibit weak DNA binding in physiological salt conditions, they do have differing DNA binding preferences. Prokaryotic MutL preferentially binds single-stranded DNA; in contrast, MutL α preferentially binds double-stranded DNA (Ban and Yang 1998, Hall, Shcherbakova et al. 2003). Furthermore, AFM studies that investigated the DNA-binding properties of MutL α under low salt conditions revealed that MutL α is able to bind cooperatively to form long tracts of protein along duplex DNA. These data also showed that

MutL α is able to interact with two different strands of duplex DNA simultaneously (Hall, Wang et al. 2001).

MutL α Endonuclease Activity

The endonuclease activity in the C-terminal domain of *S. cerevisiae* Pms1 (PMS2 in humans) shown in Figure 1.3B is essential for repair (Deschenes, Tomer et al. 2007, Erdeniz, Nguyen et al. 2007, Kadyrov, Holmes et al. 2007, van Oers, Roa et al. 2010). *In vitro* studies have shown that the endonuclease activity of MutL α is dependent on a mismatch, ATP, MutS α , and PCNA (Kadyrov, Dzantiev et al. 2006). Studies in *S. cerevisiae* with Pms1^{E707K}, a mutant of MutL α that has impaired endonuclease activity, resulted in a strong mutator phenotype (Kadyrov, Holmes et al. 2007). Other studies using endonuclease-deficient PMS2^{E702K} knock-in mice had increased genetic mutation rates and cancer predisposition (van Oers, Roa et al. 2010).

The location of the nick that results from the endonuclease activity of MutL α remains a perplexing question in the field. *In vitro* studies of MutL α show that it will strand-specifically nick the DNA in the vicinity of the mismatch on either the 5' or 3' side of the mismatch, though preferentially distally to the mismatch (Kadyrov, Dzantiev et al. 2006, Hsieh and Yamane 2008, Pluciennik, Dzantiev et al. 2010, Pluciennik, Burdett et al. 2013). These and other studies, however, also found that MutL α is capable of nicking the daughter strand up to hundreds of base pairs away from the mismatch (Kadyrov, Dzantiev et al. 2006, Kadyrov, Holmes et al. 2007). This question becomes further complicated when taking into account that PCNA must be able to activate the endonuclease activity of MutL α to strand-specifically nick the DNA when MutL α is in complex with MutS α . All of these actions must be tightly and temporally coordinated *in vivo* before histone reloading renders the mismatch inaccessible for MMR (Kunkel and Erie 2015).

The Strand Discrimination Signal

Once MutS α has recruited MutL α to the mismatch site, PCNA activates MutL α to nick the DNA in a strand-specific manner. To nick the correct strand of DNA, there must be a strand discrimination signal, which in eukaryotes is hypothesized to be PCNA, because PCNA is loaded onto the DNA asymmetrically at the replication fork or at a nick by RFC (Kadyrov, Dzantiev et al. 2006, Hsieh and Yamane 2008, Pluciennik, Dzantiev et al. 2010). Previous studies utilizing a covalently closed DNA plasmid containing a single-stranded bubble that allowed RFC to load PCNA onto DNA without strand specific orientation found that repair of a mismatch in these bubble substrates is no longer strand specific because PCNA loads randomly on either strand (Pluciennik, Burdett et al. 2009, Pluciennik, Dzantiev et al. 2010). These studies suggest that the initial orientation that PCNA is loaded onto the DNA (either at the replication fork or a nicked site) is what allows PCNA to correctly discern the daughter strand for MutL α to nick. To determine if the location of a preexisting nick affected MutL α activity, studies were done in both a reconstituted system and extracts used plasmid DNA containing a nick. These studies found that if the nick is 3' to the mismatch, MutL α is required for repair, but MutL α is not required if the nick is 5' to the mismatch (Kadyrov, Dzantiev et al. 2006, Kadyrov, Holmes et al. 2007).

MutS α and MutL α Complexes

Role of MutS α -MutL α Complexes

Fluorescence experiments, DNaseI footprinting, and other experiments have been conducted with MutS α and MutL α , and they provide some understanding as to how these proteins interact. DNaseI footprinting studies found that with MutS, approximately one turn of the DNA helix to either side of the mismatch was protected. In contrast, the MutS-MutL interactions in the

presence of ATP resulted in a very large DNaseI footprint, which indicates the presence of multiple proteins bound to the DNA (Selmane, Schofield et al. 2003). However, the assembly of MutS-MutL complexes for either prokaryotic or eukaryotic MMR proteins requires heteroduplex DNA substrates that are longer than 60 bp *in vitro* (Blackwell, Wang et al. 2001, Schofield, Nayak et al. 2001). It is unclear if longer DNA lengths is required for the assembly of MutS α -MutL α complexes, and further characterization of these complexes are needed.

Despite our current knowledge on how MMR is initiated by MutS α -MutL α complexes, there are many questions that remain to be addressed. MutS α forms a mobile sliding clamp upon binding ATP and a mismatch, but it is not known if this state or an alternate ATP-dependent state of MutS α interacts with MutL α . Additionally, we do not know what the MutS α conformational states are once it binds to the mismatch and undergoes the ATP-dependent changes, and if ATP hydrolysis has an impact on the interactions between MutS α and MutL α . Furthermore, there is little known about how MutS α and MutL α interact, whether there are multiple proteins that interact, or if there is a typical stoichiometric ratio of the two proteins. Finally, it remains unclear how MutL α in complex with MutS α interact with PCNA to potentially nick the daughter strand either near the mismatch or up to hundreds to base pairs away from the mismatch.

Several disparate models exist to address these questions. One model posits that MutL α joins MutS α to form MutS α -MutL α mobile clamps that diffuse along the DNA to interact PCNA (Figure 1.4A). This model was originally suggested based on the observation that MutS α can form mobile clamps in conjunction with fluorescence data that noted movement of MutS α -MutL α complexes (Gradia, Subramanian et al. 1999, Gorman, Wang et al. 2012). However, this model does not provide an explanation for how these clamps would result in preferential nicking near the mismatch. Another model proposes that MutL α traps MutS α mobile clamps near the

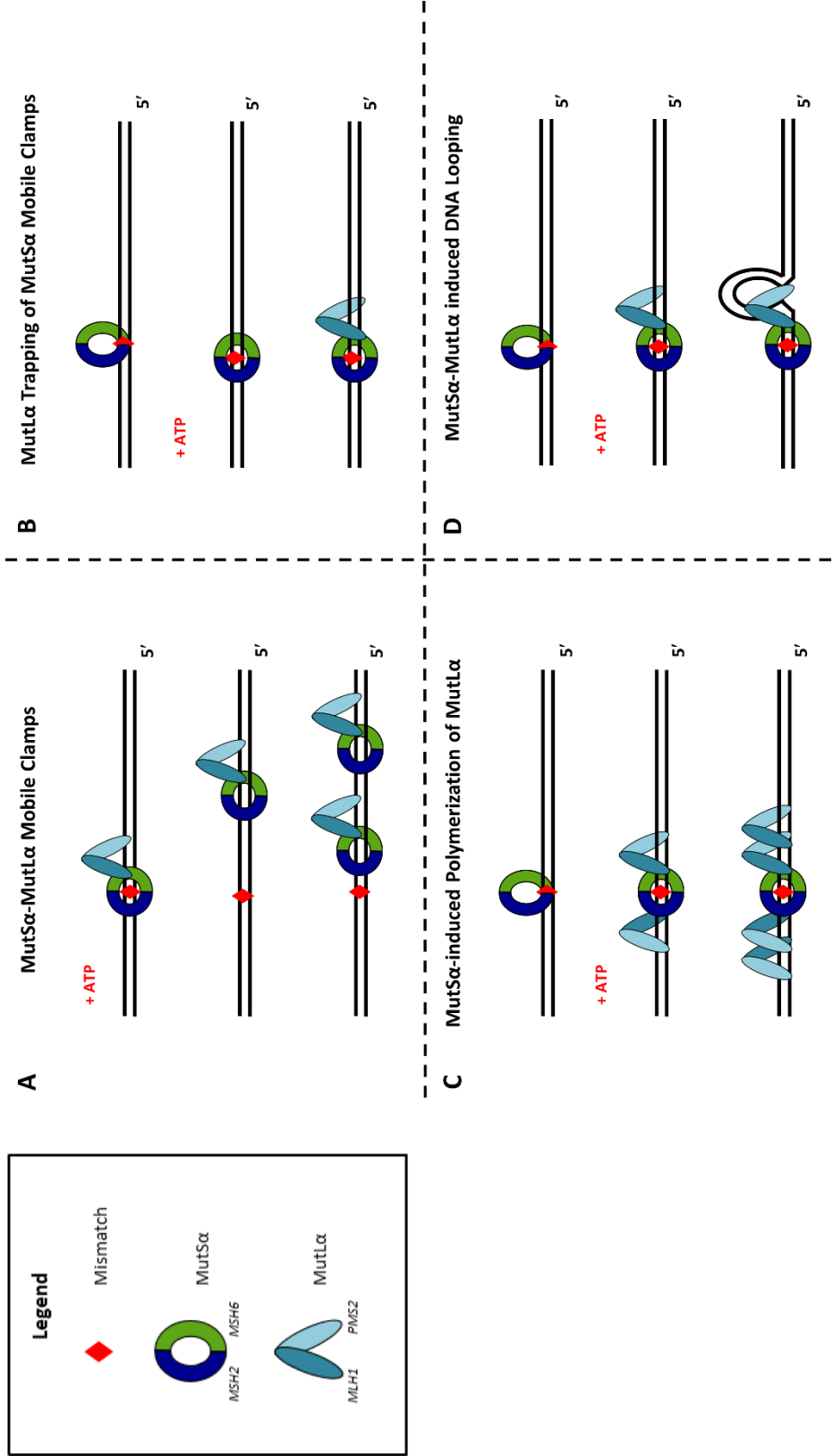


Figure 1.4 : Models of MutS α –MutL α Interactions

(A) MutL α joins MutS α at the mismatch and forms a larger mobile clamp. This clamp moves away from the mismatch to allow for a second MutS α to load onto the mismatch to form multiple MutS α –MutL α mobile clamps. (B) MutS α at the mismatch forms a mobile clamp that slides away from the mismatch. MutL α interacts with the mobile clamp of MutS α , traps MutS α , and prevents further movement. (C) MutS α recruits multiple MutL α to the mismatch site, forming long MutL α polymers along the DNA. (D) MutL α interacts with MutS α either at the mismatch as in (D) or away from the mismatch as in (B) to facilitate DNA looping.

mismatch (Figure 1.4B). This complex could then facilitate DNA looping (Figure 1.4D) to interact with downstream proteins in MMR (Kunkel and Erie 2005, Iyer, Pluciennik et al. 2006). A third model suggests that MutS α induces polymerization of MutL α along the DNA (Figure 1.4C). This model (originally proposed by Paul Modrich (Modrich 1987)) is supported by *in vivo* fluorescence studies in *S. cerevisiae* and *E. coli* suggesting that MMR foci contain more MutL α than MutS α proteins (Hombauer, Campbell et al. 2011, Elez, Radman et al. 2012). Each of these models predicts distinct MutS α -MutL α complexes, though the models may not be mutually exclusive. With structural information on the MutS α -MutL α complexes, we can gain further insight into the mechanism of MMR initiation.

Atomic Force Microscopy

Atomic force microscopy (AFM) is a high resolution, single-molecule technique that can be used to gain structural insight into biomolecular processes. Gerd Binnig developed the first AFM in 1986 from scanning tunneling microscopy (Binnig, Quate et al. 1986). The advantages of using AFM are: 1) AFM results in a three-dimensional (3D) image; 2) AFM can visualize non-conductive materials such as DNA and proteins; 3) and AFM can be conducted in air and in solution (Hansma, Laney et al. 1995).

A flow chart detailing how a general AFM experiment is conducted is shown in Figure 1.5A. Samples with protein and DNA complexes or protein alone are incubated at room temperature before glutaraldehyde is added. Glutaraldehyde is a crosslinking agent that crosslinks primary amine groups, which stabilizes protein–DNA interactions. The sample is then filtered through a size exclusion column to separate free protein from protein–DNA complexes and fractions are collected. Fractions are then deposited onto freshly cleaved mica, rinsed with water, and dried under a gentle stream of nitrogen gas before imaging.

For the purposes of this thesis, the method of tapping mode AFM will be discussed. AFM images are produced by scanning a cantilever across a sample surface, while reflecting a laser beam off the back of the cantilever (Figure 1.5B). As the cantilever progresses across the sample, small changes in sample height (z-direction) are detected as a function of changes in the position of the laser reflection in the photodiode detector. A feedback loop signals the repositioning of the piezo stage such that the position of the reflected laser beam in the detector is maintained at the same point (Figure 1.5C). Adjustments in piezo height (z) are plotted as a function of XY position on the mica surface (Last, Russell et al. 2010).

A sample AFM image is shown in Figure 1.5D. In this image the proteins appear as white spots and the DNA molecules appear as the light brown lines. These images can be analyzed to gain information such as the volumes of the protein complexes (white shapes), which can be used to estimate the number of proteins in a complex. The image can also be used to calculate the position of the proteins bound to DNA to determine if the protein bound a mismatch site. AFM images can also be used to observe different conformations of the protein complexes and the DNA, and for the examination of rare events. Because there is a linear relationship between volume of the protein complex in AFM images and its molecular weight, we can estimate the number of proteins in a complex (Ratcliff and Erie 2001, Wang, Yang et al. 2003, Yang, Wang et al. 2003). Utilizing this relationship allows us to estimate how many proteins are interacting with each other or with a single DNA molecule (stoichiometry). The visualization of the proteins bound to the DNA allows us to easily trace the DNA and pinpoint the exact location of a protein complex to see if it is bound at a mismatch site or homoduplex sites (Wang, Yang et al. 2003). The images also allow us to view the shapes of the complexes to observe how they change under different conditions as well as measure DNA bending properties to observe changes in

DNA bend angle as a function of different experimental conditions (Wang, Yang et al. 2003, Sacho, Kadyrov et al. 2008, Jiang and Marszalek 2011). Lastly, AFM is a single-molecule technique, so we can examine rare events that would otherwise be missed in bulk studies. These rare events could potentially be vital in the mechanism of the proteins being examined.

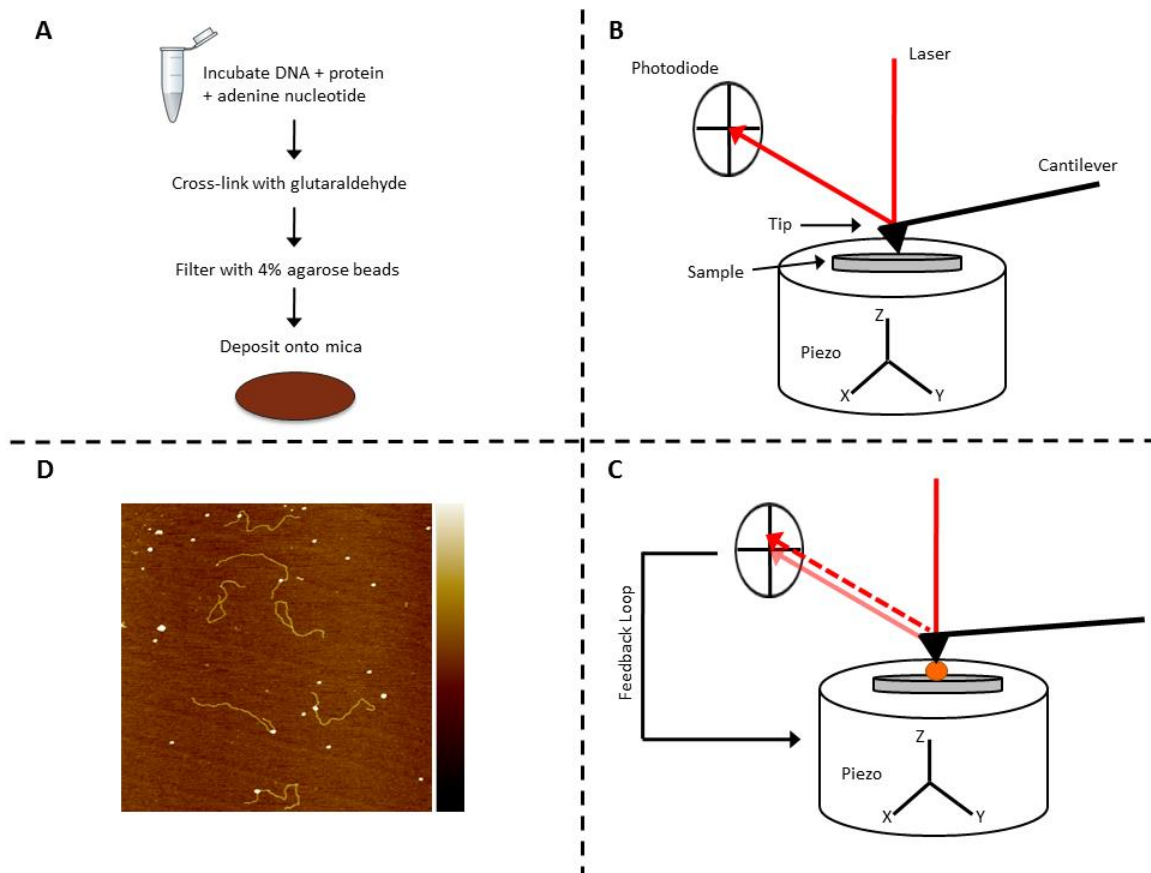


Figure 1.5 : AFM Experimental Methods

(A) Schematic overview of sample preparation. Samples are incubated before being crosslinked. Crosslinked samples are filtered through a size-exclusion column, and fractions are collected. Fractions are then deposited onto mica to be imaged. (B) The mica sample is placed onto the piezo and an oscillating tip attached to the cantilever moves across the surface in an x-y manner. A laser reflects off of the back of the tip into a photodiode. (C) The tip encounters a molecule (orange circle), and this changes the position of the reflection of the laser into the photodiode (dashed line). A feedback loop results a change in the z-movement of the piezo, and these changes are recorded to create a three-dimensional image. (D) Sample AFM image of proteins and protein-DNA complexes. This image is 2 x 2 μm at a resolution of 512 x 512 pixels. Scale bar indicates height from 0 – 2 nm (brown being low, white being high). Proteins are circular blobs and DNA molecules are light brown lines.

Thesis Statement

This project is an investigation into the initial signaling mechanism of MMR. I used AFM to investigate and gain structural insight into how MutS α and MutL α interact and form complexes on DNA containing a single Guanine-Thymine (GT-DNA) mismatch or on perfectly paired DNA (GC-DNA). I used a variety of adenine nucleotides, such as ADP, ATP, and ATP γ S as well as different incubation times to see how complexes change in various conditions. A collaboration with Peggy Hsieh's laboratory at NIDDK (NIH, Bethesda) provided me with the DNA substrate as well as with purified human MutS α and MutL α proteins. Additionally, other collaborations done with Paul Modrich's laboratory at Duke University gave us purified human MutS α . In this work, I characterized the binding positions, conformational and stoichiometric, properties of MutS α complexes on GT- and GC- linear and circular DNA in the presence of ADP, ATP, and ATP γ S. I also examined the binding positions, stoichiometries, and conformational properties of MutS α -MutL α on GT-DNA. Additionally, I examined how MutS α -induced DNA bend angles change as a function of adenine nucleotide conditions. Furthermore, I used my expertise in AFM in a collaboration with Saskia Neher's laboratory at University of North Carolina at Chapel Hill to examine the stoichiometric properties of ANGPTL4 and LPL.

In this body of work, AFM was the primary technique used to study protein-DNA interactions, protein conformational changes, and differences in protein stoichiometries. In Chapters 2 and 3, we examine the initial signaling mechanism of MMR by using AFM to determine the stoichiometries and conformation of MutS α -DNA and MutS α -MutL α -DNA complexes. AFM can differentiate between each proposed MutS α -MutL α interaction model by allowing the direct visualization of these complexes bound to DNA. The resulting images can be

used to measure the position of MutS α and MutS α –MutL α complexes on the DNA relative to a mismatch, the volumes of complexes to estimate stoichiometries of proteins within these complexes, as well as changes in the conformation of complexes in different adenine nucleotide conditions (Chapter 2 and 3). AFM was used to measure DNA bend angles in different adenine nucleotide conditions to see how MutS α induced DNA bend angles differed depending on the adenine nucleotide (Chapter 4). Chapter 5 discusses how AFM was used in several other collaborations to gain stoichiometric information on ANGPTL4 and LPL, as well as the AFM studies I conducted to investigate protein stoichiometries for other collaborations.

REFERENCES

- Acharya, S., P. L. Foster, P. Brooks and R. Fishel (2003). "The coordinated functions of the E. coli MutS and MutL proteins in mismatch repair." Mol Cell **12**(1): 233-246.
- Acharya, S., T. Wilson, S. Gradia, M. F. Kane, S. Guerrette, G. T. Marsischky, R. Kolodner and R. Fishel (1996). "hMSH2 forms specific mispair-binding complexes with hMSH3 and hMSH6." Proc Natl Acad Sci U S A **93**(24): 13629-13634.
- Antony, E. and M. M. Hingorani (2003). "Mismatch recognition-coupled stabilization of Msh2-Msh6 in an ATP-bound state at the initiation of DNA repair." Biochemistry **42**(25): 7682-7693.
- Antony, E., S. Khubchandani, S. Chen and M. M. Hingorani (2006). "Contribution of Msh2 and Msh6 subunits to the asymmetric ATPase and DNA mismatch binding activities of *Saccharomyces cerevisiae* Msh2-Msh6 mismatch repair protein." DNA Repair (Amst) **5**(2): 153-162.
- Ban, C. and W. Yang (1998). "Crystal structure and ATPase activity of MutL: implications for DNA repair and mutagenesis." Cell **95**(4): 541-552.
- Binnig, G., C. F. Quate and C. Gerber (1986). "Atomic force microscope." Phys Rev Lett **56**(9): 930-933.
- Bjornson, K. P. and P. Modrich (2003). "Differential and simultaneous adenosine di- and triphosphate binding by MutS." J Biol Chem **278**(20): 18557-18562.
- Blackwell, L. J., K. P. Bjornson, D. J. Allen and P. Modrich (2001). "Distinct MutS DNA-binding modes that are differentially modulated by ATP binding and hydrolysis." J Biol Chem **276**(36): 34339-34347.
- Blackwell, L. J., D. Martik, K. P. Bjornson, E. S. Bjornson and P. Modrich (1998). "Nucleotide-promoted release of hMutSalph α from heteroduplex DNA is consistent with an ATP-dependent translocation mechanism." J Biol Chem **273**(48): 32055-32062.
- Blackwell, L. J., S. Wang and P. Modrich (2001). "DNA chain length dependence of formation and dynamics of hMutSalph α .hMutLalph α .heteroduplex complexes." J Biol Chem **276**(35): 33233-33240.
- Constantin, N., L. Dzantiev, F. A. Kadyrov and P. Modrich (2005). "Human mismatch repair: reconstitution of a nick-directed bidirectional reaction." J Biol Chem **280**(48): 39752-39761.
- Deschenes, S. M., G. Tomer, M. Nguyen, N. Erdeniz, N. C. Juba, N. Sepulveda, J. E. Pisani and R. M. Liskay (2007). "The E705K mutation in hPMS2 exerts recessive, not dominant, effects on mismatch repair." Cancer Lett **249**(2): 148-156.

- Elez, M., M. Radman and I. Matic (2012). "Stoichiometry of MutS and MutL at unrepaired mismatches in vivo suggests a mechanism of repair." Nucleic Acids Res **40**(9): 3929-3938.
- Erdeniz, N., M. Nguyen, S. M. Deschenes and R. M. Liskay (2007). "Mutations affecting a putative MutLalpha endonuclease motif impact multiple mismatch repair functions." DNA Repair (Amst) **6**(10): 1463-1470.
- Erie, D. A. and K. R. Weninger (2014). "Single molecule studies of DNA mismatch repair." DNA Repair (Amst) **20**: 71-81.
- Geng, H., M. Sakato, V. DeRocco, K. Yamane, C. Du, D. A. Erie, M. Hingorani and P. Hsieh (2012). "Biochemical analysis of the human mismatch repair proteins hMutSalpha MSH2(G674A)-MSH6 and MSH2-MSH6(T1219D)." J Biol Chem **287**(13): 9777-9791.
- Genschel, J., L. R. Bazemore and P. Modrich (2002). "Human exonuclease I is required for 5' and 3' mismatch repair." J Biol Chem **277**(15): 13302-13311.
- Gorman, J., F. Wang, S. Redding, A. J. Plys, T. Fazio, S. Wind, E. E. Alani and E. C. Greene (2012). "Single-molecule imaging reveals target-search mechanisms during DNA mismatch repair." Proc Natl Acad Sci U S A **109**(45): E3074-3083.
- Gradia, S., S. Acharya and R. Fishel (1997). "The human mismatch recognition complex hMSH2-hMSH6 functions as a novel molecular switch." Cell **91**(7): 995-1005.
- Gradia, S., D. Subramanian, T. Wilson, S. Acharya, A. Makhov, J. Griffith and R. Fishel (1999). "hMSH2-hMSH6 forms a hydrolysis-independent sliding clamp on mismatched DNA." Mol Cell **3**(2): 255-261.
- Groothuizen, F. S., I. Winkler, M. Cristovao, A. Fish, H. H. Winterwerp, A. Reumer, A. D. Marx, N. Hermans, R. A. Nicholls, G. N. Murshudov, J. H. Lebbink, P. Friedhoff and T. K. Sixma (2015). "MutS/MutL crystal structure reveals that the MutS sliding clamp loads MutL onto DNA." Elife **4**.
- Gueneau, E., C. Dherin, P. Legrand, C. Tellier-Lebegue, B. Gilquin, P. Bonnesoeur, F. Londino, C. Quemener, M. H. Le Du, J. A. Marquez, M. Moutiez, M. Gondry, S. Boiteux and J. B. Charbonnier (2013). "Structure of the MutLalpha C-terminal domain reveals how Mlh1 contributes to Pms1 endonuclease site." Nat Struct Mol Biol **20**(4): 461-468.
- Hall, M. C., P. V. Shcherbakova, J. M. Fortune, C. H. Borchers, J. M. Dial, K. B. Tomer and T. A. Kunkel (2003). "DNA binding by yeast Mlh1 and Pms1: implications for DNA mismatch repair." Nucleic Acids Res **31**(8): 2025-2034.
- Hall, M. C., P. V. Shcherbakova and T. A. Kunkel (2002). "Differential ATP binding and intrinsic ATP hydrolysis by amino-terminal domains of the yeast Mlh1 and Pms1 proteins." J Biol Chem **277**(5): 3673-3679.

- Hall, M. C., H. Wang, D. A. Erie and T. A. Kunkel (2001). "High affinity cooperative DNA binding by the yeast Mlh1-Pms1 heterodimer." J Mol Biol **312**(4): 637-647.
- Hansma, H. G., D. E. Laney, M. Bezanilla, R. L. Sinsheimer and P. K. Hansma (1995). "Applications for atomic force microscopy of DNA." Biophys J **68**(5): 1672-1677.
- Heinen, C. D., J. L. Cyr, C. Cook, N. Punja, M. Sakato, R. A. Forties, J. M. Lopez, M. M. Hingorani and R. Fishel (2011). "Human MSH2 (hMSH2) protein controls ATP processing by hMSH2-hMSH6." J Biol Chem **286**(46): 40287-40295.
- Hess, M. T., R. D. Gupta and R. D. Kolodner (2002). "Dominant *Saccharomyces cerevisiae* msh6 mutations cause increased mispair binding and decreased dissociation from mispairs by Msh2-Msh6 in the presence of ATP." J Biol Chem **277**(28): 25545-25553.
- Hombauer, H., C. S. Campbell, C. E. Smith, A. Desai and R. D. Kolodner (2011). "Visualization of eukaryotic DNA mismatch repair reveals distinct recognition and repair intermediates." Cell **147**(5): 1040-1053.
- Hsieh, P. and K. Yamane (2008). "DNA mismatch repair: molecular mechanism, cancer, and ageing." Mech Ageing Dev **129**(7-8): 391-407.
- Iaccarino, I., G. Marra, P. Dufner and J. Jiricny (2000). "Mutation in the magnesium binding site of hMSH6 disables the hMutS α sliding clamp from translocating along DNA." J Biol Chem **275**(3): 2080-2086.
- Iyer, R. R., A. Pluciennik, V. Burdett and P. L. Modrich (2006). "DNA mismatch repair: functions and mechanisms." Chemical reviews **106**(2): 302-323.
- Jeong, C., W. K. Cho, K. M. Song, C. Cook, T. Y. Yoon, C. Ban, R. Fishel and J. B. Lee (2011). "MutS switches between two fundamentally distinct clamps during mismatch repair." Nat Struct Mol Biol **18**(3): 379-385.
- Jiang, Y. and P. E. Marszalek (2011). "Atomic force microscopy captures MutS tetramers initiating DNA mismatch repair." EMBO J **30**(14): 2881-2893.
- Kadyrov, F. A., L. Dzantiev, N. Constantin and P. Modrich (2006). "Endonucleolytic function of MutL α in human mismatch repair." Cell **126**(2): 297-308.
- Kadyrov, F. A., S. F. Holmes, M. E. Arana, O. A. Lukianova, M. O'Donnell, T. A. Kunkel and P. Modrich (2007). "*Saccharomyces cerevisiae* MutL α is a mismatch repair endonuclease." J Biol Chem **282**(51): 37181-37190.
- Kaur, G., A. Masoud, N. Raihan, M. Radzi, W. Khamizar and L. S. Kam (2011). "Mismatch repair genes expression defects & association with clinicopathological characteristics in colorectal carcinoma." The Indian journal of medical research **134**(2): 186-192.
- Kunkel, T. A. and D. A. Erie (2005). "DNA mismatch repair." Annu Rev Biochem **74**: 681-710.

- Kunkel, T. A. and D. A. Erie (2015). Eukaryotic Mismatch Repair in Relation to DNA Replication.
- Lamers, M. H., A. Perrakis, J. H. Enzlin, H. H. Winterwerp, N. de Wind and T. K. Sixma (2000). "The crystal structure of DNA mismatch repair protein MutS binding to a G x T mismatch." Nature **407**(6805): 711-717.
- Last, J. A., P. Russell, P. F. Nealey and C. J. Murphy (2010). "The applications of atomic force microscopy to vision science." Invest Ophthalmol Vis Sci **51**(12): 6083-6094.
- Longley, M. J., A. J. Pierce and P. Modrich (1997). "DNA polymerase delta is required for human mismatch repair in vitro." J Biol Chem **272**(16): 10917-10921.
- Martik, D., C. Baitinger and P. Modrich (2004). "Differential specificities and simultaneous occupancy of human MutS α nucleotide binding sites." J Biol Chem **279**(27): 28402-28410.
- Mazur, D. J., M. L. Mendillo and R. D. Kolodner (2006). "Inhibition of Msh6 ATPase activity by mispaired DNA induces a Msh2(ATP)-Msh6(ATP) state capable of hydrolysis-independent movement along DNA." Mol Cell **22**(1): 39-49.
- Mazurek, A., C. N. Johnson, M. W. Germann and R. Fishel (2009). "Sequence context effect for hMSH2-hMSH6 mismatch-dependent activation." Proc Natl Acad Sci U S A **106**(11): 4177-4182.
- Modrich, P. (1987). "DNA mismatch correction." Annual review of biochemistry **56**: 435-466.
- Modrich, P. (2006). "Mechanisms in eukaryotic mismatch repair." J Biol Chem **281**(41): 30305-30309.
- Natrajan, G., M. H. Lamers, J. H. Enzlin, H. H. Winterwerp, A. Perrakis and T. K. Sixma (2003). "Structures of Escherichia coli DNA mismatch repair enzyme MutS in complex with different mismatches: a common recognition mode for diverse substrates." Nucleic Acids Res **31**(16): 4814-4821.
- Obmolova, G., C. Ban, P. Hsieh and W. Yang (2000). "Crystal structures of mismatch repair protein MutS and its complex with a substrate DNA." Nature **407**(6805): 703-710.
- Pluciennik, A., V. Burdett, C. Baitinger, R. R. Iyer, K. Shi and P. Modrich (2013). "Extrahelical (CAG)/(CTG) triplet repeat elements support proliferating cell nuclear antigen loading and MutL α endonuclease activation." Proc Natl Acad Sci U S A **110**(30): 12277-12282.
- Pluciennik, A., V. Burdett, O. Lukianova, M. O'Donnell and P. Modrich (2009). "Involvement of the beta clamp in methyl-directed mismatch repair in vitro." J Biol Chem **284**(47): 32782-32791.

- Pluciennik, A., L. Dzantiev, R. R. Iyer, N. Constantin, F. A. Kadyrov and P. Modrich (2010). "PCNA function in the activation and strand direction of MutL α endonuclease in mismatch repair." Proceedings of the National Academy of Sciences of the United States of America **107**(37): 16066-16071.
- Qiu, R., V. C. DeRocco, C. Harris, A. Sharma, M. M. Hingorani, D. A. Erie and K. R. Weninger (2012). "Large conformational changes in MutS during DNA scanning, mismatch recognition and repair signalling." EMBO J **31**(11): 2528-2540.
- Ratcliff, G. C. and D. A. Erie (2001). "A novel single-molecule study to determine protein--protein association constants." Journal of the American Chemical Society **123**(24): 5632-5635.
- Sacho, E. J., F. A. Kadyrov, P. Modrich, T. A. Kunkel and D. A. Erie (2008). "Direct visualization of asymmetric adenine-nucleotide-induced conformational changes in MutL α ." Molecular cell **29**(1): 112-121.
- Schofield, M. J. and P. Hsieh (2003). "DNA mismatch repair: molecular mechanisms and biological function." Annu Rev Microbiol **57**: 579-608.
- Schofield, M. J., S. Nayak, T. H. Scott, C. Du and P. Hsieh (2001). "Interaction of Escherichia coli MutS and MutL at a DNA mismatch." J Biol Chem **276**(30): 28291-28299.
- Selmane, T., M. J. Schofield, S. Nayak, C. Du and P. Hsieh (2003). "Formation of a DNA mismatch repair complex mediated by ATP." J Mol Biol **334**(5): 949-965.
- Spampinato, C. P., R. L. Gomez, C. Galles and L. D. Lario (2009). "From bacteria to plants: a compendium of mismatch repair assays." Mutation research **682**(2-3): 110-128.
- Su, S. S., R. S. Lahue, K. G. Au and P. Modrich (1988). "Mispair specificity of methyl-directed DNA mismatch correction in vitro." J Biol Chem **263**(14): 6829-6835.
- Tessmer, I., Y. Yang, J. Zhai, C. Du, P. Hsieh, M. M. Hingorani and D. A. Erie (2008). "Mechanism of MutS searching for DNA mismatches and signaling repair." J Biol Chem **283**(52): 36646-36654.
- van Oers, J. M., S. Roa, U. Werling, Y. Liu, J. Genschel, H. Hou, Jr., R. S. Sellers, P. Modrich, M. D. Scharff and W. Edelmann (2010). "PMS2 endonuclease activity has distinct biological functions and is essential for genome maintenance." Proc Natl Acad Sci U S A **107**(30): 13384-13389.
- Wang, H., Y. Yang, M. J. Schofield, C. Du, Y. Fridman, S. D. Lee, E. D. Larson, J. T. Drummond, E. Alani, P. Hsieh and D. A. Erie (2003). "DNA bending and unbending by MutS govern mismatch recognition and specificity." Proc Natl Acad Sci U S A **100**(25): 14822-14827.

- Warren, J. J., T. J. Pohlhaus, A. Changela, R. R. Iyer, P. L. Modrich and L. S. Beese (2007). "Structure of the human MutSalpha DNA lesion recognition complex." Mol Cell **26**(4): 579-592.
- Yang, Y., H. Wang and D. A. Erie (2003). "Quantitative characterization of biomolecular assemblies and interactions using atomic force microscopy." Methods **29**(2): 175-187.

CHAPTER 2: STRUCTURE-FUNCTION INVESTIGATION OF HUMAN MUTSA AND MUTSA–MUTLA ON DNA CONTAINING A MISMATCH

Introduction

DNA Mismatch Repair (MMR) is a highly conserved process in prokaryotes and eukaryotes that repairs misincorporated bases and insertion-deletion loops that arise during DNA replication (Kunkel and Erie 2005, Iyer, Pluciennik et al. 2006, Hsieh and Yamane 2008). In humans, mutations in the MMR genes are linked to greater than 80% of hereditary non-polyposis colorectal cancers, which highlights the importance of understanding the mechanism of MMR (Hsieh and Yamane 2008, Martin-Lopez and Fishel 2013). In all organisms, MMR is initiated by MutS and MutL homologs. Eukaryotes have multiple MutS and MutL homologs and in humans, two of these homologs are the heterodimers MSH2-MSH6 (MutS α) and MLH1-PMS2 (MutL α). Both MutS α and MutL α contain two ATPase sites and have DNA-binding activities that are essential for MMR (Kunkel and Erie 2005, Iyer, Pluciennik et al. 2006, Hsieh and Yamane 2008). MutS α recognizes and binds to the mispaired base and forms a complex with MutL α in the presence of ATP. MutL α subsequently preferentially nicks the daughter strand near the mismatch and initiates the MMR pathway. This nicking activity has been shown *in vivo* to be a fundamental step in the repair of replication errors (Deschenes, Tomer et al. 2007, Erdeniz, Nguyen et al. 2007, Kadyrov, Holmes et al. 2007, van Oers, Roa et al. 2010); however, there is controversy in the field about how the MutS α –MutL α complex accomplishes this task.

MMR is initiated by the recognition of a mismatch by MutS α and its subsequent ATP-dependent conformational changes to a mobile clamp (Kunkel and Erie 2005, Iyer, Pluciennik et al. 2006, Hsieh and Yamane 2008). MutS α recruits MutL α to the mismatch and PCNA interacts

with this MutS α –MutL α –DNA complex. PCNA activates the latent endonuclease activity of MutL α to nick the daughter strand preferentially near the mismatch, and thus signals the downstream events of MMR (Kadyrov, Dzantiev et al. 2006, Pluciennik, Dzantiev et al. 2010).

It is well established that upon ATP-binding, MutS α forms a mobile clamp and moves away from the mismatch; however, it is unclear how MutS α and MutL α signal for MMR, and several disparate models have been proposed. One model posits that MutL α joins MutS α to form MutS α –MutL α mobile clamps that diffuse along the DNA. This model was originally suggested based on the observation that MutS α can form mobile clamps. This model, however, does not provide an explanation for how these clamps would result in preferential nicking near the mismatch (Blackwell, Martik et al. 1998, Blackwell, Wang et al. 2001, Gorman, Wang et al. 2012). Another model proposes that MutL α traps MutS α mobile clamps near the mismatch (Schofield, Nayak et al. 2001, Groothuizen, Winkler et al. 2015, Qiu, Sakato et al. 2015). This complex could then facilitate DNA looping to interact with downstream proteins in MMR. A third model suggests that MutS α induces polymerization of MutL α along the DNA. This model originally proposed by Modrich (Modrich 1987), is supported by recent *in vivo* fluorescence studies in *Saccharomyces cerevisiae* (*S. cerevisiae*) and *Escherichia coli* (*E. coli*) suggesting that MMR foci contain more MutL α than MutS α proteins (Hombauer, Campbell et al. 2011, Elez, Radman et al. 2012). These models are not mutually exclusive, but each of these models predicts structurally distinct MutS α –MutL α complexes. With structural data we can gain insight into which model (or models) closely represents how the initiation of MMR occurs.

In this study, we examine the initial signaling mechanism of MMR by using atomic force microscopy (AFM) to determine the stoichiometries and conformations of MutS α –DNA and MutS α –MutL α –DNA complexes. AFM is a single-molecule technique that can differentiate

between each proposed model by directly visualizing these complexes bound to DNA. The resulting images can be used to measure: 1) the position of MutS α and MutS α –MutL α complexes on the DNA relative to a mismatch, 2) the volumes of complexes to estimate the stoichiometries of the proteins within these complexes, and 3) the changes in the conformation of the complexes in different adenine nucleotide conditions or upon the addition of MutL α . In addition, AFM allows for the observation of rare events that may be essential to the initiation of MMR. Using these data, we will be able to distinguish between each of these disparate models so that we can shed insight into the initial signaling mechanism of MMR.

In this study, we compare MutS α –DNA complexes formed in the presence of ADP or ATP on perfectly paired DNA or on DNA containing a single guanine-thymine (GT) mismatch. We also compare these complexes to MutS α –MutL α on GT mismatch DNA (GT–DNA) in the presence of ATP. Our studies demonstrate that MutS α in the presence of ATP maintains a high specificity for the mismatch; however, we were surprised to see the formation of MutS α multimers localized to the mismatch. We also observed that the MutS α –MutL α experiments resulted in the formation of large complex formations that interacted with the DNA. The conformations of these protein-DNA complexes led us to propose a model in which MutS α bends the DNA at the mismatch and MutL α interaction with duplex DNA allows for PCNA to interact with MutL α on either side of the mismatch to preferentially nick near the mismatch.

Materials and Methods

Protein expression and purification

Human MutS α (MutS α) and human MutL α (MutL α) were purified as previously described (Geng, Du et al. 2011, Geng, Sakato et al. 2012) and generously provided by Dr. Peggy Hsieh (NIDDK, Bethesda, MD) and by Dr. Paul Modrich (Duke University).

DNA substrate preparation

We modified a pSCW02 plasmid to make the GT–DNA substrates that were used for AFM as done previously (Geng, Du et al. 2011, Geng, Sakato et al. 2012). To create linear GT–DNA or linear GC–DNA (using unmodified pSCW02 DNA), the plasmid was linearized using an endonuclease, Xmn1, which cut the DNA such that the mismatch was 375 bp (124 nm) from one end. The plasmid and DNA substrates were made by Dr. Chunwei Du and generously provided to us by Dr. Peggy Hsieh (NIDDK, Bethesda, MD).

Sample preparation and deposition

Freshly cleaved ruby mica discs (Spruce Pine Mica Company, Spruce Pine, NC) were placed in a desiccator next a piece of Parafilm containing 30 microliters of (3-aminopropyl) triethoxysilane (APTES) for 15 minutes to modify the mica surface to facilitate DNA deposition. For experiments with MutS α alone, MutS α was diluted to a concentration of 125 nM with 100 μ M ADP, 100 μ M ATP, 500 μ M ATP, or 1 mM ATP incubated with 1 ng/ μ l of the DNA substrate for 2 or 5 minutes at room temperature in imaging buffer (25 mM HEPES, pH 7.5, 100 mM NaOAc, 10 mM Mg(OAc)₂, 1 mM DTT, 5% glycerol) in a total volume of 20 microliters. Experiments with both MutS α and MutL α used final concentrations of 125 nM MutS α and 125 nM MutL α with 0.5 mM ATP or 1 mM ATP incubated with 1 ng/ μ l of the DNA substrate for 2

or 5 minutes at room temperature in imaging buffer (25 mM Hepes, pH 7.5, 100 mM NaOAc, 10 mM Mg(OAc)₂, 1 mM DTT, 5% glycerol) in a total volume of 20 microliters. The protein–DNA samples were cross-linked with 0.85% glutaraldehyde for 1-5 minutes. Cross-linking conditions were optimized to minimize artifacts, and non-cross-linked control experiments with MutS α alone were conducted (see Supplemental Methods 2.1). Variable extents of cross-linking were observed for each experiment, but the relative populations of species were found to be independent of cross-linking efficiency. Cross-linking was most important in experiments incubating MutS α and MutL α with the DNA substrate to observe a surface free from excess proteins. These cross-linked samples were filtered through a 4% agarose bead gel filtration column prior to deposition to remove excess free proteins. Fractions were collected from the filtration column and deposited onto the APTES-treated mica, rinsed with water, blotted dry, and then dried under a stream of nitrogen before imaging.

Imaging

The images were captured in air with a Nanoscope IIIa (Digital Instruments, Santa Barbara, CA) microscope in tapping mode. Pointprobe Plus tapping mode silicon cantilevers (NANOSENSORS, Switzerland) with resonance frequencies from 146-236 kHz were used. The images were collected at a speed of 1.97 Hz, a size of 2 μ m, and at a resolution of 512 x 512 pixels.

Image Analysis

A combination of NIH ImageJ64 (Rasband, with NeuronJ plug-in) software, Nanoscope III v5.3 software (Veeco, Santa Barbara, CA), ImageSXM v1.95, and a custom MATLAB program were used to measure the volumes of the complexes on the DNA, the DNA contour lengths, and the position of the proteins on the DNA. The KaleidaGraph program (Synergy

Software, Reading, PA) was used to generate statistical plots for each data set. For each data set, 20-70 images from two to three independent experiments were analyzed, compared, and pooled.

Volume analysis was performed as previously described using ImageSXM v 1.95 (Ratcliff and Erie 2001, Wang, Yang et al. 2003, Sacho, Kadyrov et al. 2008). Volumes were normalized in the MutS α alone experiments, but not in the MutS α –MutL α experiments. Individual data sets were normalized to the first peak (example shown in Supplemental Methods 2.2), which was consistent with the volume of 1 MutS α . Raw volumes were divided by the volume of the first peak to normalize each data set. The normalized individual data sets were then pooled.

DNA contour length and position analyses for the MutS α alone experiments were done as previously described using ImageJ64 software (Wang, Yang et al. 2003). To determine the positions of MutS α binding on the DNA fragments, the distance from the center of the bound MutS α complex to each end of the DNA fragment was measured. Because the mismatch is 124 nm from end of the DNA, there will be a “short arm” and a “long arm” DNA length when MutS α is bound at the mismatch (Supplemental Methods 2.3). Complexes with centers within two standard deviations of the expected mismatch position are categorized as specific complexes. We did not end label the DNA to identify the DNA ends; thus, some nonspecific complexes will be counted as specific complexes but not vice versa.

DNA contour length and position analyses for the MutS α and MutL α experiments were done using a custom MATLAB program. We observed in experiments incubating MutS α and MutL α that the total DNA length appears to shorten after a 5 minute incubation time because more of the DNA was ending up inside the protein complex (see Figure 2.C images, Supplemental, S2.6). Therefore, measuring the position of the complexes using the method

described previously will result in more complexes being miscounted as non-specifically bound to the DNA. The purpose of this program was to remove bias in measuring the DNA contour length when a large protein complex was present, so that we can account for the DNA length inside the protein complex more systematically. The positions of the complexes along the DNA were measured at the start of the complex, the end of the complex, and the total length of the DNA was also recorded. The DNA length missing from each DNA molecule was then calculated as the difference between the expected DNA length and the apparent length. We assumed the missing DNA length was included in the protein complex, so the missing DNA length was added to the overall protein complex length as shown in Figure 2.3B. A protein–DNA complex was considered specific if any part of the complex (including the missing DNA length) was within two standard deviations (as determined in the MutS α experiments conducted with ADP) of the mismatch.

Results

In the presence of ADP, one MutS α binds to the mismatch

We examined the properties of human MutS α and MutS α –MutL α bound to 2 kb DNA fragments containing either perfectly paired (GC–DNA) or a single GT mismatch 375 bp (124 nm) from one end (GT–DNA) (Figure 2.1A schematic). Because we know the position of the mismatch on the DNA, we can determine whether or not the MutS α and MutS α –MutL α complexes are bound at the mismatch (specific complex) or at homoduplex sites (nonspecific complex) by measuring the position of the complex relative to the ends of the DNA (Methods, SM2.2). In addition, because the volumes of the protein complexes in AFM images depend linearly on their molecular weight, we can estimate the number of proteins within each complex by measuring their volumes (Ratcliff and Erie 2001, Yang, Wang et al. 2003).

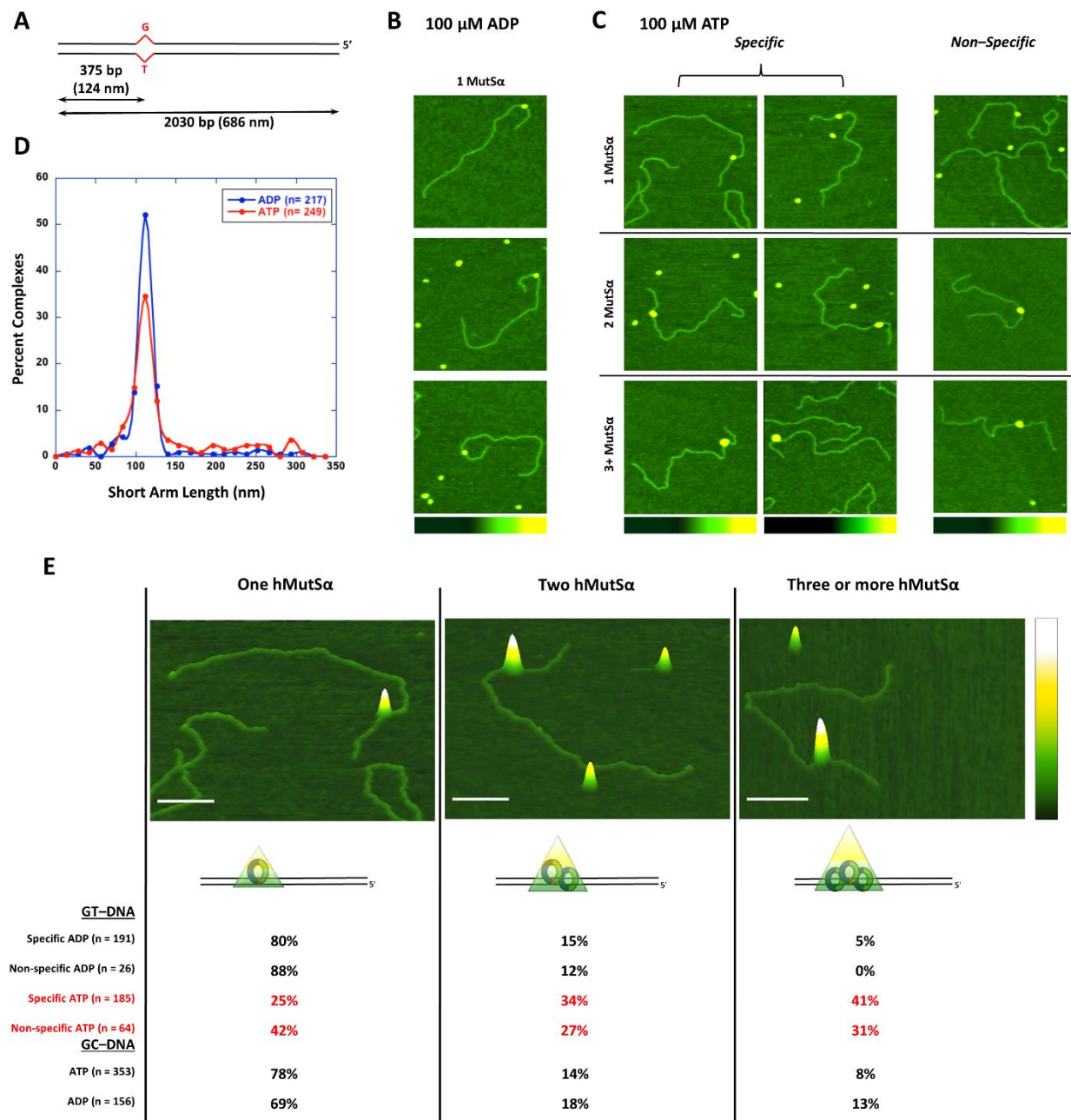


Figure 2.1 : AFM images and position and volume analysis of MutS α bound to GT–DNA

(A) Schematic view of the GT–DNA substrate used in this study. The length of the DNA fragment and the position of the mismatch in base pairs and in nanometers from the nearest end are shown by black arrows. (B) Representative images of MutS α bound to the mismatch in the presence of 100 μ M ADP. Images are 500 nm. (C) Example images of MutS α –GT–DNA complexes containing one (top row), two (middle row), and three (bottom row) MutS α proteins bound at the position of the mismatch (left panel) and at non–specific sites (right panel) in the presence of 100 μ M ATP. Images are 500 nm. (D) Distribution of positions of MutS α complexes on GT–DNA in the presence of 100 μ M ADP (blue) or 100 μ M ATP (red). In both ADP and ATP, peaks are centered at 124 nm, which is consistent with the position of the GT mismatch. (E) Top, 3D topographic images show single MutS α –GT–DNA complexes containing one, two, or three or more MutS α . White scale bars on images indicate 100 nm. Colored scaled bar indicates 0 – 9 nm with low being dark green and high being white. Middle, below the 3D images are cartoons depicting how MutS α may contribute to the volume observed in the images. Bottom, below the cartoon is a table that describes the distribution of each type of complex in the presence of ADP or ATP on GT–DNA or GC–DNA. In red are the conditions where more than one MutS α complexes are observed.

Figure 2.1B shows representative AFM images of MutS α bound to GT-DNA in the presence of ADP. Most DNA molecules (88%, n = 246) have one MutS α complex bound (Supplemental, S2.1). Inspection of the distribution of positions of MutS α bound to GT-DNA in the presence of ADP reveals a peak centered at the position of the mismatch (Figure 2.1D, blue line). We defined the complexes found within two standard deviations of the peak (which is at the mismatch) as specifically bound, and those outside this range of positions are considered to be non-specific. Analysis of the positions of MutS α on GT-DNA reveals that 90% (n = 217) of bound MutS α are found under this peak. In contrast, GC-DNA data exhibit a random position distribution (Supplemental, S2.2). The observed high specificity is not surprising given the high binding affinity of MutS α for a GT-mismatch (Mazur, Mendillo et al. 2006). In addition, the vast majority (80%, n = 187) of the MutS α -DNA complexes exhibited volumes consistent with one MutS α being bound to the mismatch, as expected (Figure 2.1E table, Specific ADP).

In the presence of ATP, MutS α binds with high specificity to the mismatch

Figure 2.1C shows AFM images of MutS α bound to GT-DNA in the presence of ATP. Like ADP, a significant percentage of the DNA molecules have one MutS α complex bound (87%, n = 287) (Supplemental, S2.1). One notable difference is that many of the complexes appear to be larger, suggesting that they contain more than one MutS α (second and third rows of Figure 2.1C). These results suggest that ATP promotes MutS α -MutS α interactions on GT-DNA. Additionally, we noted an increase in non-specific complexes (third column of Figure 2.1C), which is consistent with mobile clamp formation (Blackwell, Martik et al. 1998, Gradia, Subramanian et al. 1999, Blackwell, Bjornson et al. 2001, Acharya, Foster et al. 2003). Surprisingly, when we measured the positions of single MutS α complexes, we observed a significant peak centered at the mismatch (Figure 2.1D, red line), with 74% of complexes (n =

249) being within two standard deviations of the mismatch. In contrast, MutS α bound to GC–DNA in the presence of ATP yielded a random distribution of positions, suggesting MutS α binds the mismatch with high specificity (Supplement, S2.3). This high specificity for the mismatch in the presence of ATP is consistent with biochemical studies, which show that MutS α binds to a GT mismatch with ~ 100 nM K_d in the presence of ATP (Mazur, Mendillo et al. 2006). This high specificity is somewhat surprising, due to the contrast with other previous data that suggests multiple MutS α mobile clamps load onto the DNA non-specifically in the presence of ATP (Blackwell, Martik et al. 1998).

Although the relative specificities of MutS α for the mismatch in the presence of ADP vs. ATP are consistent with the measurements of binding affinities, we expected to see a more significant increase in the number of non-specifically bound complexes in the presence of ATP as a result of mobile clamp formation. Previous kinetic experiments have shown that addition of ATP leads to the rapid dissociation of MutS α from the DNA (Blackwell, Martik et al. 1998). To determine if the low percentage of non-specifically bound complexes is the result of the rapid dissociation of MutS α proteins from the DNA ends, we examined the number of MutS α complexes formed on circular plasmid DNA containing a single GT mismatch (Supplement, S2.1). We found no significant differences in the number of MutS α –DNA complexes, suggesting that MutS α is not dissociating from the ends of the linear DNA.

ATP induces mismatch-dependent multimerization of MutS α

As noted previously, close inspection of MutS α –DNA complexes in the presence of ATP revealed that many complexes appear to contain more than one MutS α protein (Figure 2.1B and 2.1E). Consequently, we measured the volumes of these complexes to determine the number of MutS α in each complex.

By measuring the volumes of single complexes in the presence of ATP, we observed, unexpectedly, that 74% of mismatch-bound MutS α complexes contained two or more MutS α (Figure 2.1E table, Specific ATP). We also noted that these multimeric complexes formed along the contour of the DNA fragment such that each MutS α interacts with the DNA as well as other MutS α proteins within the multimeric complex (Figure 2.1E images of two and three MutS α , S2.4 specific images). The multimeric complexes are slightly elongated and follow the contour of the DNA molecule. This elongation suggests that each MutS α was loaded onto the DNA via the mismatch instead of associating with the MutS α proteins already bound to the DNA. This result is in contrast to AFM studies done with *Thermus aquaticus* (*Taq*) MutS wherein MutS will associate and dimerize in the absence of DNA, and MutS not associated with DNA could interact with a MutS complex already bound to the DNA (Wang, Yang et al. 2003).

While the majority of the observed multimers localized to the mismatch (74%), we noted that some multimers were located non-specifically on the DNA (Figure 2.1E table, Non-specific ATP). Interestingly, these multimers followed the contour of the DNA similarly to the multimers that were specific (Supplemental, S2.4 non-specific images). The observation of multimers localized to the mismatch provides an explanation for why we did not observe as many non-specific complexes as we would expect upon the formation of the mobile clamp of MutS α in the presence of ATP. MutS α has a footprint on the DNA that covers ~ 11 bases surrounding the mismatch, meaning that only one MutS α can interact with the mismatch at a time (Warren, Pohlhaus et al. 2007). These data suggest that the first mismatch-bound MutS α formed a mobile clamp and moved away from the mismatch, a second MutS α can bind to the mismatch, and these MutS α proteins can associate to form a multimer.

The power in AFM lies in being able to observe rare events that may be essential to the initiation mechanism of MMR. Close examination of the topographic images of complexes consisting of two or more MutS α on the mismatch reveals that most complexes are tall, round, and condensed structures (S2.5A) and it is difficult to distinguish individual MutS α proteins from each other. However, we did observe a distinct species of asymmetrical complexes that are being formed (S2.5B and S2.5C). These complexes contain one MutS α that is bound specifically at the mismatch, and other MutS α proteins on the DNA that are associating with the mismatch-bound MutS α . Additionally, the MutS α localized to the mismatch appears to be “taller” relative to the other MutS α , suggesting that the MutS α proteins not on the mismatch are adopting a different conformation. Because the “short” MutS α are usually just past the site of the mismatch, it is likely that these MutS α are mobile clamps that have associated with a mismatch-bound MutS α . Comparing S2.B and S2.C, the “short” MutS α can be on either side of the bound MutS α suggesting that MutS α can move in either direction on the DNA once it has formed a mobile clamp as expected (Blackwell, Martik et al. 1998).

To explore the possibility that ATP induces the formation of multimers independent of the mismatch, we examined MutS α bound to GC–DNA (Figure 2.1E, table, GC–DNA). Volume analysis of these complexes show that the majority of bound complexes contained one MutS α (78%), suggesting that the presence of both ATP and a mismatch are required for multimers to be formed on the DNA.

MutS α and MutL α form large complexes on the DNA

To examine how the properties of MutS α –MutL α –DNA complexes differ from MutS α –DNA complexes, we incubated equal concentrations of MutS α and MutL α with 1 mM ATP and

GT-DNA for two minutes (2 min) and five minutes (5 min). Figure 2.2A shows representative images of the different conformational shapes of MutS α –MutL α –DNA complexes that we observed in the 2 min experiments. Most DNA molecules had one complex bound with 7% containing two or more complexes (Supplemental, S2.1). MutS α –MutL α complexes exhibited more conformational shapes on the DNA than was seen in the MutS α alone data. With the exception of the small round complexes (and large round complexes seen in the ATP data), these shapes were rarely observed in the MutS α alone data, suggesting that the addition of MutL α increased the variety of protein-DNA complex conformations (Supplemental, S2.6). These shapes included large elongated complexes (Long), complexes that appear to be coming off of the DNA (L-shaped), and complexes that seem to mediate DNA looping (Loop). We also observed that these conformational shapes were found at the mismatch site as well as at homoduplex sites.

We noted that these complexes appeared larger than the complexes observed previously with the MutS α alone data, and consequently we measured their volumes (Figure 2.2B, column 1, compare rows 1 and 2). Note that the volume distributions in Figure 2.2B are shown as raw volumes because, upon the addition of MutL α , it is difficult to normalize the volumes of these bound complexes as was done with MutS α alone. The 2 min complex volumes of MutS α –MutL α are shifted towards larger species relative to MutS α alone, suggesting that the addition of MutL α led to more proteins being bound to the DNA molecule. This finding is consistent with previous DNase1 footprinting studies done with *E. coli* proteins that found that upon addition of MutS and MutL to DNA containing a mismatch, a larger region of the DNA was protected than that with MutS alone (Schofield, Nayak et al. 2001).

To determine whether the complex size is dependent on the length of incubation, we incubated MutS α and MutL α with 1 mM ATP and GT-DNA for 5 min. We observed that 96% (n = 184) of protein-DNA complexes contained one complex on the DNA (Supplemental, S2.1). We again observed a variety of conformational shapes of MutS α -MutL α complexes being formed on the DNA molecule; however we observed that the distribution of complex shapes was shifted in favor of forming mainly large round shapes (Supplemental, S2.6).

We analyzed the volumes of these complexes, and observed a significant shift in volume distribution towards larger complexes relative to the 2 min experiments (Figure 2.2B, column 1, compare rows 2 and 3). These data suggest that, with a longer incubation time, more MutL α is recruited to the DNA molecule. The larger complexes are consistent with previous findings that suggest MutS α recruits multiple MutL α to the DNA molecule (Hombauer, Campbell et al. 2011, Elez, Radman et al. 2012).

Large MutS α -MutL α complexes exhibit shortened DNA lengths

Upon closer examination of the images of the 5 min experiments, it appears that the total DNA contour lengths are shorter than expected (Supplemental, S2.7, Figure 2.3C images). Consequently, the total DNA contour lengths of the 2 min and 5 min MutS α -MutL α experiments were measured and compared to the total DNA contour lengths in the MutS α alone experiments. Figure 2.2B shows that with the addition of MutL α and increasing incubation times, the total measurable DNA contour length becomes shorter. These data suggests that DNA is being pulled inside of the large complexes, and this interaction is dependent upon MutL α . To plot the positions of the protein-DNA complexes for both the 2 min and 5 min experiments, we developed a custom MATLAB program (Methods). Figure 2.3A shows three sample DNA molecules with a single complex bound. The blue bar depicts the total DNA contour length, and

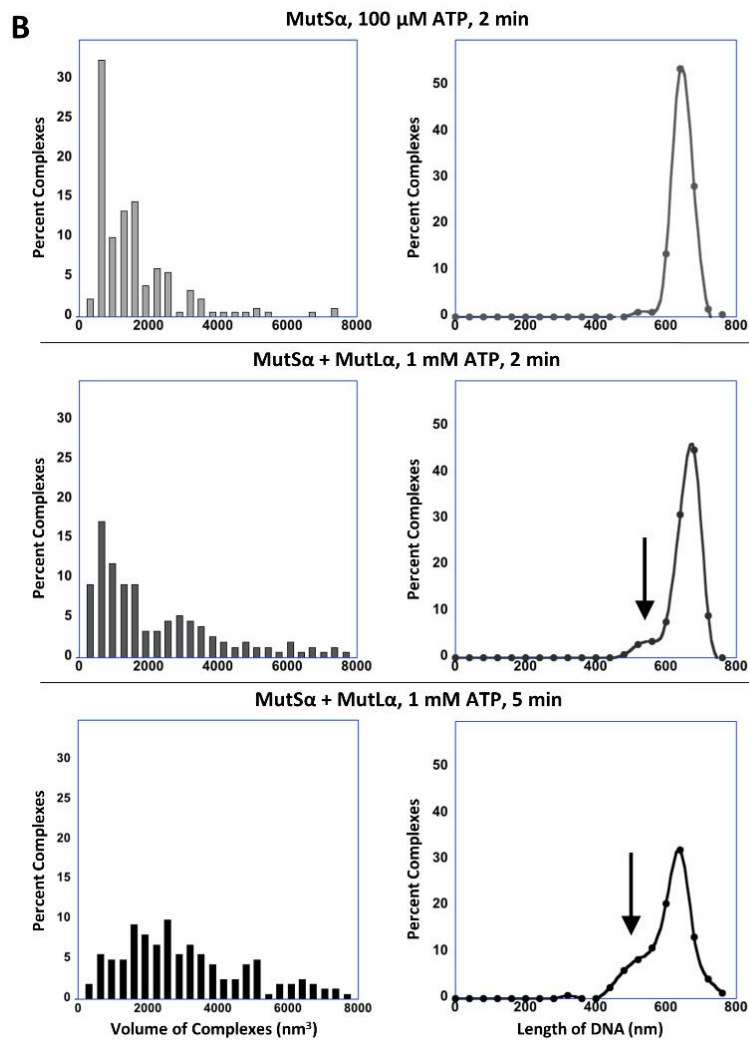
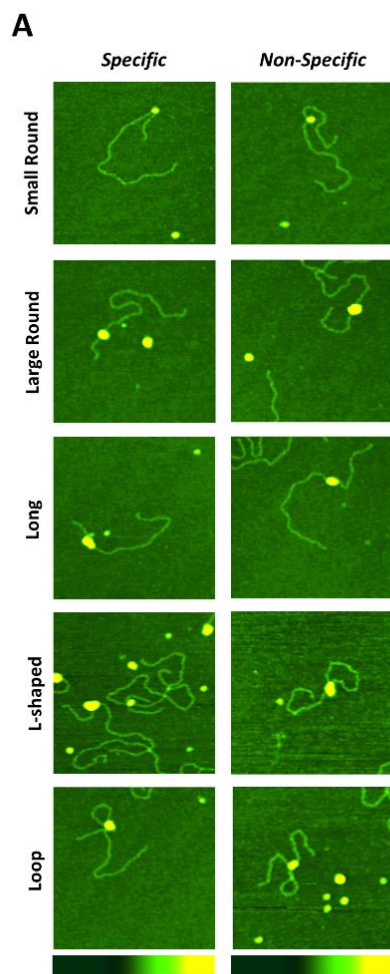


Figure 2.2 : AFM images and volume analysis of MutS α –MutL α complexes bound to GT–DNA

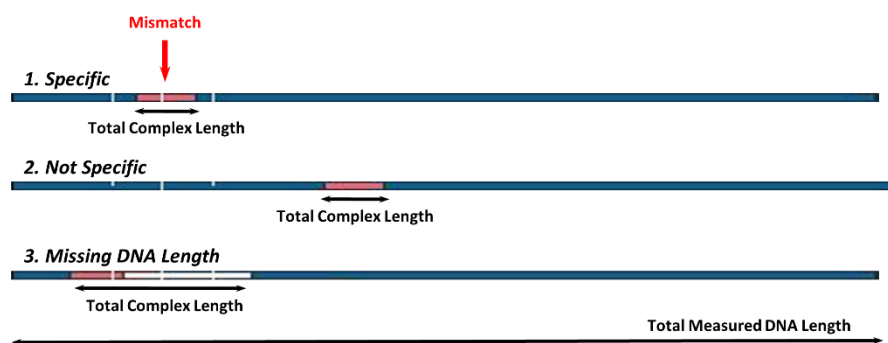
(A) Sample images of different conformational shapes of the MutS α –MutL α complexes in the presence of 1 mM ATP. Left column shows MutS α –MutL α complexes that are bound to the mismatch. Right column shows MutS α –MutL α complexes that are non-specifically bound. Images are 500 nm. (B) Volume analysis (left column) and total DNA length measurements (right column) are shown for MutS α alone in the presence of 100 μ M ATP ($n = 184$, top row), MutS α –MutL α in the presence of 1 mM ATP incubated for 2 min ($n = 153$, middle row), MutS α –MutL α in the presence of 1 mM ATP incubated for 5 min ($n = 161$, bottom row). Note that the volume distributions in (B) are shown as raw volumes because upon the addition of MutL α , it is difficult to normalize the volumes of these bound complexes as was done with MutS α alone. Volume analysis shows upon addition of MutL α and increasing incubation times, larger protein species are observed. Total DNA length analysis indicates that total DNA lengths decreases as a function of the addition of MutL α and longer incubation times. Red arrows point to the population of shorter DNA lengths. Note that large complexes are seen both at the mismatch and at non-specific sites, but only if the DNA contains a mismatch.

the pink bar represents the length and position of the protein complex. In molecules where the DNA lengths are shorter than expected (see sample 3), the missing DNA length is added in white bars; thus, the length of the combined white and pink bars correspond to the total length of DNA contained within the protein complex. Figure 2.3B shows the positions of MutS α –MutL α complexes in the 2 min and 5 min experiments. In the 5 min experiments, we observed that the MutS α –MutL α complexes span a greater length of DNA than the 2 min complexes (compare the length of the pink bars). We also observed that the 5 min complexes contain more DNA within them, leading to the original observation of shortened DNA lengths (compare the combined length of the white and pink bars).

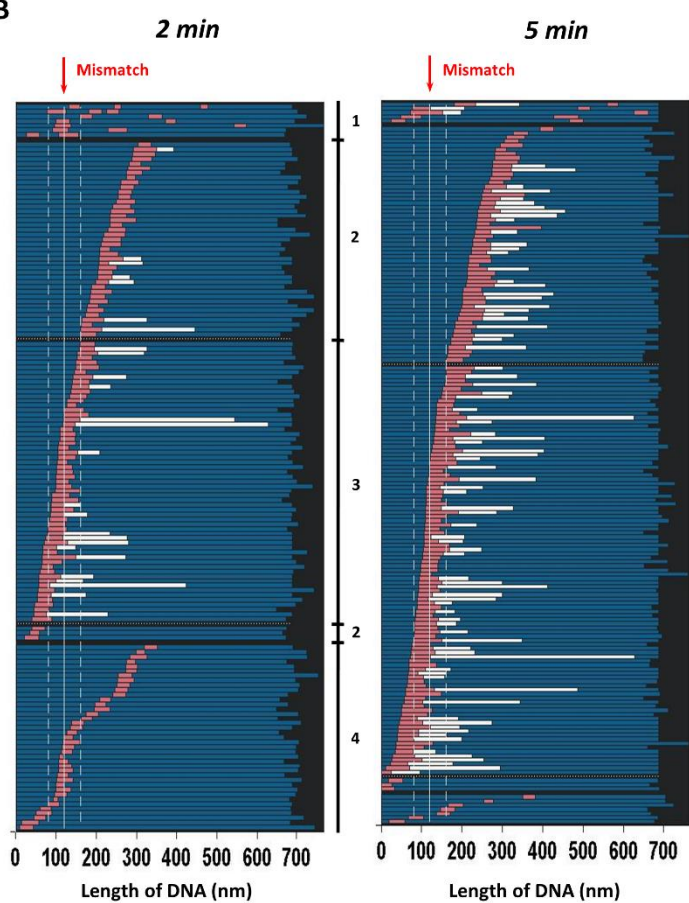
MutS α –MutL α complexes are less specific to the mismatch

To determine the specificity of MutS α –MutL α complexes for the mismatch, the positions of MutS α –MutL α complexes on GT–DNA were measured. We observed 58% and 61% of the protein complexes were bound to the mismatch site for the 2 min (n = 152) and the 5 min (n = 158), respectively (Figure 2.3B). Interestingly, we observe an increase in the number of non-specific complexes relative to the MutS α alone data. We may be unable to observe non-specifically bound mobile clamps in the MutS α alone data because the clamps slid off of the ends of the linear DNA. These data suggest that MutL α is able to recognize and trap MutS α that has formed a mobile clamp and moved away from the mismatch, because we observe a significant population of non-specific complexes in the presence of MutL α . These results are similar to recent data with *E. coli* and *Taq* MutS (Groothuizen, Winkler et al. 2015, Qiu, Sakato et al. 2015) that suggested that MutL α is able to recognize and trap mobile clamps of MutS. Alternatively, MutL α may have interacted with MutS α while MutS α was bound to the mismatch and together the MutS α –MutL α complex slid away, contributing to the larger population of non-

A



B



C

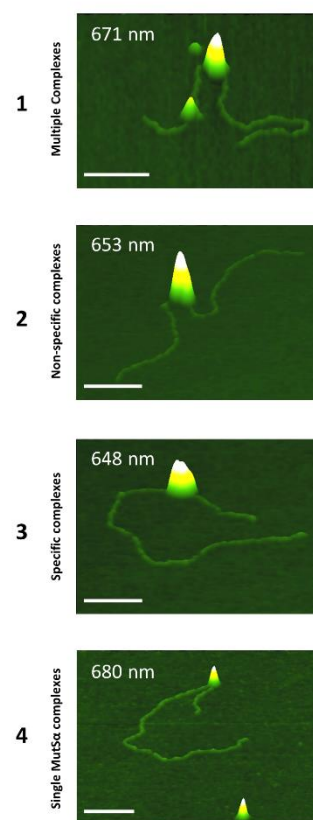


Figure 2.3 : Position analysis of MutS α –MutL α complexes bound to GT–DNA

(A) Sample DNA molecule with a MutS α –MutL α complex bound. Blue bar denotes the total measured DNA length. Pink bar is the length of the complex on the DNA. White bar represents the missing DNA length. The total amount of DNA that the protein complex covers is the summation of the pink and white bars. A solid black arrow points to the mismatch site and dashed arrows on either side indicate the standard deviation of binding to the mismatch. (B) Left panel: positions of MutS α –MutL α complexes on GT–DNA in the presence of 1 mM ATP and incubated for 2 min, right panel: positions of MutS α –MutL α complexes on GT–DNA in the presence of with 1 mM ATP and incubated for 5 min. Black solid arrows and dashed arrows above each panel indicate position of the mismatch and standard deviations, respectively. To the right of each panel, bars group up sections of the MutS α –MutL α complexes into four distinct categories. (C) Sample AFM images representing each category seen in (B). White numbers in the top left corner of each image denotes the total DNA length. White scale bars indicate 100 nm.

specifically bound complexes. This is consistent with *in vitro* fluorescence experiments in which MutS α –MutL α mobile clamps were observed (Gorman, Wang et al. 2012). Furthermore, because the complexes formed on the GT–DNA are larger than those observed with MutS α alone, it is possible that once MutS α is bound to the DNA, it recruits multiple MutL α consistent with the results in the fluorescence *in vitro* experiments which suggested that there is a higher ratio of MutL α to MutS α (Hombauer, Campbell et al. 2011, Elez, Radman et al. 2012).

Discussion

Multimers of MutS α localize to the mismatch in the presence of ATP

In this study, we make the unexpected observation that MutS α forms multimers localized to the mismatch in the presence of ATP. These multimers are consistent with previous studies that found MutS forms a mobile clamp and moves away from the mismatch (Blackwell, Martik et al. 1998, Gradia, Subramanian et al. 1999, Blackwell, Bjornson et al. 2001, Acharya, Foster et al. 2003). These freely diffusing mobile clamps of MutS along the DNA allows for multiple MutS to load on to the DNA. The results found in this study, however, indicate that mobile MutS α clamps can interact with MutS α that are bound at the mismatch. The localization of these complexes to the mismatch is supported by previous data that show that MutS α maintains a high affinity for binding a GT mismatch, even in the presence of ATP (Martik, Baitinger et al. 2004).

An interesting result from this study is that ATP appears to promote MutS α –MutS α interaction: the mobile clamp form of MutS α can interact with mismatch-bound MutS α . In some images, we observed different conformations of MutS α , where the MutS α bound at the mismatch is taller than the adjacent MutS α . The adjacent MutS α is presumably in a mobile clamp state that encircles the DNA more completely, leading to the “shorter” MutS α bound to

the DNA. Because these multimers form in the presence of ATP, it is possible that multiple MutS α proteins can recruit MutL α to the DNA. The volume data in this study suggests that up to two or more MutS α proteins can interact at the mismatch and could function to recruit MutL α .

MutL α traps MutS α mobile clamps and multiple MutL α are recruited

Upon the addition of MutL α , we observe complexes that are large indicating that multiple MutL α are recruited to the DNA. These data are supported by *in vivo* studies in *S. cerevisiae* and *E. coli* suggesting that MMR foci contain more MutL than MutS proteins (Hombauer, Campbell et al. 2011, Elez, Radman et al. 2012) as well as footprinting studies of *E. coli* MutS and MutL that show very large footprints in the presence of MutL (Schofield, Nayak et al. 2001). Furthermore, we noted that the large complexes have shortened measurable DNA lengths, suggesting that more of the DNA is ending up inside these large complexes. Alternatively, the DNA may be coated by MutL α and folded over into a condensed structure, which is consistent with DNase1 footprinting data that shows that more DNA is protected in the presence of both *E. coli* MutS and MutL (Schofield, Nayak et al. 2001). Previous studies reconstituting the mismatch repair system showed that in the absence of EXO1, MutL will continue to nick the DNA (Constantin, Dzantiev et al. 2005). With the data in this paper, the observation of more DNA ended up inside these large complexes could be indicative of a “reeling” activity of MutL α as it searches for the protein EXO, the next step in the MMR pathway, and could result in the shortened DNA contour lengths observed in this study.

Using the data presented in this chapter and from several other studies, we can provide a possible model for how MutS α and MutL α interact to signal repair. Previous studies have shown different MutS homologs exhibit DNA bending activity under different adenine nucleotide

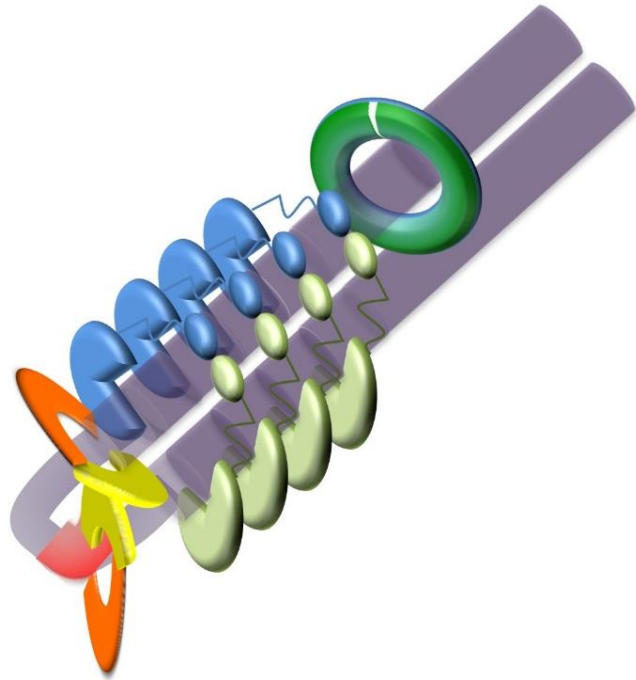
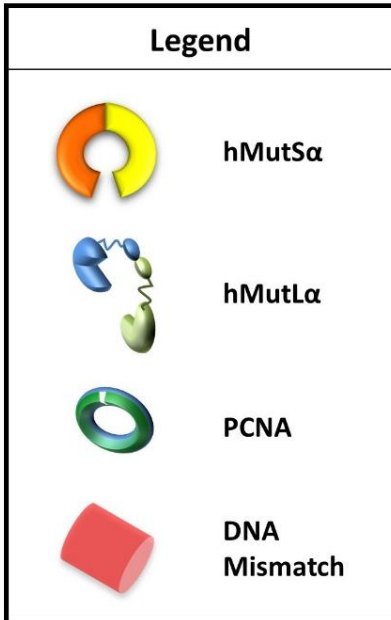


Figure 2.4 : Model of MutSα and MutLα Interaction

Up to two MutSα interact at the mismatch on the DNA. The MutSα at the mismatch bends the DNA and the other mobile clamp MutSα recruits MutLα. Multiple MutLα are recruited, and with the bend in the DNA, bring the flanking DNA on either side of the mismatch together to form a zipper-like structure. PCNA can direct MutLα to nick the DNA on either side of the mismatch. *Adapted from image prepared by Dorothy Eerie.*

conditions (Wang, Yang et al. 2003, Warren, Pohlhaus et al. 2007, DeRocco, Sass et al. 2014). Additionally, an AFM study with yeast MutL α under low salt conditions suggested that MutL α can bind cooperatively to form long tracts of protein along duplex DNA, and was also shown to interact with two different strands of DNA simultaneously (Hall, Wang et al. 2001). Figure 2.4 depicts a model based on these findings. In this model, one or two MutS α proteins interact at the mismatch with multiple MutL α polymerizing away from the mismatch. The inherent bend of the DNA by MutS α bound to the mismatch could potentially allow for MutL α to more easily access and interact with the DNA strands flanking either side of the mismatch. The second MutS α could function as a flag to recruit more MutL α , leading to the DNA flanking the mismatch to come together. This formation of a zipper-like structure could allow for PCNA to interact with MutL α and direct it to nick the nascent strand on either side of the mismatch depending on the orientation of the MutL α on that DNA. Additionally, if a MutS α formed a mobile clamp and moved away from the mismatch before associating with a second MutS α , MutL α can trap the MutS α mobile clamp either close to or away from the mismatch, creating additional areas on the DNA to be nicked, and thereby amplifying the nicking signal.

AFM is a powerful single molecule technique, but the limitation of these experiments is that we cannot distinguish MutS α from MutL α . In spite of this limitation, we are able to detect significant changes in conformational shapes, volumes, and DNA lengths in the MutS α –MutL α –DNA complexes in response to the addition of MutL α . This study and previous experiments demonstrate that MutS α and MutL α have the capacity to form large complexes under certain conditions.

Together, these data suggest that one or two MutS α are localized to the mismatch and recruit MutL α to the DNA. With increasing concentrations of ATP and longer incubation times,

more MutL α can be recruited to the mismatch, resulting in a variety of complexes being formed. Each of the noted conformational “shapes” of the complexes could correspond to a step in a pathway of MutS α –MutL α conformational changes that allow the MutS α –MutL α complex to better interact with the DNA or potentially PCNA or EXO1. The longer incubations show that MutL α will continue to be recruited and incorporate more of the DNA inside the complex, perhaps in search of EXO1 or PCNA.

Future work that examines the dynamics of MutS α –MutL α complexes on DNA containing a mismatch will shed additional insight on MutS α –MutL α interactions. Studies that examine MutS α -mediated DNA bending and how it affects MutL α will yield additional insight into the mechanism of MutS α -mediated recruitment of MutL α . These experiments will be useful in determining what MutS α –MutL α interactions occur once a mobile clamp of MutS α moves away from the mismatch. Finally, experiments that examine the adenine-nucleotide state of MutS α to see how it changes as MutS α forms a mobile clamp and interacts with MutL α will provide insight into the initiation of MMR.

REFERENCES

- Acharya, S., P. L. Foster, P. Brooks and R. Fishel (2003). "The coordinated functions of the E. coli MutS and MutL proteins in mismatch repair." *Mol Cell* 12(1): 233-246.
- Blackwell, L. J., K. P. Bjornson, D. J. Allen and P. Modrich (2001). "Distinct MutS DNA-binding modes that are differentially modulated by ATP binding and hydrolysis." *J Biol Chem* 276(36): 34339-34347.
- Blackwell, L. J., D. Martik, K. P. Bjornson, E. S. Bjornson and P. Modrich (1998). "Nucleotide-promoted release of hMutSalpha from heteroduplex DNA is consistent with an ATP-dependent translocation mechanism." *J Biol Chem* 273(48): 32055-32062.
- Blackwell, L. J., S. Wang and P. Modrich (2001). "DNA chain length dependence of formation and dynamics of hMutSalpha.hMutLalpha.heteroduplex complexes." *J Biol Chem* 276(35): 33233-33240.
- Constantin, N., L. Dzantiev, F. A. Kadyrov and P. Modrich (2005). "Human mismatch repair: reconstitution of a nick-directed bidirectional reaction." *J Biol Chem* 280(48): 39752-39761.
- DeRocco, V. C., L. E. Sass, R. Qiu, K. R. Weninger and D. A. Erie (2014). "Dynamics of MutS-mismatched DNA complexes are predictive of their repair phenotypes." *Biochemistry* 53(12): 2043-2052.
- Deschenes, S. M., G. Tomer, M. Nguyen, N. Erdeniz, N. C. Juba, N. Sepulveda, J. E. Pisani and R. M. Liskay (2007). "The E705K mutation in hPMS2 exerts recessive, not dominant, effects on mismatch repair." *Cancer Lett* 249(2): 148-156.
- Elez, M., M. Radman and I. Matic (2012). "Stoichiometry of MutS and MutL at unrepaired mismatches in vivo suggests a mechanism of repair." *Nucleic Acids Res* 40(9): 3929-3938.
- Erdeniz, N., M. Nguyen, S. M. Deschenes and R. M. Liskay (2007). "Mutations affecting a putative MutLalpha endonuclease motif impact multiple mismatch repair functions." *DNA Repair (Amst)* 6(10): 1463-1470.
- Geng, H., C. Du, S. Chen, V. Salerno, C. Manfredi and P. Hsieh (2011). "In vitro studies of DNA mismatch repair proteins." *Anal Biochem* 413(2): 179-184.
- Geng, H., M. Sakato, V. DeRocco, K. Yamane, C. Du, D. A. Erie, M. Hingorani and P. Hsieh (2012). "Biochemical analysis of the human mismatch repair proteins hMutSalpha MSH2(G674A)-MSH6 and MSH2-MSH6(T1219D)." *J Biol Chem* 287(13): 9777-9791.
- Gorman, J., F. Wang, S. Redding, A. J. Plys, T. Fazio, S. Wind, E. E. Alani and E. C. Greene (2012). "Single-molecule imaging reveals target-search mechanisms during DNA mismatch repair." *Proc Natl Acad Sci U S A* 109(45): E3074-3083.

- Gradia, S., D. Subramanian, T. Wilson, S. Acharya, A. Makhov, J. Griffith and R. Fishel (1999). "hMSH2-hMSH6 forms a hydrolysis-independent sliding clamp on mismatched DNA." *Mol Cell* 3(2): 255-261.
- Groothuizen, F. S., I. Winkler, M. Cristovao, A. Fish, H. H. Winterwerp, A. Reumer, A. D. Marx, N. Hermans, R. A. Nicholls, G. N. Murshudov, J. H. Lebbink, P. Friedhoff and T. K. Sixma (2015). "MutS/MutL crystal structure reveals that the MutS sliding clamp loads MutL onto DNA." *Elife* 4.
- Hall, M. C., H. Wang, D. A. Erie and T. A. Kunkel (2001). "High affinity cooperative DNA binding by the yeast Mlh1-Pms1 heterodimer." *J Mol Biol* 312(4): 637-647.
- Hombauer, H., C. S. Campbell, C. E. Smith, A. Desai and R. D. Kolodner (2011). "Visualization of eukaryotic DNA mismatch repair reveals distinct recognition and repair intermediates." *Cell* 147(5): 1040-1053.
- Hsieh, P. and K. Yamane (2008). "DNA mismatch repair: molecular mechanism, cancer, and ageing." *Mech Ageing Dev* 129(7-8): 391-407.
- Iyer, R. R., A. Pluciennik, V. Burdett and P. L. Modrich (2006). "DNA mismatch repair: functions and mechanisms." *Chemical reviews* 106(2): 302-323.
- Kadyrov, F. A., L. Dzantiev, N. Constantin and P. Modrich (2006). "Endonucleolytic function of MutLalpha in human mismatch repair." *Cell* 126(2): 297-308.
- Kadyrov, F. A., S. F. Holmes, M. E. Arana, O. A. Lukianova, M. O'Donnell, T. A. Kunkel and P. Modrich (2007). "Saccharomyces cerevisiae MutLalpha is a mismatch repair endonuclease." *J Biol Chem* 282(51): 37181-37190.
- Kunkel, T. A. and D. A. Erie (2005). "DNA mismatch repair." *Annu Rev Biochem* 74: 681-710.
- Martik, D., C. Baitinger and P. Modrich (2004). "Differential specificities and simultaneous occupancy of human MutSalphalpha nucleotide binding sites." *J Biol Chem* 279(27): 28402-28410.
- Martin-Lopez, J. V. and R. Fishel (2013). "The mechanism of mismatch repair and the functional analysis of mismatch repair defects in Lynch syndrome." *Fam Cancer* 12(2): 159-168.
- Mazur, D. J., M. L. Mendillo and R. D. Kolodner (2006). "Inhibition of Msh6 ATPase activity by mispaired DNA induces a Msh2(ATP)-Msh6(ATP) state capable of hydrolysis-independent movement along DNA." *Mol Cell* 22(1): 39-49.
- Modrich, P. (1987). "DNA mismatch correction." *Annual review of biochemistry* 56: 435-466.
- Pluciennik, A., L. Dzantiev, R. R. Iyer, N. Constantin, F. A. Kadyrov and P. Modrich (2010). "PCNA function in the activation and strand direction of MutLalpha endonuclease in mismatch repair." *Proceedings of the National Academy of Sciences of the United States of America* 107(37): 16066-16071.

- Qiu, R., M. Sakato, E. J. Sacho, H. Wilkins, X. Zhang, P. Modrich, M. M. Hingorani, D. A. Erie and K. R. Weninger (2015). "MutL traps MutS at a DNA mismatch." *Proc Natl Acad Sci U S A* 112(35): 10914-10919.
- Ratcliff, G. C. and D. A. Erie (2001). "A novel single-molecule study to determine protein--protein association constants." *Journal of the American Chemical Society* 123(24): 5632-5635.
- Sacho, E. J., F. A. Kadyrov, P. Modrich, T. A. Kunkel and D. A. Erie (2008). "Direct visualization of asymmetric adenine-nucleotide-induced conformational changes in MutL alpha." *Molecular cell* 29(1): 112-121.
- Schofield, M. J., S. Nayak, T. H. Scott, C. Du and P. Hsieh (2001). "Interaction of Escherichia coli MutS and MutL at a DNA mismatch." *J Biol Chem* 276(30): 28291-28299.
- van Oers, J. M., S. Roa, U. Werling, Y. Liu, J. Genschel, H. Hou, Jr., R. S. Sellers, P. Modrich, M. D. Scharff and W. Edelmann (2010). "PMS2 endonuclease activity has distinct biological functions and is essential for genome maintenance." *Proc Natl Acad Sci U S A* 107(30): 13384-13389.
- Wang, H., Y. Yang, M. J. Schofield, C. Du, Y. Fridman, S. D. Lee, E. D. Larson, J. T. Drummond, E. Alani, P. Hsieh and D. A. Erie (2003). "DNA bending and unbending by MutS govern mismatch recognition and specificity." *Proc Natl Acad Sci U S A* 100(25): 14822-14827.
- Warren, J. J., T. J. Pohlhaus, A. Changela, R. R. Iyer, P. L. Modrich and L. S. Beese (2007). "Structure of the human MutSalph DNA lesion recognition complex." *Mol Cell* 26(4): 579-592.
- Yang, Y., H. Wang and D. A. Erie (2003). "Quantitative characterization of biomolecular assemblies and interactions using atomic force microscopy." *Methods* 29(2): 175-187.

CHAPTER 3: INVESTIGATION OF THE ROLE OF ATP HYDROLYSIS IN MUTSA MOBILE CLAMP FORMATION AND MOVEMENT: AN AFM STUDY WITH ATP γ S

Introduction

DNA mismatch repair (MMR) is a highly conserved process that repairs misincorporated bases that arise during DNA replication (Kunkel and Erie 2005, Iyer, Pluciennik et al. 2006, Hsieh and Yamane 2008, Erie and Weninger 2014). MMR contributes greatly to genome stability and maintenance, and the loss of MMR results in increasing spontaneous mutation rates and cancer, such as hereditary non-polyposis colorectal cancer in humans (Hsieh and Yamane 2008).

The post-replicative process of MMR is initiated when the heterodimer, MSH2-MSH6 (MutS α) recognizes and binds to a mismatch (Kunkel and Erie 2005, Iyer, Pluciennik et al. 2006, Hsieh and Yamane 2008, Erie and Weninger 2014). MutS α then undergoes ATP-conformational dependent change(s) in to a mobile clamp that allows it to interact with other proteins and, together, facilitate the downstream events of MMR.

MutS α belongs to the ABC transporter family of ATPases, and the ATPase activities of MSH2 and MSH6 are essential for DNA repair (Kunkel and Erie 2005, Iyer, Pluciennik et al. 2006, Hsieh and Yamane 2008). However, the relative affinities for adenine nucleotides differ between MSH2 and MSH6, with MSH2 having a higher affinity for binding ADP, and MSH6 a higher affinity for ATP (Antony and Hingorani 2003, Bjornson and Modrich 2003, Martik, Baitinger et al. 2004, Antony, Khubchandani et al. 2006, Mazur, Mendillo et al. 2006). Studies

have also shown a cooperative adenine nucleotide binding effect, such that when MSH6 binds ATP, MSH2 more readily exchanges ADP for ATP (Mazur, Mendillo et al. 2006).

It is well established that upon mismatch binding, MutS α undergoes an ATP-conformational dependent change(s) to form a mobile sliding clamp (Blackwell, Martik et al. 1998, Blackwell, Bjornson et al. 2001, Acharya, Foster et al. 2003, Jeong, Cho et al. 2011, Qiu, DeRocco et al. 2012). It is not known, however, the role ATP hydrolysis plays in the formation or movement of the mobile clamp. Additionally, it is not well understood how the differing affinities of the two ATPase sites of MutS α for ATP contribute to the formation and movement of the mobile clamp.

There is much debate in the field on the role of ATP hydrolysis in mobile clamp formation and movement. Some studies indicate that ATP hydrolysis is not needed for the formation of MutS α mobile clamps along the DNA (Acharya, Wilson et al. 1996, Gradia, Subramanian et al. 1999, Schofield, Nayak et al. 2001). Because these studies used short DNA substrates, it remains unclear if ATP hydrolysis is needed for MutS(α) mobile clamps to travel distances longer DNA fragments (Erie and Weninger 2014). Other studies found that MutS α failed to form long-lived mobile clamps in the presence of slow hydrolyzing (ATP γ S) or non-hydrolyzable ATP analogs (AMPPNP) (Blackwell, Martik et al. 1998). Further studies using a mutant form of MutS α capable of binding but not hydrolyze ATP showed the formation of a long lived mobile clamp (Iaccarino, Marra et al. 2000).

In this study, we examine the role of ATP hydrolysis in the formation and position of MutS α mobile clamps by using atomic force microscopy (AFM) to determine the position, stoichiometry, and conformation of MutS α -DNA complexes in the presence of ATP γ S and a combination of ATP γ S and ADP. AFM is a single-molecule technique that can directly visualize

these complexes bound to DNA. The resulting images can be analyzed to find the position of MutS α complexes on the DNA relative to a mismatch, the volumes of complexes to estimate stoichiometries of proteins within these complexes, and changes in the conformation of complexes in the two different adenine nucleotide conditions. Using these data, we are able to distinguish between MutS α that formed mobile clamps from MutS α complexes that are localized to the mismatch by measuring the position of these complexes along the DNA. We find that MutS α remains localized to the mismatch in both adenine nucleotide conditions studied, and that in the presence of ATP γ S, up to two MutS α are bound at the mismatch.

Materials and Methods

Protein expression and purification

Human MutS α (MutS α) was purified as previously described (Geng, Du et al. 2011, Geng, Sakato et al. 2012), and generously provided to us by Dr. Peggy Hsieh (NIDDK, Bethesda, MD).

DNA substrate preparation

We modified a pSCW02 plasmid to produce the Guanine-Thymine–DNA (GT–DNA) substrates that were used for AFM as done previously (Geng, Du et al. 2011, Geng, Sakato et al. 2012). To create linear GT–DNA or linear GC–DNA (using unmodified pSCW02 DNA), the plasmid was linearized using the endonuclease XmnI, which cut the DNA such that the mismatch was 124 nm from one end. This plasmid and DNA substrates were made by Dr. Chunwei Du and generously provided to us by Dr. Peggy Hsieh (NIDDK, Bethesda, MD).

Sample preparation and deposition

Freshly cleaved ruby mica (Spruce Pine Mica Company, Spruce Pine, NC) were incubated with 30 microliters of (3-aminopropyl)triethoxysilane (APTES) on a piece of parafilm for 15 minutes in a desiccator to modify the mica surface to facilitate DNA deposition. hMutS α was diluted to a concentration of 125 nM with 100 μ M ATP γ S or with 50 μ M ATP γ S and 50 μ M ADP and incubated with 1 ng/ μ l of the DNA substrate for 2 minutes at room temperature in imaging buffer (25 mM HEPES, pH 7.5, 100 mM NaOAc, 10 mM Mg(OAc)₂, 1 mM DTT, 5% glycerol) in a total volume of 20 microliters. The protein–DNA samples were cross-linked with 0.85% glutaraldehyde for 1-5 minutes. Cross-linking conditions were minimized to prevent artifacts. Variable extents of cross-linking were observed for each experiment, but the relative populations of species were found to be independent of cross-linking efficiency. These cross-linked samples were filtered through a 4% agarose bead gel filtration column prior to deposition to remove excess free proteins. Fractions were collected from the filtration column and deposited onto the APTES-treated mica, rinsed with water, blotted dry, and then dried under a stream of nitrogen before imaging.

Imaging

The images were captured in air with a Nanoscope IIIa and III (Digital Instruments, Santa Barbara, CA) microscope in tapping mode. Pointprobe Plus tapping mode silicon cantilevers (NANOSENSORS, Switzerland) with resonance frequencies from 146-236 kHz were used. The images were collected at a speed of 1.97 Hz, a size of 2 x 2 μ m, and at a resolution of 512 x 512 pixels.

Image Analysis

A combination of NIH ImageJ64 (Rasband, with NeuronJ plug-in) software, Nanoscope III v5.3 software (Veeco, Santa Barbara, CA), and ImageSXM v1.95 software were used to measure the volumes of the complexes on the DNA, the DNA contour lengths, and the position of the proteins on the DNA. The KaleidaGraph program (Synergy Software, Reading, PA) was used to generate statistical plots for each data set. For each data set, images from two to three independent experiments were analyzed, compared, and pooled. Volume analysis was performed as previously described using ImageSXM v 1.95 (Ratcliff and Erie 2001, Wang, Yang et al. 2003, Yang, Wang et al. 2003, Sacho, Kadyrov et al. 2008). DNA contour length and position analysis for hMutS α alone experiments were done as previously described using ImageJ64 software (Wang, Yang et al. 2003).

Results

In the presence of ATP γ S, up to two MutS α bind the mismatch

To investigate the role of ATP hydrolysis in MutS α mobile clamp formation, we examined the properties of MutS α bound to a 2 kb DNA fragment that contained a single guanine-thymine mismatch 375 bp from one end (GT-DNA) in the presence of 100 μ M ATP γ S. Because we know the position of the mismatch on the DNA, we can determine whether the MutS α complexes are bound at the mismatch (specific complex) or at homoduplex sites (nonspecific complex) by measuring the distance of the complex from the ends of the DNA fragments. In addition, because the volumes of the protein complexes in AFM images are linearly dependent on their molecular weight, analyzing the volumes allows us to estimate the number of proteins within each complex (Ratcliff and Erie 2001, Yang, Wang et al. 2003).

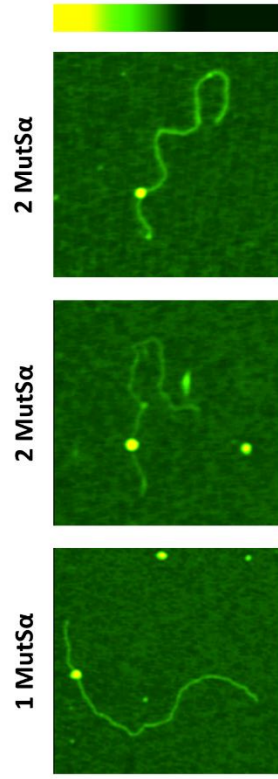
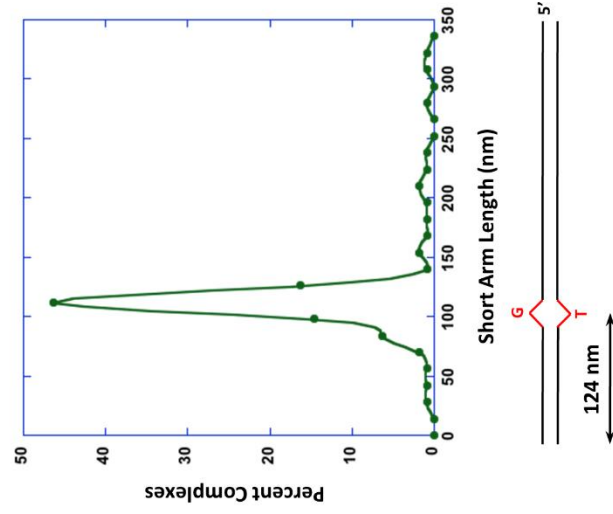
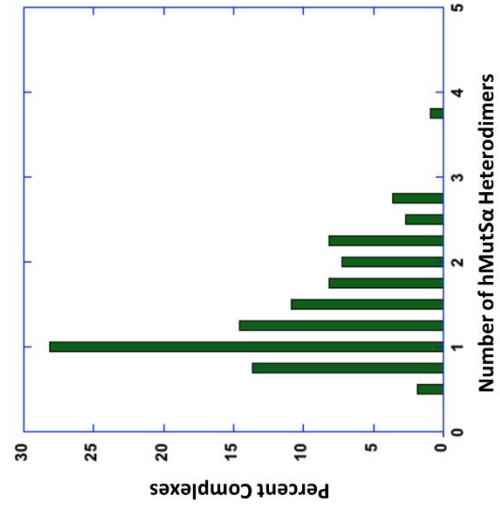
A**B****C**

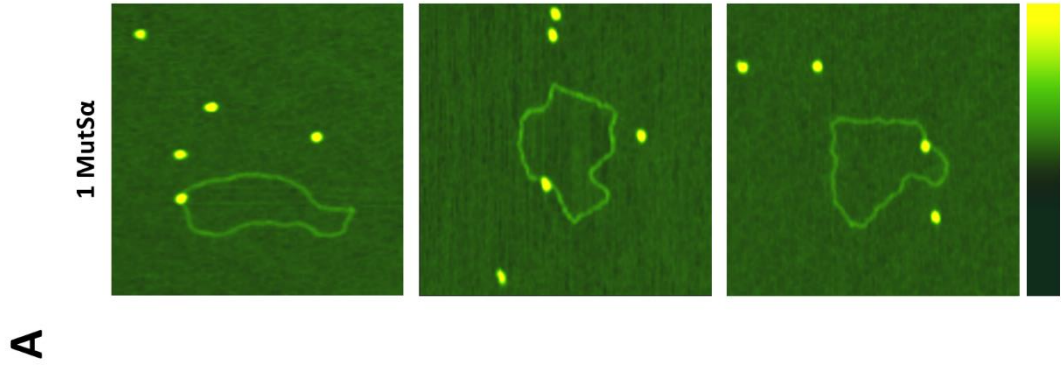
Figure 3.1 : AFM images and analysis of MutS α bound to GT-DNA in the presence of ATP γ S

(A) Representative AFM images of MutS α bound to the mismatch in the presence of 100 μ M ATP γ S. The first panel shows one MutS α protein bound, the other two panels show two MutS α proteins bound to the DNA. (B) Distribution of positions of MutS α complexes on GT-DNA in the presence of 100 μ M ATP γ S. The peak is centered at 124 nm, which is consistent with the position of the GT mismatch. (C) Distribution of the number of MutS α bound to the mismatch in the presence of 100 μ M ATP γ S. The histogram shows one or two MutS α were in each complex bound to the DNA.

Figure 3.1A shows representative AFM images of MutS α bound to GT-DNA in the presence of ATP γ S. The vast majority of bound DNA molecules contained a single complex (93%, $n = 117$) of MutS α . Examination of the distribution of positions of MutS α bound to GT-DNA reveals a peak centered at the position of the mismatch (Figure 3.1B, green line). Analysis of the positions of MutS α on GT-DNA reveals that the majority of MutS α are bound at the mismatch in the presence of ATP γ S ($n = 110$, 86% are within two standard deviations of the mismatch). This high specificity is not surprising given the high binding affinity of MutS α for a GT mismatch (Martik, Baitinger et al. 2004).

To determine the stoichiometry of MutS α , we examined the volumes of MutS α complexes bound at the mismatch (Figure 3.1C). Unexpectedly, only 54% of complexes contained a single MutS α while 43% contained 2 or more MutS α ($n = 110$). These data differ from previous AFM studies where we observed, in the presence of ADP, primarily 1 MutS α in each mismatch-bound complex; but yet are similar to results in the presence of ATP we observed volumes consistent with 1, 2, and 3 MutS α in each mismatch-bound complex (see Chapter 2). These data suggest that more than 1 MutS α is able to associate with the DNA in a single complex located at the GT-mismatch.

To investigate the possibility that mobile clamps of MutS α were sliding off of the free ends of the linear DNA in the presence of ATP γ S, we repeated the experiment using a covalently closed circular plasmid with a single GT-mismatch. Figure 3.2A shows sample AFM images of MutS α bound to circular GT-DNA. Figure 3.2B shows that, similarly to the linear GT-DNA data, the majority (89%, $n = 373$) of bound molecules to have one MutS α complex bound). Closer examination of these DNA-bound MutS α complexes reveals that the majority of these complexes



B

DNA Type	1 Complex	2+ Complexes
Linear GT–DNA ($n = 107$)	93%	7%
Circular GT– DNA ($n= 373$)	89%	11%

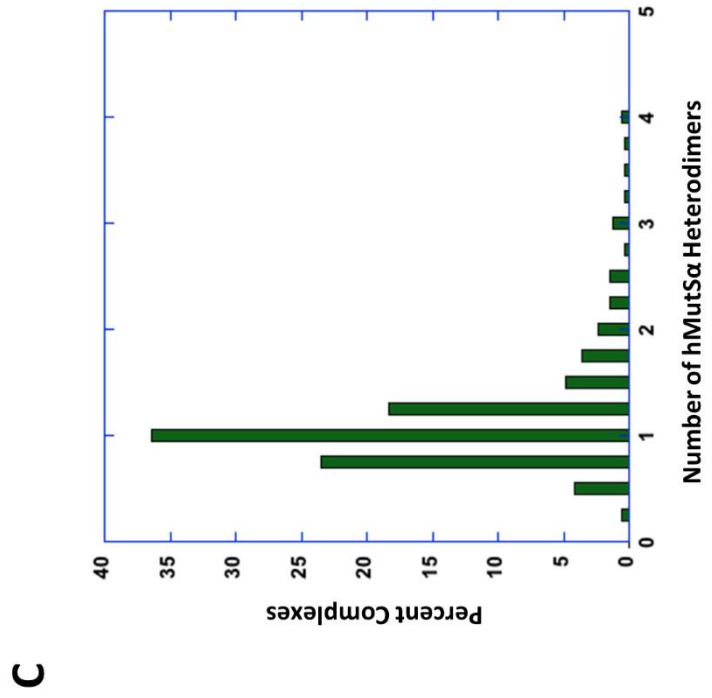


Figure 3.2 : AFM images and analysis of MutS α bound to circular GT–DNA in the presence of ATP γ S

(A) Representative images of MutS α bound to circular GT–DNA in the presence of 100 μ M ATP γ S. All panels show one MutS α bound. (B) Table comparing the number of complexes observed on the DNA between the linear and circular GT–DNA. (C) Distribution of the number of MutS α bound to the circular GT–DNA in the presence of 100 μ M ATP γ S. The histogram shows primarily one MutS α were in each complex bound to the DNA.

have volumes consistent with 1 MutS α (82%, n = 332), shown in Figure 3.2C. These data suggest that multiple MutS α are not being loaded on and then sliding off of the free ends in the linear GT–DNA experiments and are instead forming multimers at the mismatch.

In the presence of ATP γ S and ADP, one MutS α binds the mismatch

We next examined how the differing affinities of MSH2 and MSH6 for ADP and ATP affected mobile clamp formation and movement. Because MutS α readily hydrolyzes ATP (Kunkel and Erie 2005), we utilized the slowly hydrolyzing ATP-analog, ATP γ S, in equal concentrations with ADP to observe how MutS α mobile clamp behavior changes. Figure 3.3A shows representative AFM images of MutS α bound to GT–DNA in the presence of ATP γ S and ADP. The majority of bound DNA molecules contained a single complex (87%, n = 138) of MutS α . Examination of the distribution of positions of MutS α bound to GT–DNA reveals a peak centered at the position of the mismatch (Figure 3.3B, orange line). Analysis of the positions of MutS α on GT–DNA reveals that the majority of MutS α are bound at the mismatch in the presence of ATP γ S and ADP (n = 120, 89% are within two standard deviations of the mismatch). Again, this high specificity is not surprising given the high binding affinity of MutS α for a GT mismatch in the presence of different adenine nucleotides (Martik, Baitinger et al. 2004). We then examined the volumes of MutS α complexes at the mismatch (Figure 3.3C), and observed that the majority, 79% (n = 107) of complexes, contained a single MutS α heterodimer. These data are similar to previous data done in the presence of ADP, in which we observed 1 MutS α in each complex.

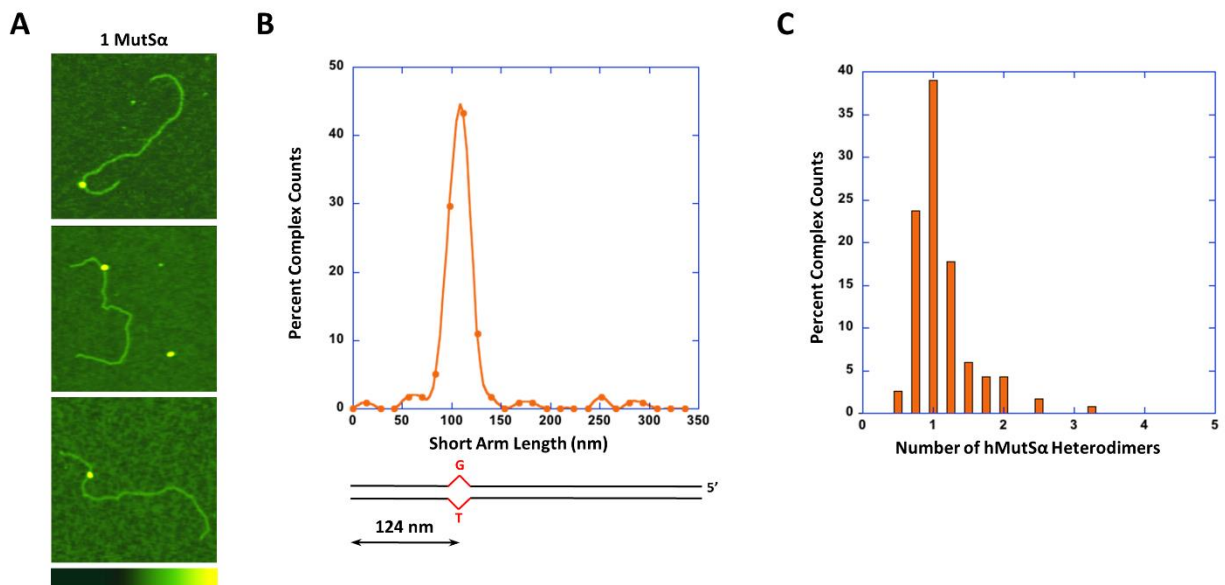


Figure 3.3 : AFM images and analysis of MutS α bound to GT-DNA in the presence of ATP γ S and ADP

(A) Representative example images of MutS α bound to the mismatch in the presence of 50 μ M ATP γ S and 50 μ M ADP. All panels show one MutS α protein bound. (B) Distribution of positions of MutS α complexes on GT-DNA in the presence of 50 μ M ATP γ S and 50 μ M ADP. The peak is centered at 124 nm, which is consistent with the position of the GT mismatch. (C) Distribution of the number of MutS α bound to the mismatch in the presence of 50 μ M ATP γ S and 50 μ M ADP. The histogram shows one MutS α was in each complex bound to the DNA.

Discussion

Previous studies have shown that in the presence of ATP, the mobile clamp state of MutS α will clear the mismatch, allowing a second MutS α to recognize and bind to the mismatch. Once a second MutS α has loaded on the mismatch, the original mobile clamp MutS α will associate with the newly mismatch-bound MutS α and form a larger complex, typically located at the mismatch. We hypothesize this larger complex is to help promote association with MutL α , the next protein to interact in the MMR pathway.

ATP γ S is a slowly hydrolyzing substrate, meaning that if the mobile clamp movement of MutS α is dependent on ATP hydrolysis we would expect to see one MutS α at the site of the GT-mismatch. In this study, we observed the majority of MutS α are bound to the mismatch in the presence of ATP γ S. However, we also observe an intermediate number of proteins in these complexes than what we observed in previous AFM studies in the presence of either ADP or ATP. A possible explanation for these differences could be that while ATP γ S is slowly hydrolyzable, it is conceivable that a small population of it was hydrolyzed during the initial recognition of the GT-mismatch. Once MutS α bound to the mismatch, it underwent an ATP γ S-induced conformational change into the mobile clamp, and moved away from the mismatch to allow for another MutS α to be loaded on, which would explain the population of two MutS α proteins that we observed. However, because ATP γ S is not as readily hydrolyzable as ATP, these complexes will be smaller than what we observed in the ATP conditions.

Another consideration to take into account is the relative affinities of MSH2 and MSH6 for each type of adenine nucleotide because these differing affinities could impact MutS α mobile clamp formation. Previous studies have shown that MSH2 has a higher affinity for ADP and MSH6 has a higher affinity for ATP (Antony and Hingorani 2003, Bjornson and Modrich 2003,

Martik, Baitinger et al. 2004, Antony, Khubchandani et al. 2006, Mazur, Mendillo et al. 2006). The affinity of yeast Msh2 for ATP is $\sim 37 \mu\text{M}$, in contrast to the affinity of Msh2 for ADP, which is $1.4 \mu\text{M}$. However, once Msh6 binds ATP, it lowers the affinity of Msh2 for ADP, and thus allows for ATP to bind in the Msh2 subunit (Mazur, Mendillo et al. 2006). The lowering of MSH6-ATP of MSH2 for ADP was also observed in the human proteins (Heinen, Cyr et al. 2011). Additionally, studies have suggested that the mobile clamp state is formed when ATP occupies both subunits of MutS α (Heinen, Cyr et al. 2011, Qiu, DeRocco et al. 2012). At the nucleotide concentrations of these experiments ($100 \mu\text{M}$ of adenine nucleotide), it is possible that the rate of ADP–ATP exchange in the subunit of MSH2 is being affected such that MutS α lingers on the mismatch. Once the first MutS α has formed a mobile clamp and moved away, there is a higher probability of it interacting with a long-lived state of MutS α that is localized to the mismatch. We have already noted in previous AFM experiments done with ATP that upon forming a mobile clamp MutS α becomes “sticky”; that is can associate with other MutS α proteins (see Chapter 2). Therefore, in these experiments we observe MutS α forming multimers at the mismatch because we have created a higher probability of MutS α mobile clamps interacting with MutS α that linger at the mismatch. The reason why we did not observe these results in the ATP γ S and ADP experiments could simply be because the adenine nucleotide concentrations were too low to allow for the MSH2 subunit to exchange ADP for ATP.

Future Directions

Future work should incubate MutS α in the presence of 1 mM ATP γ S for 5 minutes on both linear and circular GT–DNA to discover if mobile clamp formation and movement is dependent on ATP-hydrolysis. AFM studies with higher concentrations of ATP with a longer (5 minute) incubation time resulted in the formation of large complexes containing multiple MutS α

on circular GT-DNA, and revealed on linear GT-DNA that multiple (up to 3) MutS α could be loaded onto linear GT-DNA without being associated together. These data suggest that working at an adenine concentration of 100 μ M may be limiting the exchange of ADP to ATP of MSH2.

REFERENCES

- Acharya, S., P. L. Foster, P. Brooks and R. Fishel (2003). "The coordinated functions of the E. coli MutS and MutL proteins in mismatch repair." Mol Cell **12**(1): 233-246.
- Acharya, S., T. Wilson, S. Gradia, M. F. Kane, S. Guerrette, G. T. Marsischky, R. Kolodner and R. Fishel (1996). "hMSH2 forms specific mispair-binding complexes with hMSH3 and hMSH6." Proc Natl Acad Sci U S A **93**(24): 13629-13634.
- Antony, E. and M. M. Hingorani (2003). "Mismatch recognition-coupled stabilization of Msh2-Msh6 in an ATP-bound state at the initiation of DNA repair." Biochemistry **42**(25): 7682-7693.
- Antony, E., S. Khubchandani, S. Chen and M. M. Hingorani (2006). "Contribution of Msh2 and Msh6 subunits to the asymmetric ATPase and DNA mismatch binding activities of *Saccharomyces cerevisiae* Msh2-Msh6 mismatch repair protein." DNA Repair (Amst) **5**(2): 153-162.
- Bjornson, K. P. and P. Modrich (2003). "Differential and simultaneous adenosine di- and triphosphate binding by MutS." J Biol Chem **278**(20): 18557-18562.
- Blackwell, L. J., K. P. Bjornson, D. J. Allen and P. Modrich (2001). "Distinct MutS DNA-binding modes that are differentially modulated by ATP binding and hydrolysis." J Biol Chem **276**(36): 34339-34347.
- Blackwell, L. J., D. Martik, K. P. Bjornson, E. S. Bjornson and P. Modrich (1998). "Nucleotide-promoted release of hMutSalph from heteroduplex DNA is consistent with an ATP-dependent translocation mechanism." J Biol Chem **273**(48): 32055-32062.
- Erie, D. A. and K. R. Weninger (2014). "Single molecule studies of DNA mismatch repair." DNA Repair (Amst) **20**: 71-81.
- Geng, H., C. Du, S. Chen, V. Salerno, C. Manfredi and P. Hsieh (2011). "In vitro studies of DNA mismatch repair proteins." Anal Biochem **413**(2): 179-184.
- Geng, H., M. Sakato, V. DeRocco, K. Yamane, C. Du, D. A. Erie, M. Hingorani and P. Hsieh (2012). "Biochemical analysis of the human mismatch repair proteins hMutSalph MSH2(G674A)-MSH6 and MSH2-MSH6(T1219D)." J Biol Chem **287**(13): 9777-9791.
- Gradia, S., D. Subramanian, T. Wilson, S. Acharya, A. Makhov, J. Griffith and R. Fishel (1999). "hMSH2-hMSH6 forms a hydrolysis-independent sliding clamp on mismatched DNA." Mol Cell **3**(2): 255-261.
- Heinen, C. D., J. L. Cyr, C. Cook, N. Punja, M. Sakato, R. A. Forties, J. M. Lopez, M. M. Hingorani and R. Fishel (2011). "Human MSH2 (hMSH2) protein controls ATP processing by hMSH2-hMSH6." J Biol Chem **286**(46): 40287-40295.

- Hsieh, P. and K. Yamane (2008). "DNA mismatch repair: molecular mechanism, cancer, and ageing." Mech Ageing Dev **129**(7-8): 391-407.
- Iaccarino, I., G. Marra, P. Dufner and J. Jiricny (2000). "Mutation in the magnesium binding site of hMSH6 disables the hMutSalphalpha sliding clamp from translocating along DNA." J Biol Chem **275**(3): 2080-2086.
- Iyer, R. R., A. Pluciennik, V. Burdett and P. L. Modrich (2006). "DNA mismatch repair: functions and mechanisms." Chemical reviews **106**(2): 302-323.
- Jeong, C., W. K. Cho, K. M. Song, C. Cook, T. Y. Yoon, C. Ban, R. Fishel and J. B. Lee (2011). "MutS switches between two fundamentally distinct clamps during mismatch repair." Nat Struct Mol Biol **18**(3): 379-385.
- Kunkel, T. A. and D. A. Erie (2005). "DNA mismatch repair." Annu Rev Biochem **74**: 681-710.
- Martik, D., C. Baitinger and P. Modrich (2004). "Differential specificities and simultaneous occupancy of human MutSalphalpha nucleotide binding sites." J Biol Chem **279**(27): 28402-28410.
- Mazur, D. J., M. L. Mendillo and R. D. Kolodner (2006). "Inhibition of Msh6 ATPase activity by mispaired DNA induces a Msh2(ATP)-Msh6(ATP) state capable of hydrolysis-independent movement along DNA." Mol Cell **22**(1): 39-49.
- Qiu, R., V. C. DeRocco, C. Harris, A. Sharma, M. M. Hingorani, D. A. Erie and K. R. Weninger (2012). "Large conformational changes in MutS during DNA scanning, mismatch recognition and repair signalling." EMBO J **31**(11): 2528-2540.
- Ratcliff, G. C. and D. A. Erie (2001). "A novel single-molecule study to determine protein--protein association constants." Journal of the American Chemical Society **123**(24): 5632-5635.
- Sacho, E. J., F. A. Kadyrov, P. Modrich, T. A. Kunkel and D. A. Erie (2008). "Direct visualization of asymmetric adenine-nucleotide-induced conformational changes in MutL alpha." Molecular cell **29**(1): 112-121.
- Schofield, M. J., S. Nayak, T. H. Scott, C. Du and P. Hsieh (2001). "Interaction of Escherichia coli MutS and MutL at a DNA mismatch." J Biol Chem **276**(30): 28291-28299.
- Wang, H., Y. Yang, M. J. Schofield, C. Du, Y. Fridman, S. D. Lee, E. D. Larson, J. T. Drummond, E. Alani, P. Hsieh and D. A. Erie (2003). "DNA bending and unbending by MutS govern mismatch recognition and specificity." Proc Natl Acad Sci U S A **100**(25): 14822-14827.
- Yang, Y., H. Wang and D. A. Erie (2003). "Quantitative characterization of biomolecular assemblies and interactions using atomic force microscopy." Methods **29**(2): 175-187.

- Acharya, S., P. L. Foster, P. Brooks and R. Fishel (2003). "The coordinated functions of the E. coli MutS and MutL proteins in mismatch repair." Mol Cell **12**(1): 233-246.
- Acharya, S., T. Wilson, S. Gradia, M. F. Kane, S. Guerrette, G. T. Marsischky, R. Kolodner and R. Fishel (1996). "hMSH2 forms specific mispair-binding complexes with hMSH3 and hMSH6." Proc Natl Acad Sci U S A **93**(24): 13629-13634.
- Antony, E. and M. M. Hingorani (2003). "Mismatch recognition-coupled stabilization of Msh2-Msh6 in an ATP-bound state at the initiation of DNA repair." Biochemistry **42**(25): 7682-7693.
- Antony, E., S. Khubchandani, S. Chen and M. M. Hingorani (2006). "Contribution of Msh2 and Msh6 subunits to the asymmetric ATPase and DNA mismatch binding activities of *Saccharomyces cerevisiae* Msh2-Msh6 mismatch repair protein." DNA Repair (Amst) **5**(2): 153-162.
- Bjornson, K. P. and P. Modrich (2003). "Differential and simultaneous adenosine di- and triphosphate binding by MutS." J Biol Chem **278**(20): 18557-18562.
- Blackwell, L. J., K. P. Bjornson, D. J. Allen and P. Modrich (2001). "Distinct MutS DNA-binding modes that are differentially modulated by ATP binding and hydrolysis." J Biol Chem **276**(36): 34339-34347.
- Blackwell, L. J., D. Martik, K. P. Bjornson, E. S. Bjornson and P. Modrich (1998). "Nucleotide-promoted release of hMutSalph from heteroduplex DNA is consistent with an ATP-dependent translocation mechanism." J Biol Chem **273**(48): 32055-32062.
- Erie, D. A. and K. R. Weninger (2014). "Single molecule studies of DNA mismatch repair." DNA Repair (Amst) **20**: 71-81.
- Geng, H., C. Du, S. Chen, V. Salerno, C. Manfredi and P. Hsieh (2011). "In vitro studies of DNA mismatch repair proteins." Anal Biochem **413**(2): 179-184.
- Geng, H., M. Sakato, V. DeRocco, K. Yamane, C. Du, D. A. Erie, M. Hingorani and P. Hsieh (2012). "Biochemical analysis of the human mismatch repair proteins hMutSalph MSH2(G674A)-MSH6 and MSH2-MSH6(T1219D)." J Biol Chem **287**(13): 9777-9791.
- Gradia, S., D. Subramanian, T. Wilson, S. Acharya, A. Makhov, J. Griffith and R. Fishel (1999). "hMSH2-hMSH6 forms a hydrolysis-independent sliding clamp on mismatched DNA." Mol Cell **3**(2): 255-261.
- Heinen, C. D., J. L. Cyr, C. Cook, N. Punja, M. Sakato, R. A. Forties, J. M. Lopez, M. M. Hingorani and R. Fishel (2011). "Human MSH2 (hMSH2) protein controls ATP processing by hMSH2-hMSH6." J Biol Chem **286**(46): 40287-40295.
- Hsieh, P. and K. Yamane (2008). "DNA mismatch repair: molecular mechanism, cancer, and ageing." Mech Ageing Dev **129**(7-8): 391-407.

- Iaccarino, I., G. Marra, P. Dufner and J. Jiricny (2000). "Mutation in the magnesium binding site of hMSH6 disables the hMutSalpha sliding clamp from translocating along DNA." J Biol Chem **275**(3): 2080-2086.
- Iyer, R. R., A. Pluciennik, V. Burdett and P. L. Modrich (2006). "DNA mismatch repair: functions and mechanisms." Chemical reviews **106**(2): 302-323.
- Jeong, C., W. K. Cho, K. M. Song, C. Cook, T. Y. Yoon, C. Ban, R. Fishel and J. B. Lee (2011). "MutS switches between two fundamentally distinct clamps during mismatch repair." Nat Struct Mol Biol **18**(3): 379-385.
- Kunkel, T. A. and D. A. Erie (2005). "DNA mismatch repair." Annu Rev Biochem **74**: 681-710.
- Martik, D., C. Baitinger and P. Modrich (2004). "Differential specificities and simultaneous occupancy of human MutSalpha nucleotide binding sites." J Biol Chem **279**(27): 28402-28410.
- Mazur, D. J., M. L. Mendillo and R. D. Kolodner (2006). "Inhibition of Msh6 ATPase activity by mispaired DNA induces a Msh2(ATP)-Msh6(ATP) state capable of hydrolysis-independent movement along DNA." Mol Cell **22**(1): 39-49.
- Qiu, R., V. C. DeRocco, C. Harris, A. Sharma, M. M. Hingorani, D. A. Erie and K. R. Weninger (2012). "Large conformational changes in MutS during DNA scanning, mismatch recognition and repair signalling." EMBO J **31**(11): 2528-2540.
- Ratcliff, G. C. and D. A. Erie (2001). "A novel single-molecule study to determine protein--protein association constants." Journal of the American Chemical Society **123**(24): 5632-5635.
- Sacho, E. J., F. A. Kadyrov, P. Modrich, T. A. Kunkel and D. A. Erie (2008). "Direct visualization of asymmetric adenine-nucleotide-induced conformational changes in MutL alpha." Molecular cell **29**(1): 112-121.
- Schofield, M. J., S. Nayak, T. H. Scott, C. Du and P. Hsieh (2001). "Interaction of Escherichia coli MutS and MutL at a DNA mismatch." J Biol Chem **276**(30): 28291-28299.
- Wang, H., Y. Yang, M. J. Schofield, C. Du, Y. Fridman, S. D. Lee, E. D. Larson, J. T. Drummond, E. Alani, P. Hsieh and D. A. Erie (2003). "DNA bending and unbending by MutS govern mismatch recognition and specificity." Proc Natl Acad Sci U S A **100**(25): 14822-14827.
- Yang, Y., H. Wang and D. A. Erie (2003). "Quantitative characterization of biomolecular assemblies and interactions using atomic force microscopy." Methods **29**(2): 175-187.

CHAPTER 4: EXAMINATION OF THE EFFECT OF DIFFERENT ADENINE NUCLEOTIDES ON MUTS α -INDUCED DNA BENDING: AN AFM BEND ANGLE ANALYSIS STUDY

Introduction

DNA mismatch repair (MMR) is a highly conserved process that repairs misincorporated bases that arise during DNA replication (Kunkel and Erie 2005, Iyer, Pluciennik et al. 2006, Hsieh and Yamane 2008, Erie and Weninger 2014). MMR is important to genome stability and maintenance, and the loss of MMR results in increased spontaneous mutation rates and predisposition to cancer such as Lynch syndrome in humans (Hsieh and Yamane 2008).

In humans, MMR is initiated when the heterodimer, MSH2-MSH6 (MutS α) recognizes and binds to a mismatch (Kunkel and Erie 2005, Iyer, Pluciennik et al. 2006, Hsieh and Yamane 2008, Erie and Weninger 2014). MutS α then undergoes ATP-conformational dependent change(s) into a mobile clamp that allows it to interact with MutL α , and together they facilitate the downstream events of MMR. Previous evidence suggests that upon recognition of the mismatch, MutS homologs bend the DNA into some initial recognition complex; however, very little information exist on the human MutS α -DNA interaction complex (Obmolova, Ban et al. 2000, Yang, Wang et al. 2003, Qiu, DeRocco et al. 2012).

Some evidence for MutS-induced DNA bending come from AFM studies with *Thermus aquaticus* (*Taq*) and *Escherichia coli* (*E. coli*) MutS (Wang, Yang et al. 2003). These studies show that MutS induces a variety of bend angles on the DNA depending on the conformational state of MutS. When bound non-specifically to the DNA, *Taq* MutS induces an intermediate bend in the DNA during what is thought to be its searching mechanism, and upon recognizing a

mismatch, *Taq* MutS induces a “kink” or sharply bend the DNA. It will then produce an “unbent” DNA, which is proposed to be *Taq* MutS forming a mobile clamp, differing from the original “searching” clamp (Wang, Yang et al. 2003).

Crystal structures of human MutS α in complex with DNA containing a single guanine-thymine (GT) mismatch gave the first structural insight into the recognition of MutS α for a mismatch. This crystal structure shows that in domain 1 of MSH6, which interacts with the GT-mismatch, the Glu434 of the conserved Phe-X-Glu motif forms a hydrogen bond with the mispaired thymine, which is located between Phe432 and Met459 (Warren, Pohlhaus et al. 2007). In *Taq* MutS, contacts with domain 1 of the non-mismatch binding monomer have been hypothesized to contribute to DNA bending in the *Taq* MutS–DNA complexes (Obmolova, Ban et al. 2000); however, MSH2 does not make similar interactions. Interactions between MSH6 and the DNA substrate are thought to result in DNA bending, without any contribution from MSH2. The crystal structure shows MutS α induces a 45° kink in the DNA at the site of the mismatch with ADP bound in the ATPase sites (Warren, Pohlhaus et al. 2007). These experiments yielded the first structural insight into mismatch recognition by human MutS α ; however, there have been no crystal structures solved that depicts the human MutS α –ATP liganded state.

The goal of this study is to determine the DNA bend angle(s) of MutS α –DNA complexes in the presence of ADP, ATP, ATP γ S, and ATP γ S with ADP using AFM. The resulting images can be used to measure the MutS α –induced DNA bends at the mismatch and non-specifically along on the DNA. Using these data, we may be able to distinguish between MutS α complexes that have formed the mobile clamp state from MutS α complexes that are localized to the mismatch by measuring the position of these complexes along the DNA. We can identify which

of these complexes contain only one MutS α and then measure the MutS α –induced DNA bend angle when MutS α is located at the mismatch or is non–specifically bound to the DNA.

Using a variety of adenine nucleotides in the presence of homoduplex DNA (GC–DNA) or DNA containing a mismatch (GT–DNA), we aim to look for conformational differences of human MutS α by looking at the bend angles induced on the DNA. All bend angles were measured for complexes of MutS α containing a single protein on a GT–mismatch, unless otherwise noted. We also included bend angle analysis of single MutS α proteins bound to GC–DNA and non–specifically to GT–DNA to see how non–specific bending of MutS α differs from DNA bends induced at the GT–mismatch. Our results in ADP conditions are consistent with the crystal structure, and we observe a MutS α –induced DNA bend of 45°, although the distribution is broad. Upon the addition of ATP, we find that MutS α induces two distinct bend angles, suggesting that in the presence of ATP, MutS α undergoes several conformational changes, which we hypothesize will lead to different DNA bends. Our results suggest that DNA bending is important for initial mismatch recognition; however, the ability of MutS α to induce distinct DNA bends is dependent upon MutS α being located on the mismatch.

Materials and Methods

Protein expression and purification

Human MutS α (MutS α) was purified as previously described (Geng, Du et al. 2011, Geng, Sakato et al. 2012) and generously provided to us by Dr. Peggy Hsieh (NIDDK, Bethesda, MD).

DNA substrate preparation

We modified a pSCW02 plasmid to make the GT–DNA substrates that were used for AFM as done previously (Geng, Du et al. 2011, Geng, Sakato et al. 2012). To create linear GT–DNA or linear GC–DNA (using unmodified pSCW02 DNA), the plasmid was linearized using an endonuclease, Xmn1, which cuts the DNA such that the mismatch was 124 nm from one end. This plasmid and DNA substrates were made by Dr. Chunwei Du and generously provided to us by Dr. Peggy Hsieh (NIDDK, Bethesda, MD).

Sample preparation and deposition

Freshly cleaved ruby mica (Spruce Pine Mica Company, Spruce Pine, NC) was incubated in a desiccator with 30 microliters of (3–aminopropyl)triethoxysilane (APTES) on a piece of parafilm for 15 minutes to modify the mica surface for better DNA deposition. MutS α (125 nM) was incubated 1 ng/ μ l of the DNA substrate and 100 μ M ADP, 100 μ M ATP, 100 μ M ATP γ S or 50 μ M ATP γ S and 50 μ M ADP for 2 minutes at room temperature in imaging buffer (25 mM HEPES, pH 7.5, 100 mM NaOAc, 10 mM Mg(OAc) $_2$, 1 mM DTT, 5% glycerol) in a total volume of 20 microliters. The protein–DNA samples were cross–linked with 0.85% glutaraldehyde for 1–5 minutes. Cross–linking conditions were optimized to prevent artifacts. The extent of cross–linking was observed for each experiment, and the relative populations of species were found to be independent of cross–linking efficiency. These cross–linked samples were filtered through a 4% agarose bead gel filtration column prior to deposition to remove excess free proteins. Fractions were collected from the filtration column and deposited onto the APTES–treated mica, rinsed with water, blotted dry, and then dried under a stream of nitrogen before imaging.

Imaging

The images were captured in air with a Nanoscope IIIa and III (Digital Instruments, Santa Barbara, CA) microscope in tapping mode. Pointprobe Plus tapping mode silicon cantilevers (NANOSENSORS, Switzerland) with resonance frequencies from 146–236 kHz were used. The images were collected at a speed of 1.97 Hz, a scan size of 2 μm , and at a resolution of 512 x 512 pixels.

Image Analysis

Nanoscope III v5.3 software (Veeco, Santa Barbara, CA) was used to measure the MutS α –induced bend angle on the DNA. KaleidaGraph (Synergy Software, Reading, PA) was used to generate statistical plots for each data set. For each data set, 20 – 70 images from two to three independent experiments were analyzed, compared, and pooled.

MutS α complexes that were positioned at the mismatch, with the exception of homoduplex (GC–DNA), and had volumes consistent with one MutS α were analyzed for DNA bend angles. The position and volumes for each complex was measured as discussed previously in Chapter 2 and 3. MutS α –induced DNA bends were determined as shown in Figure 4.1. First, the direction of the short DNA arm as it enters the protein through the center of the complex is determined (Figure 4.1B). The line drawn out of the complex (Figure 4.1B) represents the

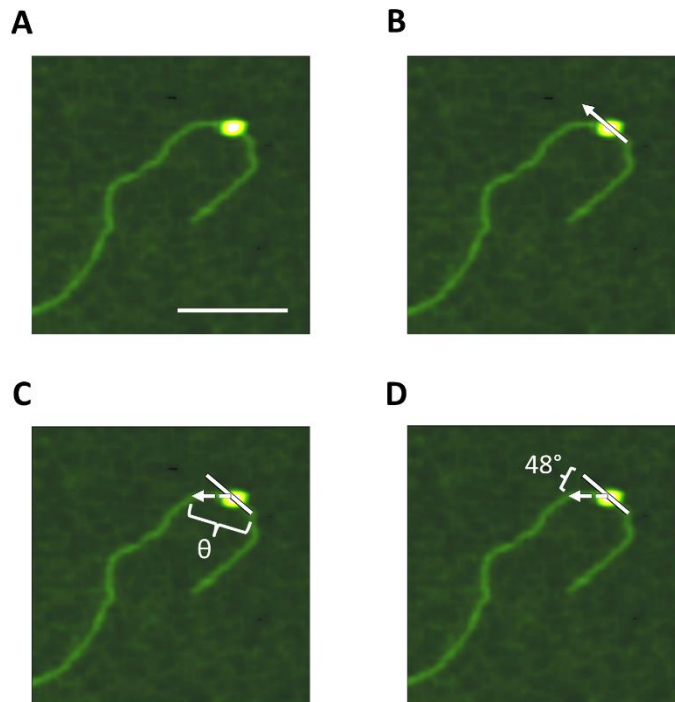


Figure 4.1 : AFM bend angle analysis

(A) Representative AFM image of MutS α bound to the mismatch in the presence of 100 μ M ADP. The image is 250 x 250 nm and the white scale bar is 100 nm. (B) A line (white arrow) is drawn as the DNA from the short arm side enters the protein complex. This line represents the path of the DNA molecule when it is not bent. (C) A second line (white dashed arrow) is drawn that traces the DNA from the center of the complex as it exits the complex. The angle of the DNA as it enters and exits the complex is θ . (D) The DNA bend angle is defined as the deviation of the DNA from the normal line (shown in panel B) and is found by subtracting $180^\circ - \theta$. For this sample image, the MutS α -induced DNA bend angle is 48° .

predicted path of the DNA in the absence of a MutS α -induced DNA bend. This is also referred as the “normal” line. Next, a line is drawn from the center of the complex and tracing the long arm of the DNA as it exits the complex (Figure 4.1C). The angle of the DNA as it enters and leaves the complex is θ (Figure 4.1C) and the MutS α -induced DNA bend angle is the deviation from “normal” and is defined as $180^\circ - \theta$ (Figure 4.1D).

Results

In the presence of ADP, MutS α at the mismatch bends the DNA at 45°

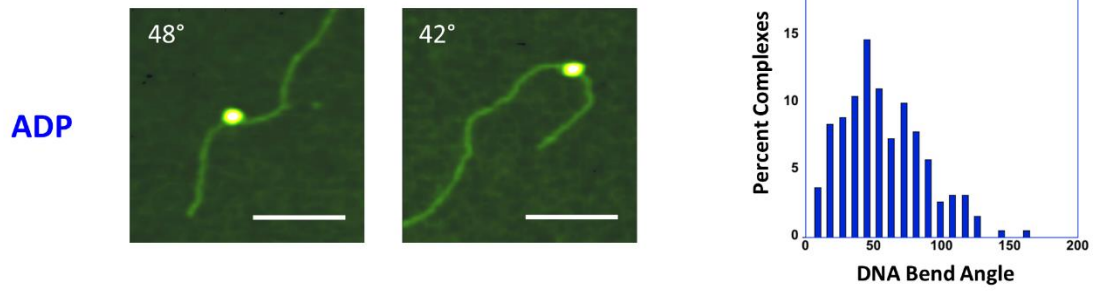
Previous MutS α crystal structure data showed that when liganded to ADP, MutS α induces a 45° bend at a GT-mismatch (Warren, Pohlhaus et al. 2007). We examined the DNA bend angle properties of MutS α bound to a 2 kb DNA fragment that contained a single GT-mismatch 375 bp from one end (GT-DNA) in the presence of 100 μ M ADP. Figure 4.2A shows sample AFM images with MutS α on the mismatch inducing DNA bend angles at approximately 45° (two left panels). Examination of the DNA bend angles of these mismatch-bound MutS α revealed a single broad peak centered around 45° . While our AFM data agree with previous data that suggest that MutS α exhibits a DNA bend of 45° at a mismatch site, the broad distribution around this bend angle implies that MutS α may induce a variety of DNA bends and/or is flexible at the mismatch.

To confirm that the 45° DNA bend angle was the result of MutS α bound to the mismatch in the presence of ADP, we conducted a similar experiment with MutS α and ADP utilizing GC–DNA. Examination of these complexes revealed that MutS α exhibited a broad range of DNA bend angles with a peak centered around 70° (Figure 4.3A). Comparison of the GT–DNA and GC–DNA bend angle distributions indicates a shift of the broad central GC–DNA peak towards a 45° bend angle in the presence of the mismatch. This result suggests that ADP and a mismatch are required for MutS α to induce a 45° DNA bend angle.

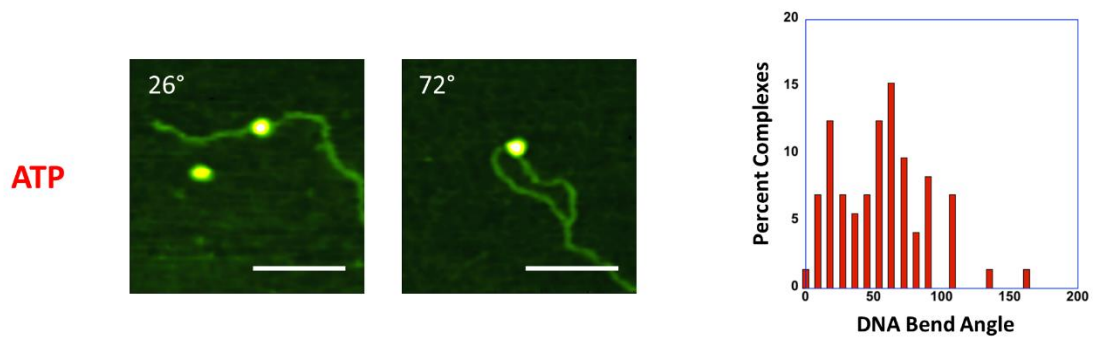
Mismatch-bound MutS α in the presence of ATP exhibits two DNA bend angles

ATP is known to induce a conformational change in MutS α to form a mobile clamp, we expected to observe DNA bend angles that were unbent or only slightly bent, consistent with the formation of the MutS α mobile clamp (Kunkel and Erie 2005, Iyer, Pluciennik et al. 2006, Hsieh and Yamane 2008). To determine the effects of ATP on MutS α -induced DNA bending, we incubated MutS α with GT–DNA and ATP. Figure 4.2B shows the bend angles of MutS α bound to the mismatch in the presence of ATP, and example images of the dominant DNA bend angles observed are shown (two left panels). Examination of these GT–bound MutS α complexes revealed two distinct peaks of DNA bend angles: the first at 20° and a second at 65°. The less bent 20° MutS α –induced DNA bend angle could represent the DNA bend angle associated with the MutS α mobile clamp. The 65° DNA bend angle could be consistent with the conformation of MutS α when it undergoes ADP–ATP exchange (Qiu, DeRocco et al. 2012). These AFM data suggest that MutS α undergoes several

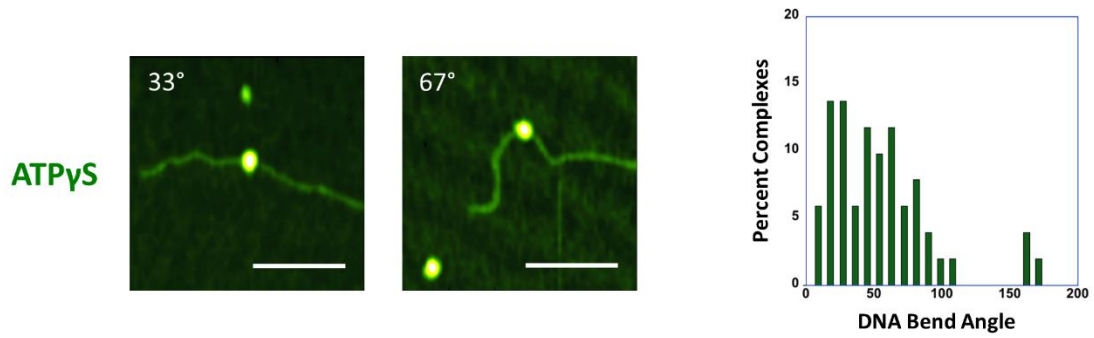
A



B



C



D

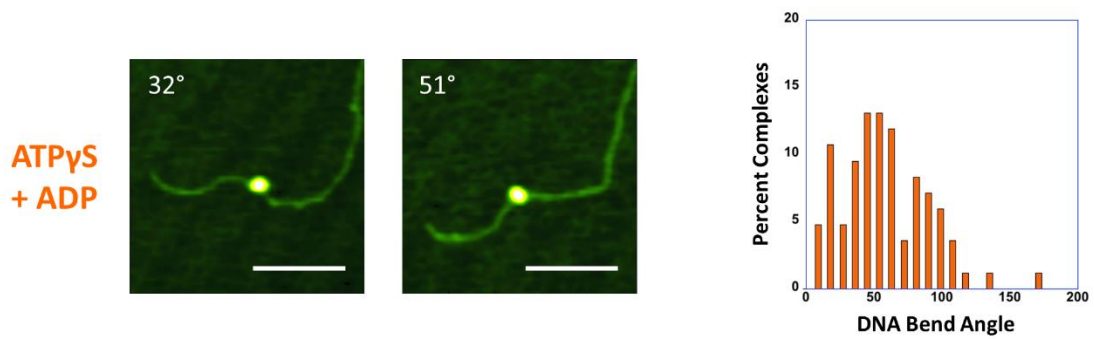


Figure 4.2 : MutS α -induced GT-DNA bend angles in the presence of various adenine nucleotides

For all rows: right, two panels show sample images of MutS α bound to the mismatch. Numbers in top left corner indicate DNA bend angles. Images are 250 x 250 nm and white scale bars are 100 nm. (A) MutS α bound to the mismatch in the presence of 100 μ M ADP (n = 190). Sample images have DNA bend angles at $\sim 45^\circ$. Histogram shows a broad distribution of DNA bend angles with a peak that centers at 45° . (B) MutS α bound to the mismatch in the presence of 100 μ M ATP (n = 74). Sample images have two different DNA bend angles. Histogram shows two DNA bend angle peaks, one at 20° and 65° . (C) MutS α bound to the mismatch in the presence of 100 μ M ATP γ S (n = 51). Sample images display similar DNA bend angles to the ATP images. Histogram shows similar distribution of peaks to ATP histogram: 20° , 55° , and 80° . (D) MutS α bound to the mismatch in the presence of 50 μ M ATP γ S and 50 μ M ADP (n = 84). Sample images have different DNA bend angles. Histogram of DNA bend angles shows three broad peaks that center on: 20° , 50° , and 90° .

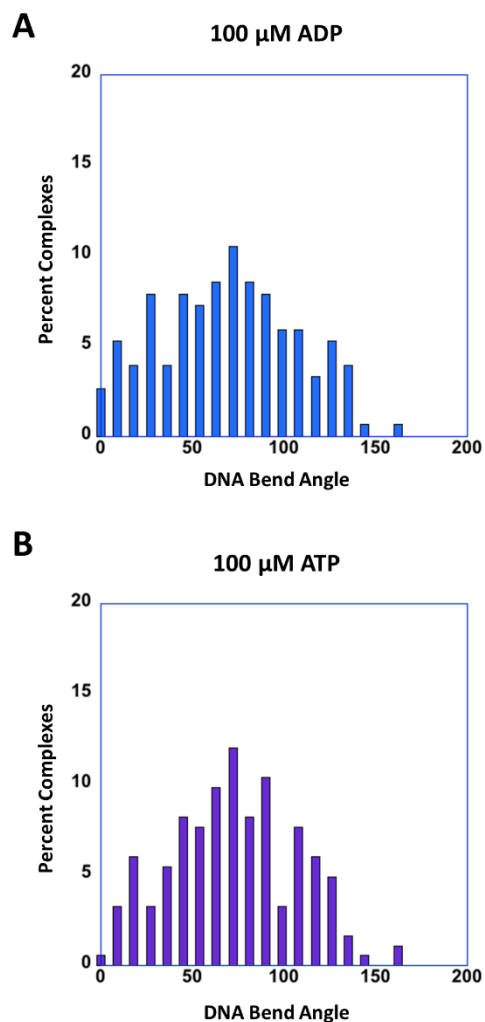


Figure 4.3 : MutS α -induced GC-DNA bend angles

(A) MutS α -induced DNA bend angles on GC-DNA in the presence of 100 μ M ADP (n = 152).

Histogram shows a broad angle distribution with a peak centered on $\sim 70^\circ$.

(B) MutS α -induced DNA bend angles on GC-DNA in the presence of 100 μ M ATP (n = 183).

Histogram shows a broad angle distribution with a peak centered on $\sim 70^\circ$.

conformational changes in the presence of ATP, and these conformations induce distinct bends in the DNA that differ from what was observed with ADP.

In the presence of ATP, we also observed a population of MutS α that were bound non-specifically on the GT-DNA, suggesting that mobile clamp formation and movement had occurred. We examined the DNA bend angle distributions of these complexes, and observed a broad distribution of angles (Figure 4.4). Interestingly, this broad distribution appears to center at $\sim 65^\circ$, which coincides with one of the mismatch bound bend angle population. Given the variation of bend angles, it appears that MutS α is likely to induce many DNA bend angles when it is not on the mismatch.

To confirm that the two dominant conformational states observed were the result of MutS α being bound to the mismatch in the presence of ATP, MutS α was incubated with GC-DNA in the presence of ATP. The DNA bend angle distribution of the GC-DNA data in the presence of ATP is shown in Figure 4.3B. Note that the GC-DNA bend angle distribution is broad and centers around 70° , similarly to what we observed for the GC-DNA in the presence of ADP (Figure 4.3A). Comparing the DNA bends of the GC-DNA data (Figure 4.3A) to the GT-DNA data (Figure 4.2B) reveals that similar populations of bend angles in the GT-DNA are also observed in the presence of GC-DNA. In the absence of a mismatch, however, MutS α appears to induce a larger range of DNA bends, which is expected because of sequence variability. Interestingly, the populations of bent states observed in the presence of GC-DNA (Figure 4.3B) are similar to the states observed for non-specifically bound MutS α on GT-DNA (Figure 4.4). In both data sets, the population distributions are broad, suggesting that the two distinct bend angle states at 20° and 65° require the presence of the mismatch.

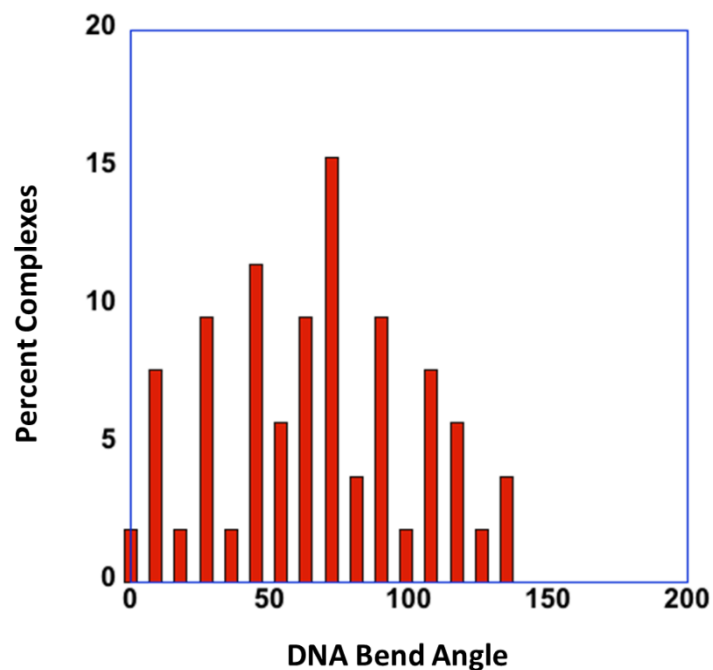


Figure 4.4 : Non-specifically bound MutS α -induced GT-DNA bend angles in the presence of ATP

MutS α -induced DNA bend angles on GT-DNA in the presence of 100 μ M ATP (n = 52).

Histogram shows the DNA bend angles of MutS α bound on homoduplex sites of GT-DNA.

Histogram shows a broad angle distribution with a peak centered on $\sim 65^\circ$.

MutS α induced DNA bend angles are independent of ATP hydrolysis

To determine if ATP–hydrolysis plays a role in MutS α –induced DNA bending, we incubated MutS α on GT–DNA with ATP γ S, a slow hydrolyzing ATP analog. If ATP hydrolysis is not needed for MutS α to form a mobile clamp, then we would expect to see similar bend angle distributions to the ATP data (Figure 4.2B). Figure 4.2C shows sample images of MutS α bound to the GT–DNA at the mismatch in the presence of ATP γ S. Similar MutS α –induced DNA bend angles were observed in both the presence of ATP (Figure 4.2B) and in the presence of ATP γ S (Figure 4.2C). Three populations of DNA bend angles are observed in the presence of ATP γ S: 20°, 55°, and 80°. Because the DNA bend angles observed for MutS α –DNA complexes in the presence of the mismatch and ATP γ S are similar to those observed in the presence of ATP, the data are consistent with the formation of the MutS α mobile clamp being ATP–hydrolysis independent. It is important to note that in the time scale these experiments were done, a small population of ATP γ S could have been hydrolyzed. Minimal amounts of hydrolysis could explain the presence of the 55° DNA bend angle, which could be consistent with the ADP–ATP exchange bend angle we observed in the ATP data.

We also examined the different adenine nucleotide binding properties of the two subunits of MutS α . MSH2 has a higher affinity for binding ADP whereas MSH6 has been shown to bind ATP with higher affinity (Mazur, Mendillo et al. 2006, Heinen, Cyr et al. 2011). To provide insight on what DNA bends are induced by MutS α in an MSH2–ADP:MSH6–ATP bound state on the mismatch, we incubated MutS α with GT–DNA and an equal concentration of ATP γ S and ADP. Figure 4.2D shows sample AFM images of MutS α in these conditions and shows the distribution of DNA bend angles induced by MutS α . We observe three DNA bend angle peaks in

these conditions: a 20° peak, a broad 50° peak, and a 90° peak. Because we are unable to identify what the nucleotide occupancy of MutS α is in any given MutS α –DNA complex, we cannot say whether these DNA bend angles are the result of a specific combination of nucleotides. However, by comparing these data to the other data in this chapter, these data suggest that the broad 50° is likely due to MutS α binding to the mismatch with ADP in one or both subunits, and one of the other peaks could be the ATP–dependent conformational change exhibited by MutS α as it forms the mobile clamp.

Table 4.1 : Summary of MutS α -induced DNA bend angles

Nucleotide	DNA Bend Angles
<i>GT - DNA</i>	
ADP (n = 190)	45°
ATP (specific) (n = 74)	20°, 65°
ATP (non-specific) (n = 52)	65°
ATPyS (n = 51)	20°, 55°, 80°
ATPyS + ADP (n = 84)	20°, 50°, 90°
<i>GC - DNA</i>	
ADP (n = 152)	~70°
ATP (n = 183)	~70°

Discussion

In this study we examined the DNA bend angle properties of a single MutS α on GT–DNA, as summarized in Table 4.1. In the presence of ADP, we observed that MutS α induces a 45° bend in the DNA, which is consistent with the DNA bending observed in the crystal structure (Warren, Pohlhaus et al. 2007). We also noted that this bend angle distribution is broad, suggesting that MutS α is flexible on the mismatch.

The DNA bend angle properties of human MutS α in the presence of ATP were also examined. We observe two distinct DNA bend angles: a 20° bend and a 65° bend. Comparing these bend angles to the ADP data we hypothesize that ATP induces at least two conformational states that result in the two distinct DNA bend angles observed. The 20° DNA bend angle is likely consistent with MutS α forming a mobile clamp, whereas the 65° bend angle could be result of the ADP–ATP exchange step of the mismatch recognition of MutS α . This two–step process is not unprecedented, as other data suggests that *Taq* MutS undergoes at least two conformational states in the presence of ATP (Wang, Yang et al. 2003, Qiu, DeRocco et al. 2012, Qiu, Sakato et al. 2015).

These DNA bend angles of MutS α on a GT–mismatch are similar to those found for *Taq* and *E. coli* MutS (Wang, Yang et al. 2003, Qiu, DeRocco et al. 2012, DeRocco, Sass et al. 2014). These studies show that MutS bends the DNA during the “searching mechanism”, and upon recognition of the mismatch puts a sharp bend in the DNA before inducing a final slightly bent state. Based on the data presented in this chapter, we have created a model where MutS α bends the DNA while searching for the mismatch (Figure 4.5). This model is consistent with the broad distribution of DNA bend angles observed in the GC–DNA data (Figure 4.3), which may be attributed to the ease of MutS α bending the DNA within different sequence contexts. Upon

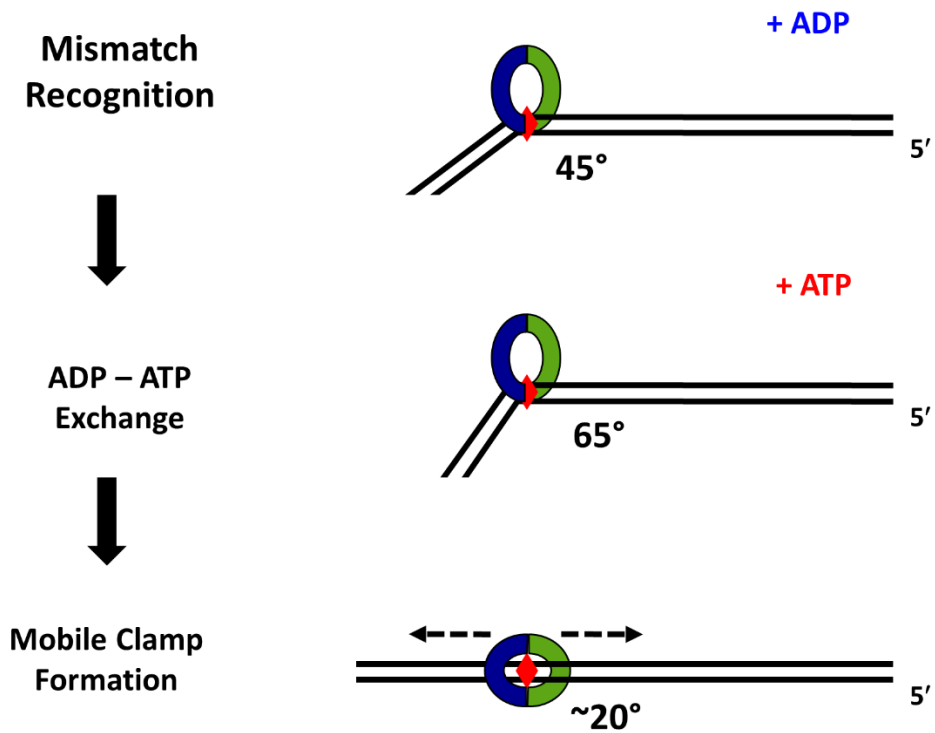


Figure 4.5 : Model of MutS α -induced DNA Bending

In this model, MutS α recognizes a mismatch and in the presence of ADP, it will induce a bend at $\sim 45^\circ$. In the presence of ATP, MutS α will undergo ADP-ATP exchange leading to the 65° DNA bend before forming a sliding clamp. The mobile clamp state of MutS α will induce a 20° bend in the DNA.

recognition of the mismatch, MutS α in an ADP-bound state bends the DNA at a 45° angle (Figure 4.2A) (Warren, Pohlhaus et al. 2007). After the addition of ATP, MutS α induces two distinct DNA bend angles (Figure 4.2B). Because the 20° DNA bend angle state is only observed when MutS α is bound at the mismatch in the presence of ATP, it is likely that this is the mobile clamp state of MutS α . Additionally, because we observe this bent state in the ATP γ S data, this provides further evidence that MutS α forms a mobile clamp that is independent of ATP hydrolysis. Therefore, the ADP-ATP exchange could lead to MutS α to induce a sharply kinked 65° bent state on the DNA before forming a mobile clamp leading to the slightly bent 20° state.

Future Directions

AFM is a powerful technique to examine the properties of singly bound human MutS α complexes on a mismatch and to gain insight into the DNA bend angle conformations that are induced by MutS α . However, a complementary technique should be employed to study these bend angles. While AFM provides detailed static images for analysis, the breadth of the distributions presented in this chapter in combination with data from previous studies (DeRocco, Sass et al. 2014) suggest that MutS α -DNA binding is dynamic. To appropriately evaluate the properties of MutS α bound to a mismatch in the presence of various adenine nucleotides, single-molecule fluorescence studies should be utilized to study how MutS α conformations change in real time. These experiments should be done both by pre-incubating MutS α in each adenine nucleotide as well as flowing in different adenine nucleotides while measuring how MutS α -induced DNA bend dynamics change over time. These studies, in addition to more replicates of the AFM experiments will more cleanly define which DNA bend angle conformation MutS α

samples the most, and will provide a clearer picture of MutS α -induced DNA bend dynamics on a mismatch.

REFERENCES

- Blackwell, L. J., D. Martik, K. P. Bjornson, E. S. Bjornson and P. Modrich (1998). "Nucleotide-promoted release of hMutSalphalpha from heteroduplex DNA is consistent with an ATP-dependent translocation mechanism." J Biol Chem **273**(48): 32055-32062.
- DeRocco, V. C., L. E. Sass, R. Qiu, K. R. Weninger and D. A. Erie (2014). "Dynamics of MutS-mismatched DNA complexes are predictive of their repair phenotypes." Biochemistry **53**(12): 2043-2052.
- Erie, D. A. and K. R. Weninger (2014). "Single molecule studies of DNA mismatch repair." DNA Repair (Amst) **20**: 71-81.
- Geng, H., C. Du, S. Chen, V. Salerno, C. Manfredi and P. Hsieh (2011). "In vitro studies of DNA mismatch repair proteins." Anal Biochem **413**(2): 179-184.
- Geng, H., M. Sakato, V. DeRocco, K. Yamane, C. Du, D. A. Erie, M. Hingorani and P. Hsieh (2012). "Biochemical analysis of the human mismatch repair proteins hMutSalphalpha MSH2(G674A)-MSH6 and MSH2-MSH6(T1219D)." J Biol Chem **287**(13): 9777-9791.
- Gradia, S., D. Subramanian, T. Wilson, S. Acharya, A. Makhov, J. Griffith and R. Fishel (1999). "hMSH2-hMSH6 forms a hydrolysis-independent sliding clamp on mismatched DNA." Mol Cell **3**(2): 255-261.
- Heinen, C. D., J. L. Cyr, C. Cook, N. Punja, M. Sakato, R. A. Forties, J. M. Lopez, M. M. Hingorani and R. Fishel (2011). "Human MSH2 (hMSH2) protein controls ATP processing by hMSH2-hMSH6." J Biol Chem **286**(46): 40287-40295.
- Hsieh, P. and K. Yamane (2008). "DNA mismatch repair: molecular mechanism, cancer, and ageing." Mech Ageing Dev **129**(7-8): 391-407.
- Iaccarino, I., G. Marra, P. Dufner and J. Jiricny (2000). "Mutation in the magnesium binding site of hMSH6 disables the hMutSalphalpha sliding clamp from translocating along DNA." J Biol Chem **275**(3): 2080-2086.
- Iyer, R. R., A. Pluciennik, V. Burdett and P. L. Modrich (2006). "DNA mismatch repair: functions and mechanisms." Chemical reviews **106**(2): 302-323.
- Kunkel, T. A. and D. A. Erie (2005). "DNA mismatch repair." Annu Rev Biochem **74**: 681-710.
- Mazur, D. J., M. L. Mendillo and R. D. Kolodner (2006). "Inhibition of Msh6 ATPase activity by mispaired DNA induces a Msh2(ATP)-Msh6(ATP) state capable of hydrolysis-independent movement along DNA." Mol Cell **22**(1): 39-49.
- Obmolova, G., C. Ban, P. Hsieh and W. Yang (2000). "Crystal structures of mismatch repair protein MutS and its complex with a substrate DNA." Nature **407**(6805): 703-710.

- Qiu, R., V. C. DeRocco, C. Harris, A. Sharma, M. M. Hingorani, D. A. Erie and K. R. Weninger (2012). "Large conformational changes in MutS during DNA scanning, mismatch recognition and repair signalling." EMBO J **31**(11): 2528-2540.
- Qiu, R., M. Sakato, E. J. Sacho, H. Wilkins, X. Zhang, P. Modrich, M. M. Hingorani, D. A. Erie and K. R. Weninger (2015). "MutL traps MutS at a DNA mismatch." Proc Natl Acad Sci U S A **112**(35): 10914-10919.
- Schofield, M. J., S. Nayak, T. H. Scott, C. Du and P. Hsieh (2001). "Interaction of Escherichia coli MutS and MutL at a DNA mismatch." J Biol Chem **276**(30): 28291-28299.
- Wang, H., Y. Yang, M. J. Schofield, C. Du, Y. Fridman, S. D. Lee, E. D. Larson, J. T. Drummond, E. Alani, P. Hsieh and D. A. Erie (2003). "DNA bending and unbending by MutS govern mismatch recognition and specificity." Proc Natl Acad Sci U S A **100**(25): 14822-14827.
- Warren, J. J., T. J. Pohlhaus, A. Changela, R. R. Iyer, P. L. Modrich and L. S. Beese (2007). "Structure of the human MutSalph DNA lesion recognition complex." Mol Cell **26**(4): 579-592.
- Yang, Y., H. Wang and D. A. Erie (2003). "Quantitative characterization of biomolecular assemblies and interactions using atomic force microscopy." Methods **29**(2): 175-187.
- DeRocco, V. C., L. E. Sass, R. Qiu, K. R. Weninger and D. A. Erie (2014). "Dynamics of MutS-mismatched DNA complexes are predictive of their repair phenotypes." Biochemistry **53**(12): 2043-2052.
- Erie, D. A. and K. R. Weninger (2014). "Single molecule studies of DNA mismatch repair." DNA Repair (Amst) **20**: 71-81.
- Geng, H., C. Du, S. Chen, V. Salerno, C. Manfredi and P. Hsieh (2011). "In vitro studies of DNA mismatch repair proteins." Anal Biochem **413**(2): 179-184.
- Geng, H., M. Sakato, V. DeRocco, K. Yamane, C. Du, D. A. Erie, M. Hingorani and P. Hsieh (2012). "Biochemical analysis of the human mismatch repair proteins hMutSalph MSH2(G674A)-MSH6 and MSH2-MSH6(T1219D)." J Biol Chem **287**(13): 9777-9791.
- Heinen, C. D., J. L. Cyr, C. Cook, N. Punja, M. Sakato, R. A. Forties, J. M. Lopez, M. M. Hingorani and R. Fishel (2011). "Human MSH2 (hMSH2) protein controls ATP processing by hMSH2-hMSH6." J Biol Chem **286**(46): 40287-40295.
- Hsieh, P. and K. Yamane (2008). "DNA mismatch repair: molecular mechanism, cancer, and ageing." Mech Ageing Dev **129**(7-8): 391-407.
- Iyer, R. R., A. Pluciennik, V. Burdett and P. L. Modrich (2006). "DNA mismatch repair: functions and mechanisms." Chemical reviews **106**(2): 302-323.
- Kunkel, T. A. and D. A. Erie (2005). "DNA mismatch repair." Annu Rev Biochem **74**: 681-710.

- Mazur, D. J., M. L. Mendillo and R. D. Kolodner (2006). "Inhibition of Msh6 ATPase activity by mispaired DNA induces a Msh2(ATP)-Msh6(ATP) state capable of hydrolysis-independent movement along DNA." *Mol Cell* 22(1): 39-49.
- Obmolova, G., C. Ban, P. Hsieh and W. Yang (2000). "Crystal structures of mismatch repair protein MutS and its complex with a substrate DNA." *Nature* 407(6805): 703-710.
- Qiu, R., V. C. DeRocco, C. Harris, A. Sharma, M. M. Hingorani, D. A. Erie and K. R. Weninger (2012). "Large conformational changes in MutS during DNA scanning, mismatch recognition and repair signalling." *EMBO J* 31(11): 2528-2540.
- Qiu, R., M. Sakato, E. J. Sacho, H. Wilkins, X. Zhang, P. Modrich, M. M. Hingorani, D. A. Erie and K. R. Weninger (2015). "MutL traps MutS at a DNA mismatch." *Proc Natl Acad Sci U S A* 112(35): 10914-10919.
- Wang, H., Y. Yang, M. J. Schofield, C. Du, Y. Fridman, S. D. Lee, E. D. Larson, J. T. Drummond, E. Alani, P. Hsieh and D. A. Erie (2003). "DNA bending and unbending by MutS govern mismatch recognition and specificity." *Proc Natl Acad Sci U S A* 100(25): 14822-14827.
- Warren, J. J., T. J. Pohlhaus, A. Changela, R. R. Iyer, P. L. Modrich and L. S. Beese (2007). "Structure of the human MutS α DNA lesion recognition complex." *Mol Cell* 26(4): 579-592.
- Yang, Y., H. Wang and D. A. Erie (2003). "Quantitative characterization of biomolecular assemblies and interactions using atomic force microscopy." *Methods* 29(2): 175-187.

CHAPTER 5: AFM STUDIES TO GAIN INSIGHT INTO OTHER BIOMOLECULAR PROCESSES

Introduction

Atomic force microscopy (AFM) is a high resolution, single-molecule technique that can be used to gain structural insight into biomolecular processes. The advantages of using AFM are: 1) AFM results in a three-dimensional (3D) image; 2) AFM can visualize non-conductive materials such as DNA and proteins; 3) and AFM can be conducted in air and in solution (Hansma, Laney et al. 1995). These resulting images can be analyzed to gain detailed structural information including the volumes of the protein complexes, the position of the proteins bound to DNA, the conformations of the protein complexes and the DNA, and the examination of rare events (Ratcliff and Erie 2001, Wang, Yang et al. 2003, Sacho, Kadyrov et al. 2008). The purpose of this chapter is to demonstrate the broad applicability of AFM in the context of other biomolecular questions. Because of the power of AFM to characterize proteins, I have been involved in several collaborations to examine the conformational and stoichiometric states of different proteins. I examined the properties of ANGPTL4, a protein involved in regulating LPL; TRAK, a protein involved in bacterial conjugation; and vaccinia virus endoribonuclease H5, a protein involved in viral RNA metabolism and DNA replication.

REFERENCES

- Hansma, H. G., D. E. Laney, M. Bezanilla, R. L. Sinsheimer and P. K. Hansma (1995). "Applications for atomic force microscopy of DNA." Biophys J **68**(5): 1672-1677.
- Ratcliff, G. C. and D. A. Erie (2001). "A novel single-molecule study to determine protein--protein association constants." Journal of the American Chemical Society **123**(24): 5632-5635.
- Sacho, E. J., F. A. Kadyrov, P. Modrich, T. A. Kunkel and D. A. Erie (2008). "Direct visualization of asymmetric adenine-nucleotide-induced conformational changes in MutL alpha." Molecular cell **29**(1): 112-121.
- Wang, H., Y. Yang, M. J. Schofield, C. Du, Y. Fridman, S. D. Lee, E. D. Larson, J. T. Drummond, E. Alani, P. Hsieh and D. A. Erie (2003). "DNA bending and unbending by MutS govern mismatch recognition and specificity." Proc Natl Acad Sci U S A **100**(25): 14822-14827.

CHAPTER 5.1: STRUCTURE-FUNCTION INVESTIGATION OF ANGPTL4¹

Introduction

Lipoprotein Lipase (LPL) is an important enzyme that regulates serum lipid levels by hydrolyzing triglycerides in lipoproteins such as chylomicrons and very low-density lipoproteins (VLDL). Abnormal LPL expression and/or function can be associated with obesity, diabetes, Alzheimer's disease, and other diseases (Mead, Irvine et al. 2002). LPL is composed of two domains connected by a linker, and is only active as a homodimer (Lookene, Zhang et al. 2004). Previous work has shown that LPL plays a key role in regulating lipid homeostasis and requires LPL tissue-specific activity to be well coordinated with nutritional status. Angiopoietin-like Protein 4 (ANGPTL4) is a secreted protein that directly regulates LPL activity (Kersten, Mandard et al. 2000).

ANGPTL4 is a two domain protein: The N-terminal domain is a coiled-coil that mediates oligomerization of the protein, and the C-terminal portion is a fibrinogen-like domain (Ge, Yang et al. 2004). Once ANGPTL4 is secreted, these domains are cleaved apart by the action of pro-protein convertases (Ge, Yang et al. 2004). The N-terminal domain of ANGPTL4 inhibits LPL activity, and cleavage of the two domains enhances this inhibition (Ge, Yang et al. 2004, Ge, Yang et al. 2004, Yin, Romeo et al. 2009). ANGPTL4 is thought to inhibit LPL by promoting

¹ This research was originally published in Journal of Biological Chemistry. Lafferty, M. J., K. C. Bradford, D. A. Erie and S. B. Neher. Angiopoietin-like protein 4 inhibition of lipoprotein lipase: evidence for reversible complex formation. J Biol Chem. 2013; 288(40): 28524-28534. © the American Society for Biochemistry and Molecular Biology.

dissociation of LPL dimers to form inactive monomers (Sukonina, Lookene et al. 2006). Active LPL dimers are known to undergo both reversible and irreversible dissociation into inactive monomers; however, it remains unclear how ANGPTL4 interacts with LPL to inhibit LPL activity and if the ANGPTL4-induced conformational change in LPL is irreversible.

In this study we sought to use atomic force microscopy (AFM) to complement other biochemical experiments to gain structural insight into how ANGPTL4 interacts with LPL and to investigate the stoichiometries of each of these proteins.

Materials and Methods

Protein Purification

LPL and ANGPTL4 were purified as described (Lafferty, Bradford et al. 2013). Dr. Saskia Neher (UNC-CH) generously provided these proteins.

Atomic Force Microscopy

100 nM LPL, 100 nM ANGPTL4, or 100 nM LPL plus 100 nM ANGPTL4 were incubated on ice for 15 min in 10 mM BisTris, pH 6.5, 500 mM NaCl, and 10% glycerol. Mixtures were diluted 5x into the same buffer, and 10 μ l was immediately deposited onto freshly cleaved mica. The mica surface was then immediately washed with water, and a stream of nitrogen gas was used to dry the surface. Images were acquired with a Nanoscope III 3A atomic force microscope (Veeco, Santa Barbara, CA) in tapping mode with a resolution of 512×512 pixels at a scan rate of 1.97 Hz and over a 1×1 μ m scan size. AFM tips were from NanoSensors (Neuchatel, Switzerland) with a spring constant between 21 and 98 N/m and resonance frequencies between 146 and 236 kHz. AFM images for each sample were consistent over multiple depositions (greater than three from each sample) and multiple tips (at least two for each deposition). Poor images resulting from blunted tips were excluded from analysis. Between three and five representative images of

each sample condition were 3rd order plane-fitted and flattened using NanoScope Analysis version 1.40r1 (Bruker Instruments). Volume analysis of protein peaks was conducted with Image SXM 194-2X (Steve Barrett, University of Liverpool, UK) as described (Ratcliff and Erie 2001, Yang, Wang et al. 2003). Protein molecular mass was converted into predicted AFM volume using the following equation: $V = 1.2 \cdot M - 14.7$, where V is AFM volume in nm^3 , and M is molecular mass in kDa.

Results

Results are an excerpt of those published in (Lafferty, Bradford et al. 2013).

We utilized AFM to determine the distribution of oligomeric states of the inhibited LPL-ANGPTL4 complex in the absence of cross-linking. Volume analysis of AFM images has been shown to be a powerful tool for determining the oligomerization states of proteins, because the AFM volume depends linearly on the molecular weight of the protein (Ratcliff and Erie 2001, Yang, Wang et al. 2003). ANGPTL4, LPL, and LPL-ANGPTL4 were imaged. Table 5.1 shows the predicted AFM volumes for various LPL and ANGPTL4 protein complexes. Images of ANGPTL4 alone yielded protein volumes ranging from 5 to 60 nm^3 , which is consistent with ANGPTL4 dimers and tetramers (Figure 5.1A). ANGPTL4 monomers may also be present, but with a predicted AFM volume of 3 nm^3 , proteins of this size fall below the linear range of the AFM volume dependence on molecular weight. LPL alone showed a broad distribution of volumes between 60 and 110 nm^3 , likely representing the dimer form (Figure 5.1B).

Table 5.1 : Predicted AFM volumes based on the linear dependency of AFM volume to protein molecular weight: $V = 1.2 * M - 14.7$, where V is AFM volume in nm³, and M is molecular mass in kDa

Protein complex	Mass	Predicted AFM volume (nm ³)
	<i>kDa</i>	
ANGPTL4 monomer	15	3 ^a
ANGPTL4 dimer ^b	31	22
ANGPTL4 tetramer ^b	62	59
LPL monomer	51	46
LPL dimer ^c	101	107
LPL monomer + ANGPTL4 monomer	66	65
LPL monomer + ANGPTL4 dimer	81	83
LPL monomer + ANGPTL4 tetramer ^d	112	120
LPL dimer + ANGPTL4 monomer ^d	117	125
LPL dimer + ANGPTL4 dimer ^d	132	144
LPL dimer + ANGPTL4 tetramer	163	181

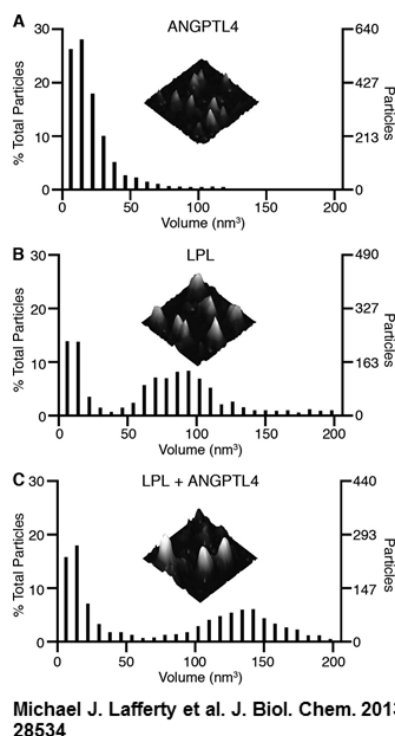
^a Out of linear range.

^b ANGPTL4 dimers and tetramers are most likely represented in Fig. 7A.

^c LPL dimers are seen in Fig. 7B.

^d Possible LPL-ANGPTL4 complexes are seen in Fig. 7C.

Distribution of AFM particle volumes in cubic nanometers.



©2013 by American Society for Biochemistry and Molecular Biology

jbc

Figure 5.1 : Distribution of AFM particle volumes in cubic nanometers

Particle distributions normalized by the percent of total particles in each size range.

Topographical images correspond to an 80×80 nm area on the surface and between 0 and 1.5 nm off the surface. (A) ANGPTL4 at 20 nM deposited onto a freshly cleaved mica surface and imaged with tapping mode AFM in air. Particles from four representative images from the same deposition and using the same tip were analyzed totaling 2150 particles. (B) same as (A), but with 20 nM LPL. Data from five representative images using the same tip totaling 1726 particles. (C) LPL at 100 nM was combined with 100 nM ANGPTL4, incubated on ice for 15 min, then diluted to a final concentration of 20 nM LPL and 20 nM ANGPTL4. Samples were immediately deposited onto freshly cleaved mica and imaged as in (A) and (B). Data from three representative images using the same tip total 1719 particles.

Topographical analysis of the LPL images show tightly spaced protein peaks, also indicative of dimeric proteins. A minor population of smaller particles was also seen, and we attribute these to an LPL cleavage fragment known to co-purify with full-length LPL. Addition of ANGPTL4 to LPL increased the observed volume of the protein particles (Figure 5.1C). If ANGPTL4 catalytically transformed LPL dimers into LPL monomers, we would expect an increase in particles near the expected monomer volume of 46 nm^3 . Furthermore, we would expect the distribution of ANGPTL4 protein volumes to remain between 5 and 60 nm^3 . If ANGPTL4 and LPL did not interact at all, we would predict a combined volume distribution representing the ANGPTL4 distribution added to the LPL distribution. Instead, we see the volume of the main peak increase to between 110 and 160 nm^3 . These AFM volumes could represent LPL dimers in complex with either ANGPTL4 monomers or ANGPTL4 dimers. They could also correspond to LPL monomers in complex with ANGPTL4 tetramers. We believe this last option to be unlikely as there was a complete loss of the LPL dimer peak seen between 60 and 110 nm^3 . With a 1:1 molar ratio of ANGPTL4 monomers to LPL dimers, there would not be sufficient ANGPTL4 tetramers to complex with each LPL monomer. By both cross-linking and AFM, we observed an increase in the molecular weight of LPL upon addition of ANGPTL4. This clearly indicates that ANGPTL4 does not simply monomerize LPL dimers but instead forms an LPL-ANGPTL4 complex.

Discussion

Other evidence within this paper showed that ANGPTL4 is a reversible, non-competitive inhibitor of LPL (Lafferty, Bradford et al. 2013). AFM in conjunction with other techniques showed that the inhibited form of LPL is bound to ANGPTL4, rather than ANGPTL4 inducing LPL to form monomers. Significantly, these data are consistent with a previous *in vivo* study

showing that, in plasma from mice overexpressing ANGPTL4, ANGPTL4 and LPL form a complex as they co-migrate during heparin-Sepharose chromatography (Lichtenstein, Berbee et al. 2007). Thus, our data show that ANGPTL4 acts as a conventional, noncompetitive inhibitor that binds to LPL and prevents it from hydrolyzing substrates.

REFERENCES

- Ge, H., G. Yang, L. Huang, D. L. Motola, T. Pourbahrami and C. Li (2004). "Oligomerization and regulated proteolytic processing of angiopoietin-like protein 4." *J Biol Chem* 279(3): 2038-2045.
- Ge, H., G. Yang, X. Yu, T. Pourbahrami and C. Li (2004). "Oligomerization state-dependent hyperlipidemic effect of angiopoietin-like protein 4." *J Lipid Res* 45(11): 2071-2079.
- Kersten, S., S. Mandard, N. S. Tan, P. Escher, D. Metzger, P. Chambon, F. J. Gonzalez, B. Desvergne and W. Wahli (2000). "Characterization of the fasting-induced adipose factor FIAF, a novel peroxisome proliferator-activated receptor target gene." *J Biol Chem* 275(37): 28488-28493.
- Lafferty, M. J., K. C. Bradford, D. A. Erie and S. B. Neher (2013). "Angiopoietin-like protein 4 inhibition of lipoprotein lipase: evidence for reversible complex formation." *J Biol Chem* 288(40): 28524-28534.
- Lichtenstein, L., J. F. Berbee, S. J. van Dijk, K. W. van Dijk, A. Bensadoun, I. P. Kema, P. J. Voshol, M. Muller, P. C. Rensen and S. Kersten (2007). "Angptl4 upregulates cholesterol synthesis in liver via inhibition of LPL- and HL-dependent hepatic cholesterol uptake." *Arterioscler Thromb Vasc Biol* 27(11): 2420-2427.
- Lookene, A., L. Zhang, M. Hultin and G. Olivecrona (2004). "Rapid subunit exchange in dimeric lipoprotein lipase and properties of the inactive monomer." *J Biol Chem* 279(48): 49964-49972.
- Mead, J. R., S. A. Irvine and D. P. Ramji (2002). "Lipoprotein lipase: structure, function, regulation, and role in disease." *J Mol Med (Berl)* 80(12): 753-769.
- Ratcliff, G. C. and D. A. Erie (2001). "A novel single-molecule study to determine protein--protein association constants." *Journal of the American Chemical Society* 123(24): 5632-5635.
- Sukonina, V., A. Lookene, T. Olivecrona and G. Olivecrona (2006). "Angiopoietin-like protein 4 converts lipoprotein lipase to inactive monomers and modulates lipase activity in adipose tissue." *Proc Natl Acad Sci U S A* 103(46): 17450-17455.
- Yang, Y., H. Wang and D. A. Erie (2003). "Quantitative characterization of biomolecular assemblies and interactions using atomic force microscopy." *Methods* 29(2): 175-187.
- Yin, W., S. Romeo, S. Chang, N. V. Grishin, H. H. Hobbs and J. C. Cohen (2009). "Genetic variation in ANGPTL4 provides insights into protein processing and function." *J Biol Chem* 284(19): 13213-13222.

CHAPTER 5.2: STRUCTURE-FUNCTION INVESTIGATIONS OF TRAK

Introduction

Bacterial conjugation is the transfer of genetic material between bacterial cells by either direct cell-to-cell contact or by pili and was originally discovered in 1946 by Joshua Lederberg and Edward Tatum (Lederberg and Tatum 1946, Holmes and Jobling 1996). Conjugal DNA transfer occurs frequently in bacterial cells and is often beneficial to the recipient cell, conferring benefits such as antibiotic resistance (Holmes and Jobling 1996). The conjugative plasmid is called the F-plasmid with a length of approximately 100 kb. It contains an origin of replication, *oriV*, an origin of transfer, *oriT*, and the *tra* and *trb* loci. The *tra* locus includes the *pilin* gene and regulatory genes, which together form the pili on the cell surface to initiate conjugation (Holmes and Jobling 1996). The exact mechanism for how the transfer of DNA occurs is unclear. One hypothesis is that the F-encoded Tra proteins act together at the cell surface to mediate the different stages of conjugal DNA transfer (Harris, Hombs et al. 2001). Yeast two-hybrid analyses of the Tra proteins: TraV, TraK, and TraB; found that these proteins constitute a protein interaction group that result in a complex in the *Escherichia coli* (*E. coli*) cell envelope. The purpose of this complex, however, is not well understood (Harris, Hombs et al. 2001). Many studies seek to investigate and understand the function of each protein, and little is known about TraK. TraK is predicted to be a 23.3 kDa protein (Frost, Ippen-Ihler et al. 1994). Electron microscopy (EM) studies of TraK-*oriT* complexes shows that binding of TraK to its recognition region apparently shrinks the length of the target DNA, suggesting that the nucleic acid becomes wrapped around a core of TraK proteins (Ziegelin, Pansegrau et al. 1992). Additionally, the

DNA binding activity of TraK appears to be cooperative, leading to large complexes of TraK on the DNA.

In this study, we use atomic force microscopy (AFM) to identify the oligomerization state of TraK alone and TraK in the presence of DNA. AFM is a single molecule technique that directly visualizes protein and protein–DNA complexes on a surface. Because the volumes of the proteins depend linearly on their molecular weight, we can estimate the number of proteins present in a given protein complex (Ratcliff and Erie 2001). From these studies, we demonstrate that TraK exists as both a monomer and a dimer, but upon binding to DNA, it forms large multimeric species. Future work should focus on doing more experiments with TraK and the DNA substrate to confirm the initial study results and to discover the preferential DNA binding site of TraK.

Materials and Methods

TraK and DNA substrate purification

TraK was purified and generously provided by Dr. Krystle McLaughlin and Dr. Matt Redinbo (University of North Carolina – Chapel Hill). A 381 bp DNA substrate was purified and provided by Dr. Krystle McLaughlin and Dr. Matt Redinbo (University of North Carolina – Chapel Hill).

Sample preparation and deposition

For experiments with TraK alone, TraK was diluted to a concentration of 40 nM in high salt imaging buffer (25 mM HEPES, pH 7.5, 100 mM NaOAc, 10 mM Mg(OAc)₂, 1 mM DTT, 5% glycerol) and 10 µl was immediately deposited onto freshly cleaved ruby mica (Spruce Pine Mica Company, Spruce Pine, NC). For experiments with TraK and the 381 bp DNA substrate,

TraK was diluted to 20 nM in low salt imaging buffer (25 mM HEPES, pH 7.5, 50 mM NaOAc, 10 mM Mg(OAc)₂, 1 mM DTT, 5% glycerol) with 1 ng/μl of the DNA substrate for 1 minute at room temperature and 10 μl was deposited onto freshly cleaved ruby mica. Mica samples were rinsed with water, blotted dry, and then dried under a stream of nitrogen before imaging.

Imaging

The images were captured in air with a Nanoscope IIIa (Digital Instruments, Santa Barbara, CA) microscope in tapping mode. Pointprobe Plus tapping mode silicon cantilevers (NANOSENSORS, Switzerland) with resonance frequencies from 146-236 kHz were used. The images were collected at a speed of 1.97 Hz, a size of 1 x 1 μm, and at a resolution of 512 x 512 pixels.

Image Analysis

A combination of NIH ImageJ64 (Rasbrand, with NeuronJ plug-in) software, Nanoscope III v5.3 software (Veeco, Santa Barbara, CA), and ImageSXM v1.95, were used to measure the volumes of the complexes on the DNA, the DNA contour lengths, and the position of the proteins on the DNA. The KaleidaGraph program (Synergy Software, Reading, PA) was used to generate statistical plots for these data sets. Volume analysis was performed as previously described using ImageSXM v 1.95 (Ratcliff and Erie 2001, Wang, Yang et al. 2003, Sacho, Kadyrov et al. 2008). DNA contour length and position analysis for the TraK and DNA substrate experiments were done as previously described using ImageJ64 software (Wang, Yang et al. 2003). To determine the positions of TraK binding on the DNA fragments, the distance from the center of the bound TraK complex to each end of the DNA fragment was measured.

Results

TraK exists as a monomer and dimer in vitro

To investigate the oligomerization state of TraK, 40 nM was deposited onto mica and imaged. Figure 5.2A shows a sample AFM image of TraK and the image shows that the protein exists in different oligomerization states. Consequently, we analyzed the volumes of these proteins to determine the distribution of oligomerization states of TraK. Figure 5.2B shows the distribution of volumes, and two peaks are observed. The first peak centered at $\sim 20 \text{ nm}^3$, is consistent with the monomer state of TraK and the second peak centered at $\sim 50 \text{ nm}^3$, is consistent with the dimer state. Figure 5.2C shows a sample surface plot of a monomer and dimer form of TraK. These data suggests that TraK can exist in either a monomer or dimer state.

Large complexes of TraK form on DNA

To investigate the region of the DNA to which TraK protein preferentially binds, we incubated 20 nM TraK with the 381 bp DNA substrate. Figure 5.3A shows a sample image of TraK bound to the DNA. In this experiment, we noted that TraK bound in three regions of the DNA, shown in Figure 5.3B: on the end of the DNA, towards one end of the DNA, and at the center of the DNA molecule. The volumes of TraK bound to the DNA are significantly larger (Figure 5.3B) than those observed with TraK alone. For example, the smallest volume shown in Figure 5.3B is 159 nm^3 , which is significantly larger than TraK monomers or dimers. These volumes suggests that multiple (>7) TraK proteins are binding the DNA, similar to previous DNaseI footprinting and electron microscopy data (Ziegelin, Pansegrau et al. 1992). We measured the DNA contour length of TraK–DNA complexes, and found that on average the total DNA length was 337 bp, which was shorter than expected ($n = 16$, expected length was 381 bp). The DNA contour lengths were more likely to be shorter when the TraK complex was bound

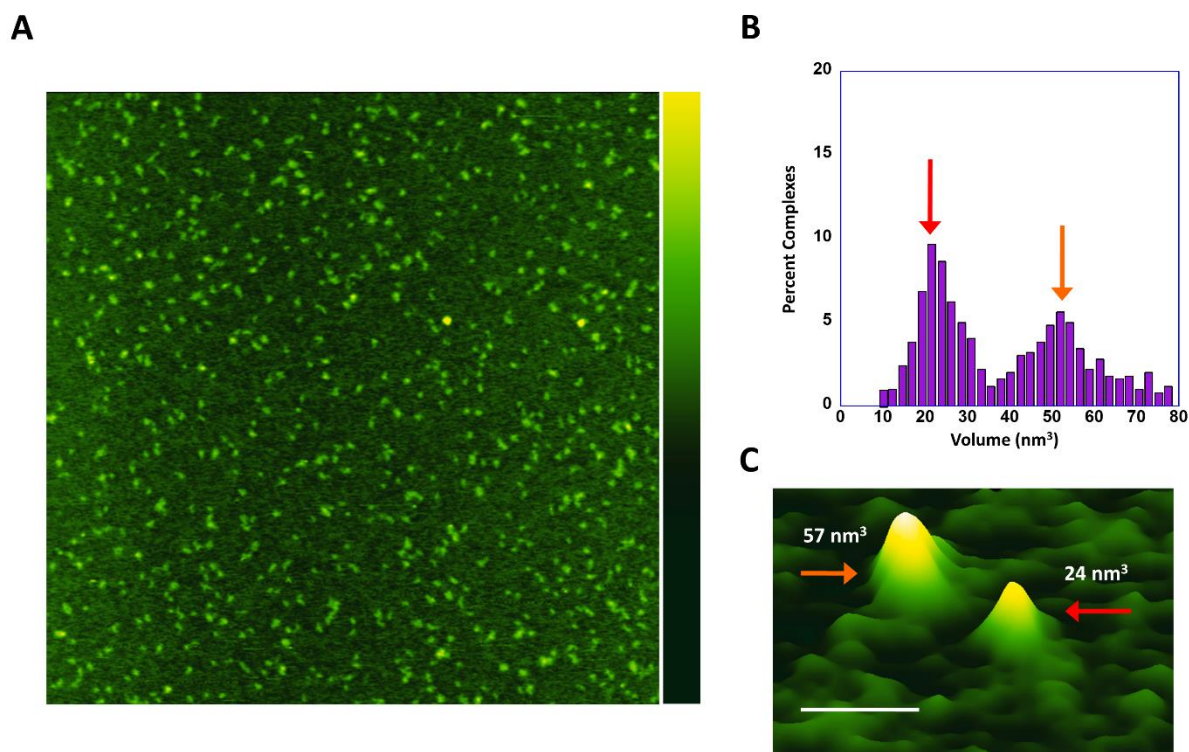


Figure 5.2 : AFM images and volume analysis of TraK

(A) 1 x 1 μm image of 40 nM TraK diluted in high salt imaging buffer. Scale bar indicates height from 0 – 3 nm. (B) Volume distribution of TraK ($n = 497$). Red arrow indicates the monomer species of TraK with a volume $\sim 20 \text{ nm}^3$. Orange arrow points to the population associated with the dimer species of TraK with a volume $\sim 50 \text{ nm}^3$. (C) 70 x 70 nm surface plot of TraK. A red arrow indicates the monomer and an orange arrow points to a dimer. White text displays the volumes of each protein complex. White scale bar indicates 20 nm.

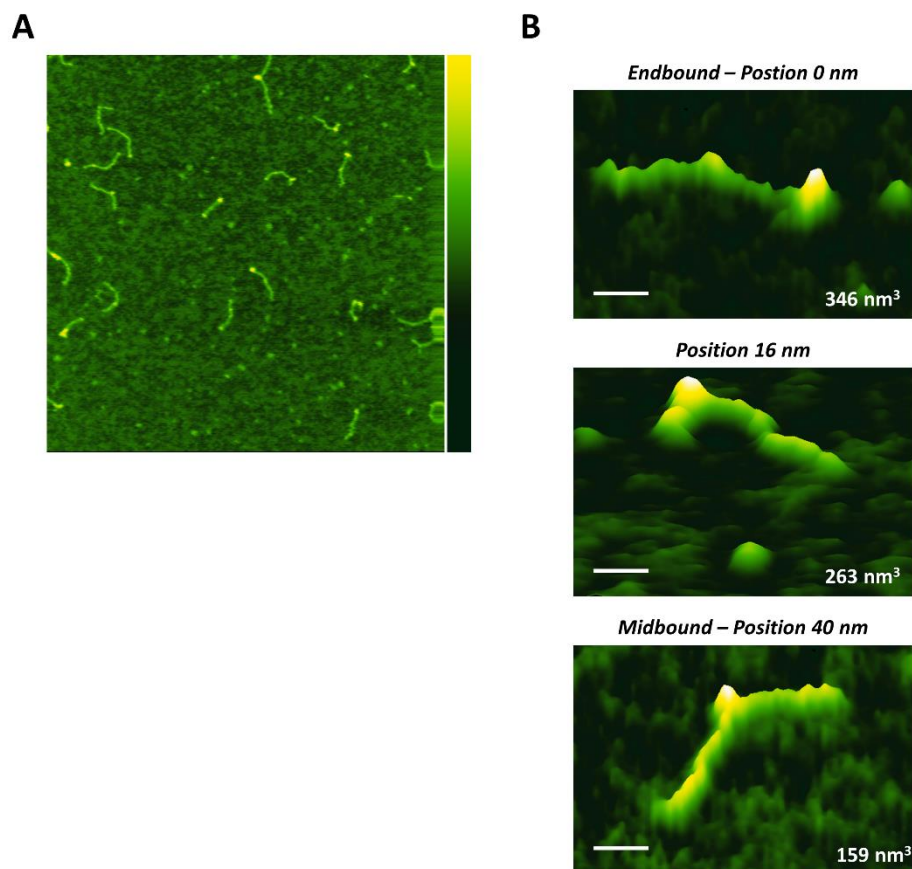


Figure 5.3 : AFM image and position analysis of TraK on DNA

(A) 1 x 1 μm image of 20 nM TraK bound to a 381 bp DNA substrate in low salt imaging buffer. Scale bar indicates height from 0 – 4 nm. (B) 130 nm surface plots of TraK bound to different regions of the DNA. The numbers above each panel image indicate the binding position. Numbers in white display the volumes of the bound protein. White scale bars indicate 20 nm. Top panel shows TraK bound to one end of the DNA, middle panel shows TraK bound towards one end of the DNA, and bottom panel shows TraK bound to the center of the DNA substrate.

towards one end or on the end of the DNA molecule, however more data are needed to confirm this result.

Conclusions and Future Work

In this AFM study, we demonstrate that TraK can exhibit both monomer and dimer oligomerization states *in vitro*. We also confirmed previous studies that found that multiple TraK proteins bound to DNA to form large complexes. Furthermore, we found that in TraK–DNA species where TraK was bound on the end of the DNA or towards one end, that the overall DNA length was shorter, similarly to what was observed in the EM experiments, suggesting that TraK wraps the DNA around the protein complex (Ziegelin, Pansegrau et al. 1992). This experiment, however, was successfully completed once, resulting in only 16 protein–DNA molecules to be analyzed. Future work should replicate these studies multiple times to ensure proper statistics and to provide more insight into the DNA binding preferences of TraK.

REFERENCES

- Frost, L. S., K. Ippen-Ihler and R. A. Skurray (1994). "Analysis of the sequence and gene products of the transfer region of the F sex factor." Microbiol Rev **58**(2): 162-210.
- Harris, R. L., V. Hombs and P. M. Silverman (2001). "Evidence that F-plasmid proteins TraV, TraK and TraB assemble into an envelope-spanning structure in Escherichia coli." Mol Microbiol **42**(3): 757-766.
- Holmes, R. K. and M. G. Jobling (1996). Genetics. Medical Microbiology. S. Baron. Galveston (TX), University of Texas Medical Branch at Galveston
- The University of Texas Medical Branch at Galveston.
- Lederberg, J. and E. L. Tatum (1946). "Gene recombination in Escherichia coli." Nature **158**(4016): 558.
- Ratcliff, G. C. and D. A. Erie (2001). "A novel single-molecule study to determine protein--protein association constants." Journal of the American Chemical Society **123**(24): 5632-5635.
- Sacho, E. J., F. A. Kadyrov, P. Modrich, T. A. Kunkel and D. A. Erie (2008). "Direct visualization of asymmetric adenine-nucleotide-induced conformational changes in MutL alpha." Molecular cell **29**(1): 112-121.
- Wang, H., Y. Yang, M. J. Schofield, C. Du, Y. Fridman, S. D. Lee, E. D. Larson, J. T. Drummond, E. Alani, P. Hsieh and D. A. Erie (2003). "DNA bending and unbending by MutS govern mismatch recognition and specificity." Proc Natl Acad Sci U S A **100**(25): 14822-14827.
- Ziegelin, G., W. Pansegrau, R. Lurz and E. Lanka (1992). "TraK protein of conjugative plasmid RP4 forms a specialized nucleoprotein complex with the transfer origin." J Biol Chem **267**(24): 17279-17286.

CHAPTER 5.3: AFM STUDIES OF THE OLIGMERIZATION STATE OF THE VACCINIA VIRUS ENDORIBONUCLEASE H5

Introduction

The vaccinia virus is one of the most well studied members of the poxvirus family. These viruses are large double-stranded DNA viruses that replicate exclusively in the host cell cytoplasm and encode all the enzymes and factors required for DNA and RNA metabolism (Beaud 1995, Kay, Bainbridge et al. 2013). Studies of poxvirus RNA metabolism, DNA replication, and virion morphogenesis have shown that the vaccinia H5 protein plays important roles in each of these processes (Kay, Bainbridge et al. 2013). H5 is a constitutively expressed, 22.3 kDa phosphoprotein that is localized in viral factories and packaged into virions. Although the molecular mass of the H5 is only 22 kDa, different biochemical estimations of molecular weight have yielded different conclusions. H5 was shown to fractionate on SDS-PAGE at 35 kDa, slightly larger than the predicted monomer state (Beaud, Beaud et al. 1995). Additionally, the purified protein has been shown to elute from gel filtration columns with an extremely large apparent molecular mass (> 400 kDa), suggesting multimerization of the protein (D'Costa, Bainbridge et al. 2008). With such differences in molecular weight from different techniques, we sought to use atomic force microscopy (AFM) to identify the oligomerization state of H5. AFM is a single molecule technique that directly visualizes protein complexes on a surface. Because the volumes of the proteins depend linearly on their molecular weight, we can estimate the number of proteins there are in a given protein complex (Ratcliff and Erie 2001). From these studies, we demonstrate that H5 in the conditions tested is most often seen as a monomer. Future

work should use different protein preparations from different organisms to test the possibility that post-translational modifications may play a role in the multimerization of H5.

Materials and Methods:

Protein Purification

H5 was purified and generously provided by Dr. Susan D'Costa (University of Florida).

Atomic Force Microscopy

90 nM of H5 was diluted into imaging buffer containing 25 mM HEPES, pH 7.5, 100 mM NaOAc, 10 mM Mg(OAc)₂, 1 mM DTT, 5% glycerol. 10 µl was deposited onto freshly cleaved ruby mica. The mica surface was then immediately washed with water, and a stream of nitrogen gas was used to dry the surface. Images were acquired with a Nanoscope III 3A atomic force microscope (Veeco, Santa Barbara, CA) in tapping mode with a resolution of 512 × 512 pixels at a scan rate of 1.97 Hz and over a 1 × 1 µm scan size. AFM tips were from NanoSensors (Neuchatel, Switzerland) with a spring constant between 21 and 98 n/m and resonance frequencies between 146 and 236 kHz. Volume analysis of protein peaks was conducted with Image SXM v 1.94 (Steve Barrett, University of Liverpool, UK) as described (Ratcliff and Erie 2001, Yang, Wang et al. 2003). Protein molecular mass was converted into predicted AFM volume using the following equation: $V = 1.2 \cdot M - 14.7$, where V is AFM volume in nm³, and M is molecular mass in kDa.

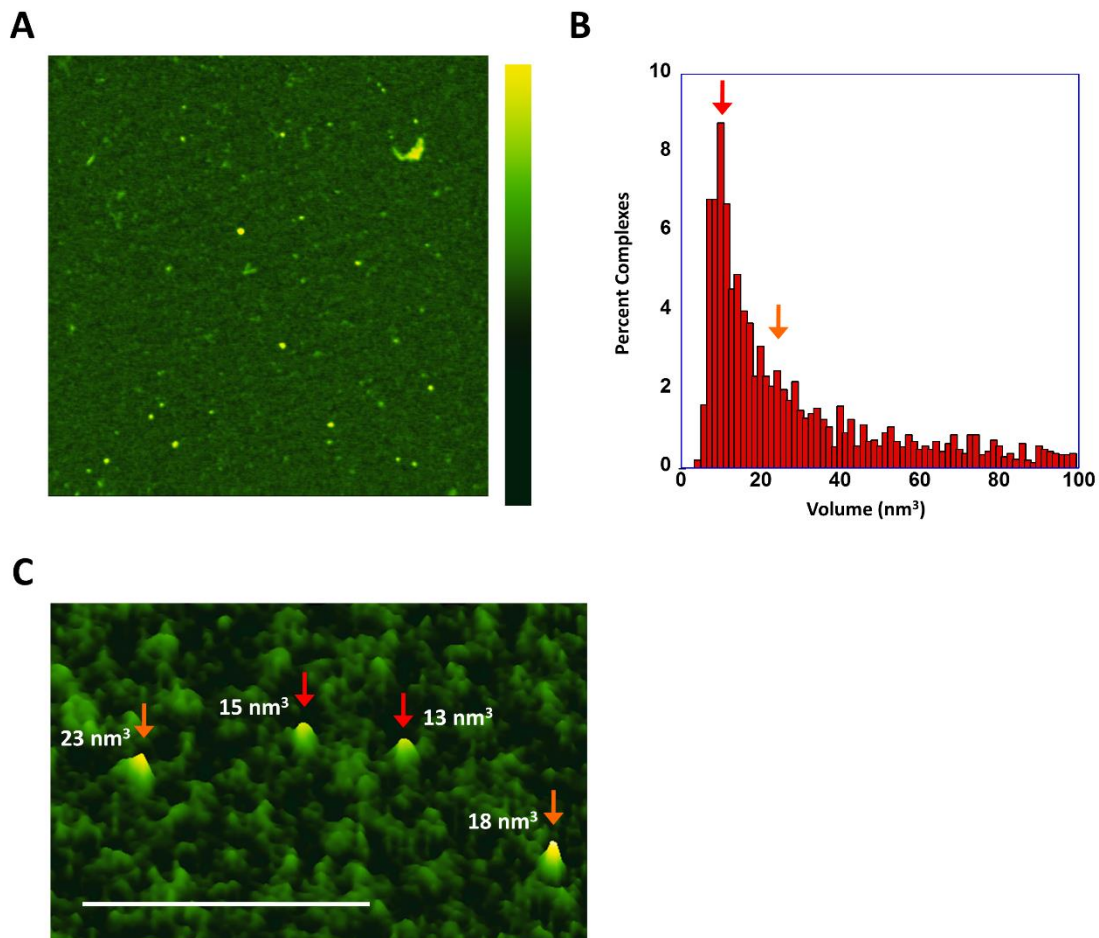


Figure 5.4 : AFM images and volume analysis of H5

(A) 1 x 1 μm image of 90 nM H5 protein deposited onto mica. Scale indicates height from 0 – 3 nm. (B) Volume distribution of H5 proteins (n = 2111). Red arrow indicates the dominant species, the monomer form of H5 with a volume of 10.9 nm³. An orange arrow indicates the population of the H5 dimers, ~ 20 nm³. (C) 200 x 200 nm surface plot of monomers and dimers of H5. Red arrows indicate monomers and orange arrows point to dimers. White text displays the volumes of each protein complex. White scale bar is 100 nm.

Results

H5 exists primarily as a monomer

Figure 5.4A shows a sample AFM image of H5 protein deposited onto mica, and this image shows that the H5 protein exhibits different oligomerization states. To investigate the distribution of oligomerization states of the H5 protein, the volumes of the protein complexes were measured. Figure 5.4B shows the distribution of volumes for H5 proteins. The most dominant population has a volume of 10.9 nm^3 , which is consistent with the monomer form of H5 (red arrow). Additionally, there were volumes consistent with the dimer form of H5 (orange arrow), and much larger species of H5. We then closely examined the H5 protein complexes to check if there were any unique conformational shapes associated with the dimer form of H5. Figure 5.4C shows a surface plot of monomers and dimers of H5. Note that the dimers, while larger, appear to have similar shapes to the monomers, suggesting that there is not a unique conformational change associated with the dimer of H5.

Conclusions and Future Work

The data from the AFM experiments indicate that the H5 protein exists primarily in a monomer form, consistent with previous SDS – PAGE data (Beaud, Beaud et al. 1995). While the SDS – PAGE gel experiments found that the protein was slightly larger (35 kDa) than its monomer form, these results were thought to be the result of the rigid structure associated with H5. However, the AFM data were inconsistent with the gel filtration column data, which found that H5 can form large species, greater than 400 kDa (D'Costa, Bainbridge et al. 2008). AFM uses lower concentrations of protein to investigate stoichiometries, and it is possible that at 90 nM concentration, the larger multimeric species of H5 would be difficult to observe. Additionally, H5 is a phosphoprotein, and it is quite possible that post-translational modifications

could impact the ability of H5 to form larger species. The purified protein used in these experiments came from *E. coli*, and the gel filtration data and SDS – PAGE experiments used protein from cell extracts of HeLa cells, a human epithelial cell strain, which may contribute to the discrepancy. Future work should include doing studies at higher concentrations of H5 protein, cross-linking studies to investigate if the large species of H5 can be formed, and using a different protein preparation of H5 that comes from a eukaryotic cell line.

REFERENCES

- Beaud, G. (1995). "Vaccinia virus DNA replication: a short review." Biochimie **77**(10): 774-779.
- Beaud, G., R. Beaud and D. P. Leader (1995). "Vaccinia virus gene H5R encodes a protein that is phosphorylated by the multisubstrate vaccinia virus B1R protein kinase." J Virol **69**(3): 1819-1826.
- D'Costa, S. M., T. W. Bainbridge and R. C. Condit (2008). "Purification and properties of the vaccinia virus mRNA processing factor." J Biol Chem **283**(9): 5267-5275.
- Kay, N. E., T. W. Bainbridge, R. C. Condit, M. R. Bubb, R. E. Judd, B. Venkatakrishnan, R. McKenna and S. M. D'Costa (2013). "Biochemical and biophysical properties of a putative hub protein expressed by vaccinia virus." J Biol Chem **288**(16): 11470-11481.
- Ratcliff, G. C. and D. A. Erie (2001). "A novel single-molecule study to determine protein--protein association constants." Journal of the American Chemical Society **123**(24): 5632-5635.
- Yang, Y., H. Wang and D. A. Erie (2003). "Quantitative characterization of biomolecular assemblies and interactions using atomic force microscopy." Methods **29**(2): 175-187.

APPENDIX A: SUPPLEMENTAL FIGURES - CHAPTER 2

Supplemental Figures



	 Single Complexes	 Multiple Complexes
<i>Linear GT-DNA ADP</i> (<i>n</i> = 246)	88%	12%
<i>Linear GT-DNA ATP</i> (<i>n</i> = 287)	87%	13%
<i>Circular GT-DNA ATP</i> (<i>n</i> = 361)	86%	14%
<i>Linear GC-DNA ADP</i> (<i>n</i> = 198)	92%	8%
<i>Linear GC-DNA ATP</i> (<i>n</i> = 371)	96%	4%
<i>Linear GT-DNA ATP S+L 2m</i> (<i>n</i> = 163)	93%	7%
<i>Linear GT-DNA ATP S+L 5m</i> (<i>n</i> = 184)	96%	4%

Figure S2.1 : Number of complexes bound to DNA

Cartoons above the table indicate what is meant by single vs. multiple complexes. Table shows the percent of single complexes vs. multiple complexes for each type of experiment conducted.

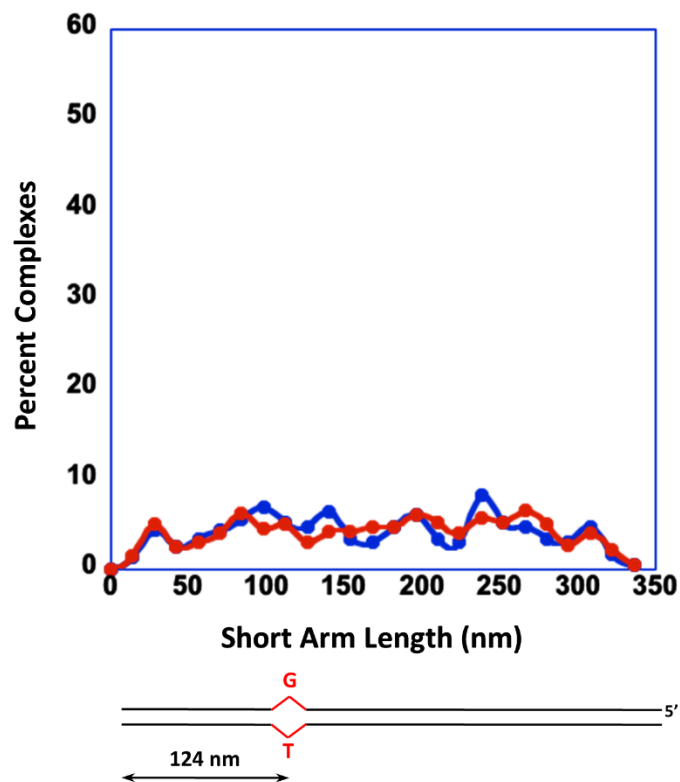


Figure S2.2 : Position distribution of MutS α on GC-DNA in the presence of ADP vs.ATP

Analysis of the distribution of positions of MutS α on GC-DNA in the presence of 100 μ M ADP (blue line) or 100 μ M ATP (red line) shows a random distribution, indicating that MutS α does not exhibit preferential binding without a mismatch present.

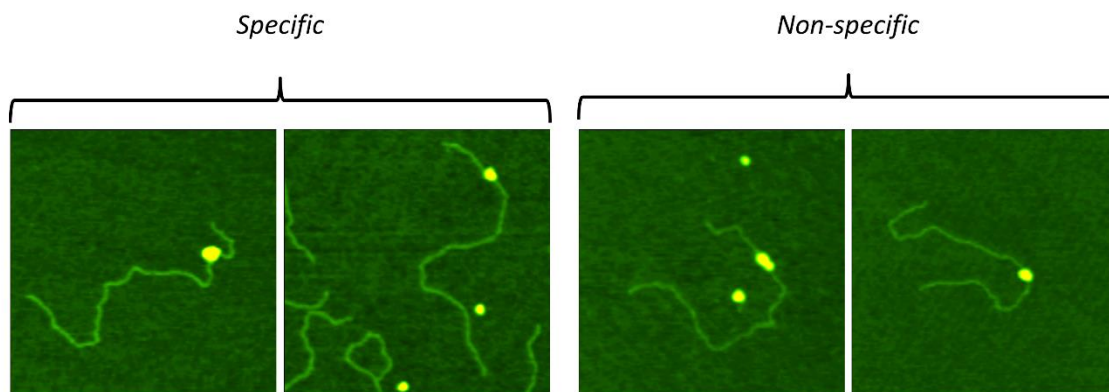


Figure S2.3 : Images of multimers of MutS α on GT-DNA in the presence of ATP

500 nm images of multimers of MutS α in the presence of 100 μ M ATP are shown. Two left panels show multimeric MutS α complexes bound to the mismatch follow the contour of the DNA. Two right panels show multimeric MutS α complexes bound non-specifically to GT-DNA follows the contour of the DNA

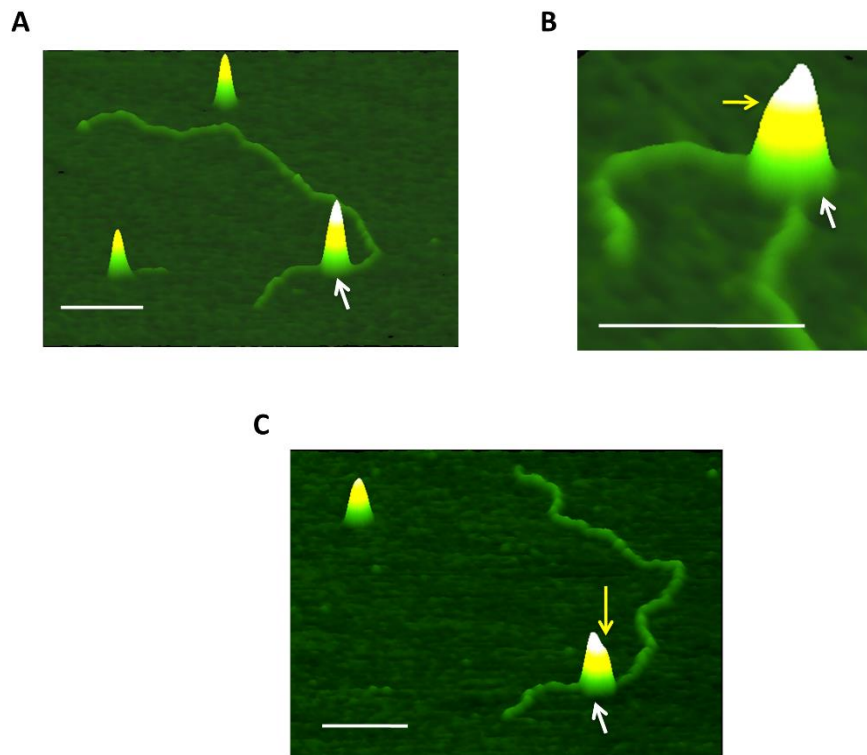


Figure S2.4 : Asymmetry of multimers of MutS α on GT-DNA in the presence of ATP

(A) Topographic image of a tall condensed complex containing two MutS α in the presence of 100 μ M ATP bound to the mismatch. White arrow indicates the mismatch. White scale bar indicates 100 nm. (B) and (C) show topographic images of a complex at the mismatch (mismatch indicated by white arrow) containing two MutS α (B) or three MutS α (C) in the presence of ATP. Yellow arrows point to the asymmetric MutS α in the complex. White scale bars indicate 100 nm.

Shapes	MutS α		MutS α –MutL α	
	ADP (n = 219)	ATP (n = 184)	2m (n = 152)	5m (n = 173)
<i>Small Round</i>	96 %	68 %	51 %	21 %
<i>Large Round</i>	2 %	24 %	20 %	41 %
<i>Long</i>	1 %	6 %	9 %	22 %
<i>L-shaped</i>	0 %	1 %	12 %	6 %
<i>Loops</i>	1 %	1 %	8 %	9 %

Figure S2.5 : Distribution of the conformational shapes of MutS α and MutS α –MutL α complexes on GT–DNA.

Table shows the percent of each shape that was observed in the MutS α alone and the MutS α –MutL α experiments under different conditions.

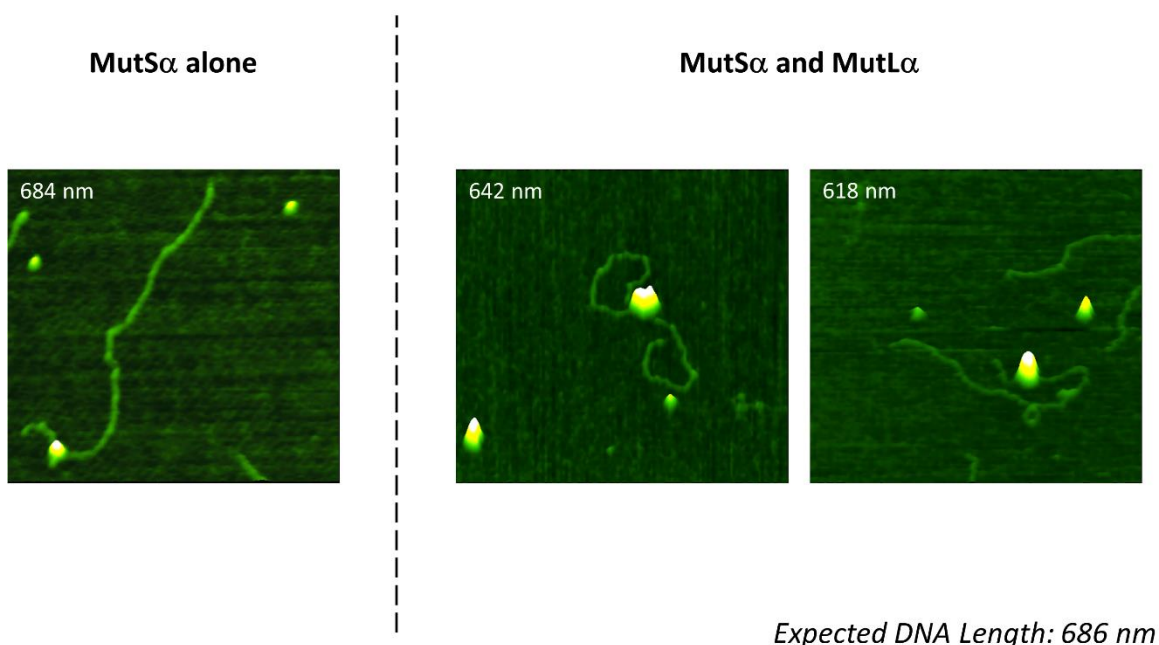


Figure S2.6 : AFM images of MutS α and MutS α –MutL α complexes bound to GT–DNA

500 nm images of MutS α and MutS α –MutL α complexes bound to GT–DNA in the presence of 1 mM ATP. Left panel shows MutS α bound to the mismatch and total DNA length is indicated in the upper left corner. Two right panels show MutS α –MutL α complexes bound to GT–DNA either at the mismatch or not. Total DNA length is indicated in the upper left corner.

Supplemental Methods Figures

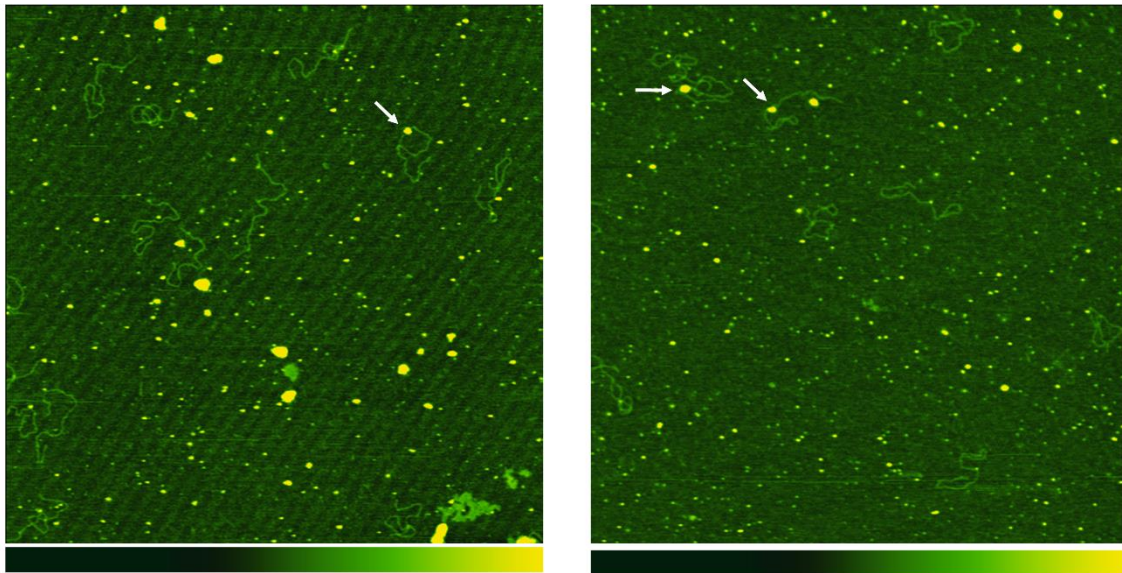


Figure SM2.1 : AFM images of the non-crosslinked control experiment of MutS α bound to GT-DNA in the presence of ATP

Images are of MutS α in the presence of 100 μ M ATP and GT-DNA. White arrows indicate multimers of MutS α bound to GT-DNA. Images are 2 μ m each and color scale bars indicate 0 – 3 nm.

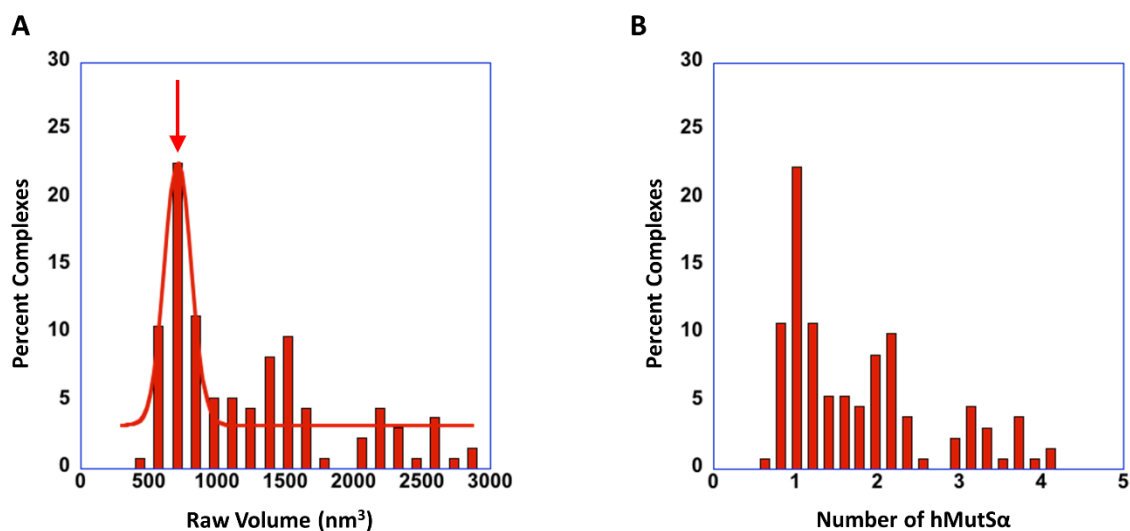


Figure SM2.2 : Normalization of MutS α volumes

(A) Histogram of raw MutS α volumes bound to GT–DNA in the presence of 100 μ M ATP. A Gaussian was fit to the first peak (red arrow) and all volumes were divided by the volume of the first peak. (B) Histogram of normalized MutS α volumes.

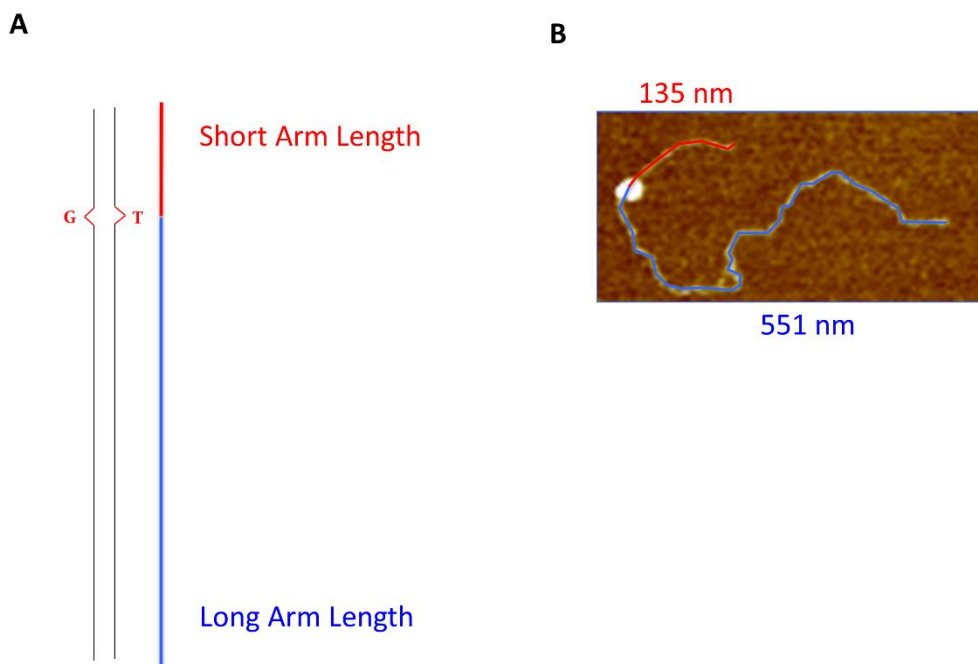


Figure SM2.3 : Position analysis of MutS α on DNA

(A) Schematic of the DNA substrate used showing the mismatch is 124 nm from end (the short arm). Short arm length is indicated in red and long arm length is indicated in blue. (B) Sample MutS α -DNA complex traced. Short arm length is indicated in red and long arm length is indicated in blue. If any part of the complex is within two standard deviations of the mismatch, it is a specific complex.

APPENDIX B: AFM DATA ANALYSIS PROTOCOL

Part 1: Flattening raw AFM images

To be done before analyzing ANY of the images via ImageSXM and ImageJ

1. Open the NanoScope Software (can only be used on a PC)
2. Select the second icon (the multi-color one, not the microscope icon)
3. Open the drive that contains all images of interest
4. Open the first image (if it contains two images (height and phase for example) Select Left Image)
5. Select Plane Fit, hit the XY button, and then Quit. This should Plane Fit the image.
6. Select Flatten, make sure it is set to 0 order flatten (or 1st or 2nd depending on the bowing within the image). Next, select No Threshold, select Execute. Then, select Z < (less than), and manipulate the number until the background is mostly black with the protein showing through. Less brown is better.
7. If there are scan lines, select Modify, Erase Scan Lines. Click on the image and highlight the scan line, click, and then hit Execute.
8. Save the image with an “f” for flattened. These images can be analyzed via ImageSXM.
9. Save the image as a tif to be analyzed via ImageJ.
10. Select the next image, rinse and repeat.

Part 2: Volume Analysis

As seen in (Ratcliff and Erie 2001, Yang, Wang et al. 2003)

Setting up the program (before opening ANY images)

1. Open Image SXM (have a Mac to use this software)
2. On Menu Bar, click on SPM and scroll down to SPM options

3. Under Display Units for both XY and Z, ensure then units are nm and check “fix” for both XY and Z. Next look at Multiple Images and be sure to Display “Image #1,” and hit OK.
4. On the Menu Bar, click on Analyze and scroll down to Options. Make sure the following are checked: Area, Mean Density, Standard Deviation, Ellipse Major Axis, Ellipse Minor Axis, and Headings. Click on OK.

Open all images to be analyzed. Also open a spreadsheet containing information on the conditions of the samples being analyzed.

1. First you need to determine the height of the surface, which is usually a non-zero number, and must be taken into consideration during your volume analysis. Click on Analyze on the Menu Bar and click on Histogram (hot key command + G). To measure the surface height, place the cursor in the middle of the distribution and read its value in the Info window at Level. This value will be used to calculate all the volumes in this particular image. Remember, for every image you analyze, you MUST write down the surface height value.
2. Go to Options on the Analyze menu and scroll down to Density Slice. Adjust the density slice, and maximize the upper limit of the density slice. Now adjust the lower limit of the density slice by moving the cursor to the right hand side of the histogram. *Remember: try to get all proteins of interest highlighted in red without highlighting too much of the background noise.*
3. With Density Slice still on, go to Analyze on the Menu Bar and select Analyze Particles. Under the Particle Analysis Options make sure the Min Particle Size (Pixels) is either 5 or 10, depending on the size of your protein. For MutS α both 5 and 10 were sufficient for

complete analysis. Max Particle Size (Pixels) should be maximized at 99999. Be sure and check Label Particles, Outline Particles, and Ignore Particles Touching the Edge. Click OK.

4. Go to the Analyze menu and select Show Results. Save both the threshold image (which now has all the proteins counted labeled with a number) and the Results table. Copy and paste the Results table into your spreadsheet.
5. Open the next image. Rinse and repeat.

Once all images and their proteins have been analyzed and all the results have been input into the spreadsheet.

1. Make a new column in the spreadsheet and title it Maj/Min. You will take the Major Axis value and divide it by the Minor Axis value for each protein. The value that comes out is usually between 1 and 2 (if your protein is symmetrical) or higher (if your protein is asymmetrical). Be sure to note when you make your histogram, all the values that are exactly equal to 2. These are false positives and should be thrown out from the analysis.
2. Next, make a new column titled Volume. The formula for the Volume is:

$$V = A (M - S)$$

Where V is volume, A is the area, M is the mean, and S represents the surface height value that you got when you looked at the surface height histogram. Calculate the volume for all proteins.

Open up KaleidaGraph once all the volumes have been determined. Note that these calculations can also be done in KaleidaGraph.

1. Copy and paste all the volumes with their maj/min values into the KaleidaGraph spreadsheet. Highlight the columns and Right-click to open up the menu and click on

Sort Ascending. Make sure both columns are selected and hit ok. Now, throw out all the volumes that match up to a maj/min value of 2.

2. Next, go to Functions on the Menu Bar and select Bin Data. For MutS α the minimum value is 300, with the maximum value 3,000. Next input a bin number to bin the data. Typically this number is the square root of the number of counted proteins, however this is not always the case. Be sure to experiment with the bin number to ensure you are getting an accurate representation of the data. Click on Copy to Clipboard and select OK. Paste onto two empty columns in the KaleidaGraph spreadsheet.
3. Next go to Gallery on the Menu Bar and select Linear then Scatter Plot. The first column listed is the x-value and the second is the y-value. Hit OK.
4. This will open up a new window with a histogram. Next, fit this histogram with a Gaussian fit. Select the Volume and Define Parameters. M1 is the background level of noise. M2 is the amplitude of the curve (the highest point of the curve). M3 is the middlemost point of the highest peak. M4 is the standard deviation, or the breadth of distribution. Hit OK and the histogram will be fit with the Gaussian fit. A table will pop up on the Histogram window containing values for M1 – M4, the ChiSq, and the R-value. The closer the R-value is to 1, the better the fit.

Part 3: DNA Contour Trace analysis

As seen in (Wang, Yang et al. 2003)

Setting up the program (before opening ANY images)

1. Open up ImageJ (available for both Macs and PCs)
2. Go to Plug-ins on the Menu Bar and select NeuronJ.

Open up the first image of interest. Unlike ImageSXM, ImageJ can only have one image open at a time.

1. Select Analyze on the Menu Bar and scroll down to Set Scale...
2. Distance in pixels should be 512, Known Distance is 2000, Unit of Length is in nm, and then check Global. Hit OK.
3. Now count how many DNA there are, free and bound and note their X&Y locations on a spreadsheet.
4. Select on the Add Tracing icon on the mini menu bar, and trace any DNA of interest.

Note: For linear DNA with no proteins bound, just measure the entire length and double-click to end the trace.

For linear DNA with a protein bound, measure from the end of the longer arm to the center of the protein then double click, then measure from the protein to the shorter arm, and double click.

For circular DNA with no proteins bound, measure the same way as linear DNA with no proteins bound, but be sure that the trace doesn't overlap on itself.

For circular DNA with proteins bound, measure the entire length the same way as the circular DNA with no proteins bound.

5. Select on the Measure Tracings and ensure that Display tracing measurements is checked. The other two on the upper half of the menu do not need to be checked. Hit OK. Another window will pop up, write down the Trace Length value for each of the DNAs measured.
6. Be sure to note interesting-looking DNA formations in the spreadsheet such as: loops, end-binding events, multiple binding events, etc.

7. *For linear DNA with protein(s) bound, there will be a short arm length value as well as a long arm length value. Write these down, then add them together to get the total length. Then take the short arm length and divide it by the total length to determine where the protein has bound on the DNA.*
8. Use KaleidaGraph to make histograms of anything from Total DNA vs. Number of Binding Events, Loops vs. End Bindings, Specificity of Binding, Bound DNA vs. Free DNA, etc.

REFERENCES

- Ratcliff, G. C. and D. A. Erie (2001). "A novel single-molecule study to determine protein--protein association constants." Journal of the American Chemical Society **123**(24): 5632-5635.
- Wang, H., Y. Yang, M. J. Schofield, C. Du, Y. Fridman, S. D. Lee, E. D. Larson, J. T. Drummond, E. Alani, P. Hsieh and D. A. Erie (2003). "DNA bending and unbending by MutS govern mismatch recognition and specificity." Proc Natl Acad Sci U S A **100**(25): 14822-14827.
- Yang, Y., H. Wang and D. A. Erie (2003). "Quantitative characterization of biomolecular assemblies and interactions using atomic force microscopy." Methods **29**(2): 175-187.